ÇUKUROVA UNIVERSITY
INSTITUTE OF NATURAL AND APPLIED SCIENCES

MSc. THESIS

Ruken AKTAŞ

FLOPPING BEHAVIOR OF SIDE-BY-SIDE CYLINDERS IN SHALLOW FLOW

DEPARTMENT OF MECHANICAL ENGINEERING

ADANA, 2007

ÇUKUROVA ÜNİVERSİTESİ

FEN BİLİMLERİ ENSTİTÜSÜ

FLOPPING BEHAVIOR OF SIDE-BY-SIDE CYLINDERS IN SHALLOW-FLOW

Ruken AKTAŞ

YÜKSEK LİSANS TEZİ

MAKİNA MÜHENDİSLİĞİ ANABİLİM DALI

Bu Tez 19/12/2007 Tarihinde Aşağıdaki Jüri Üyeleri Tarafından Oybirliği/Oyçokluğu İle Kabul Edilmiştir.

İmza:……	İmza:……	İmza:……..
Doç. Dr. Hüseyin AKILLI DANIŞMAN	Prof. Dr. Beşir ŞAHİN ÜYE	Doç. Dr. Galip SEÇKİN ÜYE

Bu Tez Enstitümüz Makina Mühendisliği Anabilim Dalında Hazırlanmıştır.

Kod No:

Prof. Dr. Aziz ERTUNÇ
Enstitü Müdürü

ABSTRACT

M.Sc. THESIS

FLOPPING BEHAVIOR OF SIDE-BY-SIDE CYLINDERS IN SHALLOW FLOW

Ruken AKTAŞ

DEPARTMENT OF MECHANICAL ENGINEERING
INSTITUTE OF NATURAL AND APPLIED SCIENCES
UNIVERSITY OF ÇUKUROVA

Supervisor: Assoc. Prof. Dr. Hüseyin AKILLI
Year: 2007, Pages: 95
Jury: Assoc. Prof. Dr. Hüseyin AKILLI
Prof. Dr. Beşir ŞAHİN
Assoc. Prof. Dr. Galip SEÇKİN

In this study, flopping regime behind two and three side-by-side circular cylinders in shallow water flow was investigated by Particle Image Velocimetry Technique. During the experiments, the cylinders used was made of plexiglas material and their diameter was 40mm. Experiments were carried out at three different water heights (10mm, 20mm and 40mm) and three different spacing (10mm, 20 mm, 30 mm) between cylinders were used. The value of Reynolds number based on the cylinder diameter was Re=5000. Time-averaged flow characteristics were obtained from averaging 3000 images which were acquired at 2 Hz frequency. Flopping regime looks completely random process of flow. However, flopping occurs in between 10 and 60 seconds time period. Moreover, this time period decreases with decreasing water height. Finally, for the flows where flopping regime occurs, instantaneous flow characteristics are more informative than the time-averaged flow characteristics.

Key Words: Flopping regime, Side-by-side circular cylinders, Shallow water, PIV.

ÖZ

YÜKSEK LİSANS TEZİ

SIĞ SUDA YAN YANA DİZİLİ SİLİNDİRLER ARKASINDA OLUŞAN GİRDAP DALGALANMASININ İNCELENMESİ

Ruken AKTAŞ

ÇUKUROVA ÜNİVERSİTESİ
FEN BİLİMLERİ ENSTİTÜSÜ
MAKİNA MÜHENDİSLİĞİ ANABİLİM DALI

Danışman: Doç.Dr. Hüseyin AKILLI
Yıl: 2007, Sayfa:95
Juri: Doç.Dr. Hüseyin AKILLI
Prof. Dr. Beşir ŞAHİN
Doç. Dr. Galip SEÇKİN

Bu çalışmada, sığ su akışında yanyana dizilmiş olan iki ve üç adet silindirler arkasında oluşan girdap dalgalanması parçacık görüntülemeli hız ölçüm tekniği kullanılarak incelenmeştir. Deneylerde 40mm çapında plastik cam malzemeden yapılan silindirler kullanıldı. Deneyler üç farklı su yüksekliğinde (10mm, 20mm and 40mm) yapıldı ve silindirler arasında üç farklı aralık (10mm, 20mm and 30mm) kullanıldı. Reynold sayısı silindir çapına bağlı olarak Re=5000 değerindedir.Akış karakteristikleri 2 Hz sıklığında alınan 3000 anlık şekiller ile elde edildi. Girdap dalgalanması tamamen rastgele olmaktadır.Ancak girdap dalgalanmasının periyodu 10 ile 60 saniye arasında meydana gelmektedir. Bu periyot su yüksekliği azaldıkça düşmektedir. Sonuçta girdap dalgalanmasının meydana geldiği akışlar için anlık akış karekteristikleri ortalama akış karekteristiklerinden daha bilgilendiricidir.

Anahtar Kelimeler: Girdap dalgalanması, Yan yana dizili silindirler, Sığ su, Parçacık görüntülemeli hız ölçüm tekniği

ACKNOWLEDGEMENTS

This list endless if I have to thank all the people that made possible this work. First and Foremost, I would like to thank my advisor Assoc. Prof. Dr. Hüseyin AKILLI for his support, guidance and encouragement. I shall always be owed to him both for what I have learned from him and for what he has allowed me to learn on my own.

I would like to thank Prof. Dr. Beşir ŞAHİN for his continues support, help and encouragements. Knowing and feeling his support during my M.Sc. thesis helped me a lot to my self-confidence.

My sincere thanks go to Research Assist Cuma KARAKUŞ for sharing his knowledge and for helping in experiments.

In addition, I would like to thank all the staff of Department of Mechanical Engineering at Çukurova University.

Last but not least, I would like to thank my family and my sister Helin AKTAŞ for their patience and trust.

NOMENCLATURE

C_f : Bed (skin) friction coefficient

Cp : Base pressure coefficient (Cp=(P-P∞) / (1/2ρU2∞),

D : Diameter of cylinder (mm)

d : Plate width (mm)

Fr : Froude number $(Fr = U / \sqrt{gh_w})$

f : Frequency of Karman vortex formation (Hz)

f_s : The vortex shedding frequency

H : Height of water level (mm)

M : Magnification factor ($M=L_i/L_r$)

N : Frame Number

P : Island wake parameter $(P = \overline{U}h^2 / K_Z D)$

Re_d : Reynolds number based on the diameter of cylinder $(\mathrm{Re}_d = UD/\nu)$

Re_h : Reynolds number based on the height of water level $(\mathrm{Re}_d = Uh_w/\nu)$

S : Wake stability parameter $(S = C_{fs} D / h_w)$

St : Strouhal number $(St = fD/\overline{U})$

t : Time(sec)

T : Distance between the cylinder axes

U : Free stream velocity (maximum velocity) (mm/sec)

$\overline{U}$: Depth-averaged velocity (mm/sec)

u,v : Component of velocity V in x y axis system (mm/sec)

u'v' : Reynolds stress correlation (mm^2/sec^2)

V : Instantaneous total velocity vector (mm/sec)

$\langle V \rangle$: Time-averaged total velocity vector (mm/sec)

W : Width of water channel (mm)

ω : Instantaneous vorticity (1/sec)

$\langle \omega \rangle$: Time-averaged vorticity (1/sec)

ψ : Instantaneous streamline

$\langle \psi \rangle$: Time-averaged streamline

θ : Momentum thickness of boundary layer (mm)

ν : Kinematic viscosity (mm/sec^2)

x : Horizontal length (mm)

TABLE OF CONTENTS **PAGE**

LIST OF FIGURES

1. INTRODUCTION

1.1. Shallow water

A shallow flow is defined as a predominatly horizontal length scale of the flow is considirably larger than its depth. Many wake flows can be characterized as shallow turbulent flow in nature and in engineering practice,e.g. in wide rivers, lakes, estuaries, shallow coastal waters, mountains or the statified atmosphere.

The wake regions in shallow water also occur in a variety of engineering applications, e.g. behind a bridge pier, other types of hydraulic structures, in various types of channels and reservoirs. Most of the wakes of island are said to be shallow because, the horizontal length scales of the flows are approximately two the orders of magnitude larger than their depths. Babarutsi et al. (1988) gave an example for shallow water flows such that the diameters of the island are 280m and 560m, while the water depth in the region around island are only two to three meters. Despite their practical importance, relatively little is known of detailed flow structure of shallow water vortices.

The presence of a bottom wall, parallel to a free surface, and with a relatively short distance between them, has important effects in several respects. An important characteristic of shallow flows is the vertical confinement restriction that prevents the three-dimensional stretching and breakdown (via secondary or spanwise instabilities) of the two-dimensional structures. Another dramatic influence of the shallow flow comes from the bottom friction effect. The bottom resistance is associated with small-scale three-dimensional turbulance, which can “stabilize” the transverse shear flow.This effect will eventually attenuate and suppress the instability of the horizontal, large-scale, quasi two-dimensional flow structure. Finally, at sufficiently high Froude number, the presence of free-surface contamination or surfactant can induce additional three-dimensionality at the vortex free-surface junction, as characterized by Lang & Manglano (2002). This free-surface distortion may play a role in modification of the near wake instability. The present investigation emphasizes shallow flows without substantial free-surface distortion,

namely subcritical in flow at low Foude number.In the following,recent advances in our understanding of vortex formation in shallow flows are reviewed.

In shallow flows, the in flow is confined between a free-surface and a bed. Turbulent flow is mainly governed by three-dimensional wall turbulance produced by shear friction at solid bottom. The characteristic length of these vortical structures is of the order of, or less than, the water depth and mostly aligned in streamwise direction, as reviewed by Nezu and Nakagawa (1993) . When an inflow boundary layer in a shallow flow encounters a vertical obstacle, three-dimensional separation is induced, and a complex horseshoe (necklace) vortex system is created.Although the physics of this horseshoe vortex have not been characterized for the case of shallow flow, considerable insight has been attained for the case of vertical blunt obstacle or cylinder in a flow of large depth.

1.2. Turbulent wakes generated by side-by-side cylinders in deep-water

Flows around two and more cylinders have received considerable attention in the past because of its inherent importance and practical significance in many branches of engineering. For example turbulent wakes are found; the blades of multistage turbo–machines, tube bundles in heat exchangers, marine structures, group of tall buildings, In the design for heat exchangers, Flow – induced vibration of tubes in heat exchangers, Oil and gas pipelines, Fuel and control guide rods in nuclear reactors, Cooling systems for nuclear power plants, Cooling tower arrays, Offshore structures, The local strong wind around a group of skyscrapers (a group of tall buildings), Bridges, Suspension bridges, Piers and bridges pilings, Chimneys, Power lines, Struts, Grids and Screen and cables.These turbulent wakes are usually formed by the interactions of a number of simple wakes generated by individual structures. Research into this kind of flows has been largely focused on the Strouhal map, the pressure, the mean and fluctuating lift and drag coefficient, measured in immediate vicinity of the cylinders (Bearman and Wadcock, 1973; Zdravkovich, 1977), while data in the downstream region in mostly limited to qualitative descriptions.

It is therefore important to understand the flow patterns and aerodynamic characteristics behind multiple bluff bodies in order to estimate gust – wind effects and aerodynamics forces on downstream structures or to determine the heat transfer of cross – flow heat exchangers. It is well kwon that the cross flow is depend on, for example Reynolds number, surface roughness, blockage and free–stream turbulence.

Flow behind two side-by-side circular cylinders has been investigated extensively, which improves our understanding tremendously.(Landweber 1942; Spivac 1946; Ishigai et al. 1972; Bearman and Wadcock 1973; Williamson 1985; Kim and Durbin 1988; Sumner et al.1999; Zhou et al.2000). When immersed in steady cross-flow of velocity U, two circular cylinders of equal diameter D, arranged in a side-by-side configuration (Figure 1.1), are known to exhibit an asymmetrical flow pattern for intermediate values of the center-to-center transverse pitch ratio T/D separating the two cylinders (Spivack 1946; Hori 1959; Ishigai et al. 1972; Bearman & Wadcock 1973; Kamemoto 1976; Kiya et al. 1980; Williamson 1985; Jendrzejczyk & Chen 1986; Kim & Durbin 1988; Le Gal et al 1990; Sumner et al. 1997).

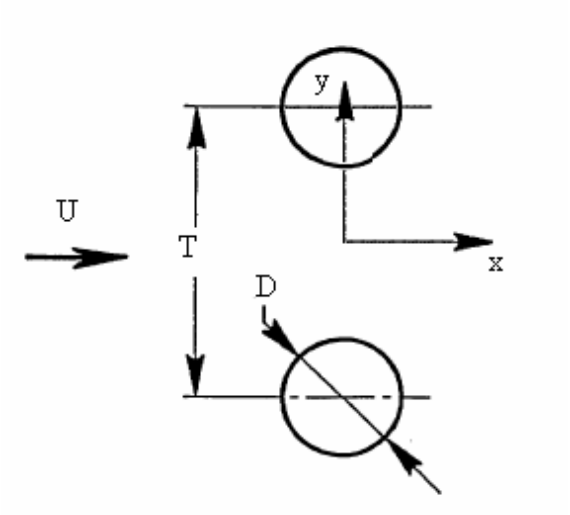

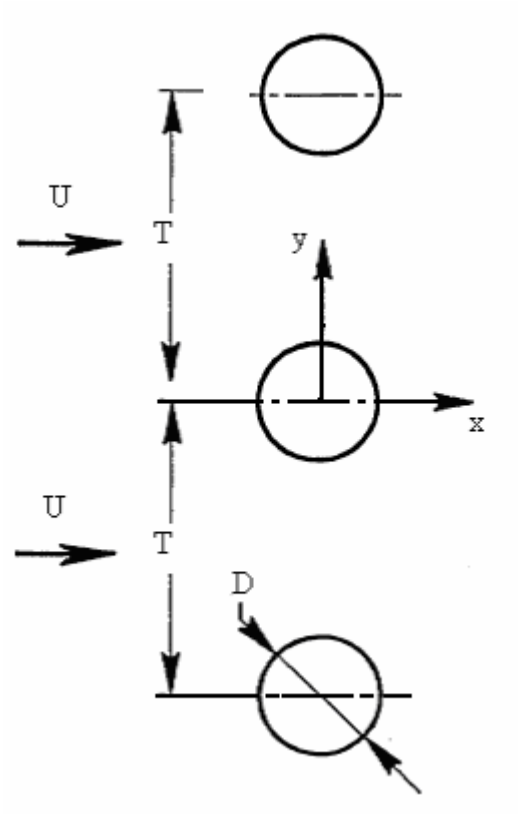

Figure 1.1. Nomenclature for two and three side-by-side circular cylinders of equal diameter in steady cross-flow.

The asymmetrical flow pattern is characterized by a narrow near-wake region behind one of the cylinders, a wide near-wake region behind the other cylinder, and two dominant vortex-shedding frequencies (which may be expressed in nondimensional form in terms of Strouhal number, $St = f_s D/U$, where f_s is the vortex shedding frequency). In some cases, the biased flow pattern switches intermittently from being directed towards one cylinder to the other, and the flow pattern is termed bi-stable (Bearman & Wadcock 1973; Kim & Durbin 1988). This biased flow pattern is observed in the range of $1.2 < T/D < 2.2$ approximately , and is nominally independent of the Reynolds number, Re (based on the cylinder diameter D and the approach velocity U).

At smaller pitch ratios, $T/D < 1.2$, the two-cylinders act like a single bluff body, forming a single Karman vortex street. For $1.2< T/D<2.2$, the gap flow between the cylinder is deflected, thus generating one narrow and one wide wake The deflected gap flow is bi-stable that is the deflection can change its direction in a

random way and stay in the same direction for a while. Two dominant frequencies are associated with the narrow and wide wakes respectively. For, T/D>2.2, two couple vortex street occur.

The flow behind three side-by-side circular cylinders bears similarity in many aspects, such as the deflected gap flow and multiple dominant frequencies, to the two side-by-side cylinders. This flow is more complicated, however. For example, there are two gap flows that may deflect in different ways and more types of flow patterns involved.Evidently, this flow is more representative of those behind a row of circular cylinders; many of its features are shared by the latter (e.g. Zdravkovich and Stonebanks 1990; Moretti 1993; Le Gal et al.1996).Kumada et al. (1984) measured the pressure distributions, velocity distributions and vortex shedding frequencies of a three-side-by-side cylinder wake at Reynold number $Re=(1.0\approx3.2)*10^4$.Four typical flow regimes were identified. When T/D was between 1.0 and 1.125, the three cylinders behaved like a single bluff body and one vortex street occurred. For T/D=1.125≈1.35, both gap flows between the cylinders deflected towards one side, thus forming narrow and wide wakes.For T/D=1.35 ≈2.225, the two gap flows were deflected towards the free-stream, respectively.

Insight into the flow structure downstream of such a side-by-side arrangement of stationary cylinders is most recently described by Williamson (1985) who found that the two-parallel vortex streets could be formed either as in-phase or an anti-phase system (See Figure1.2). When they are in anti-phase, i.e., out-of-phase, two distinct vortex streets are formed. On the other hand, in-phase oscillation of the two-vortex streets can actually lead to development of a single, large-scale wake exhibiting “binary vortices”, formed from rotation of the vortices of one wake above those from its neighbor. When the gap size lies bellow a threshold value. The flow pattern downstream of the cylinders is asymmetric, but a large-scale wake is formed.

a) Anti-phase

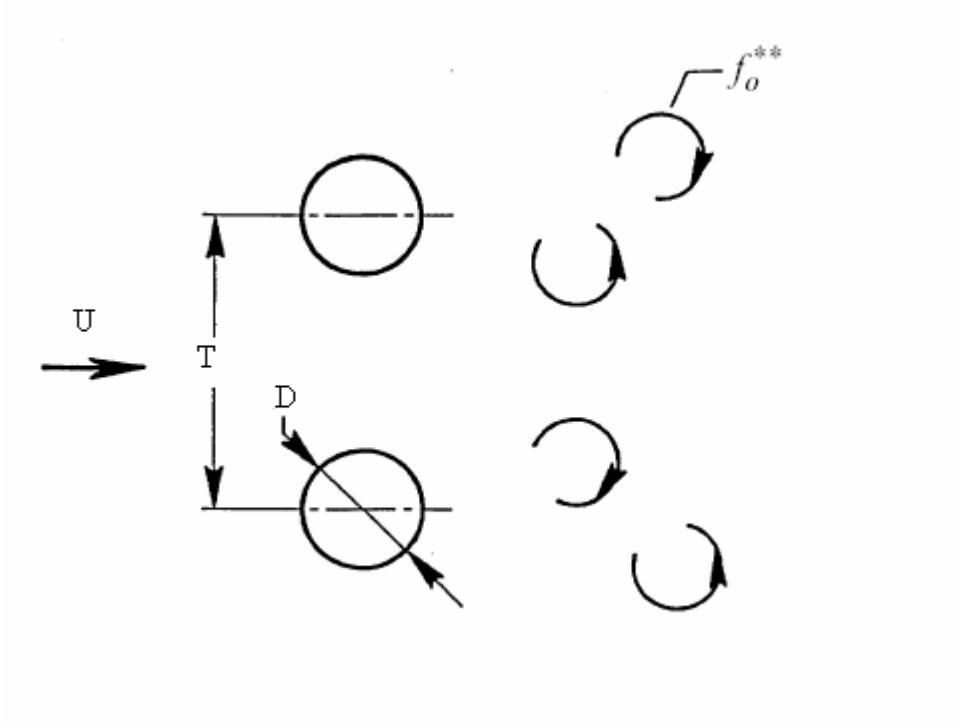

b) In-phase

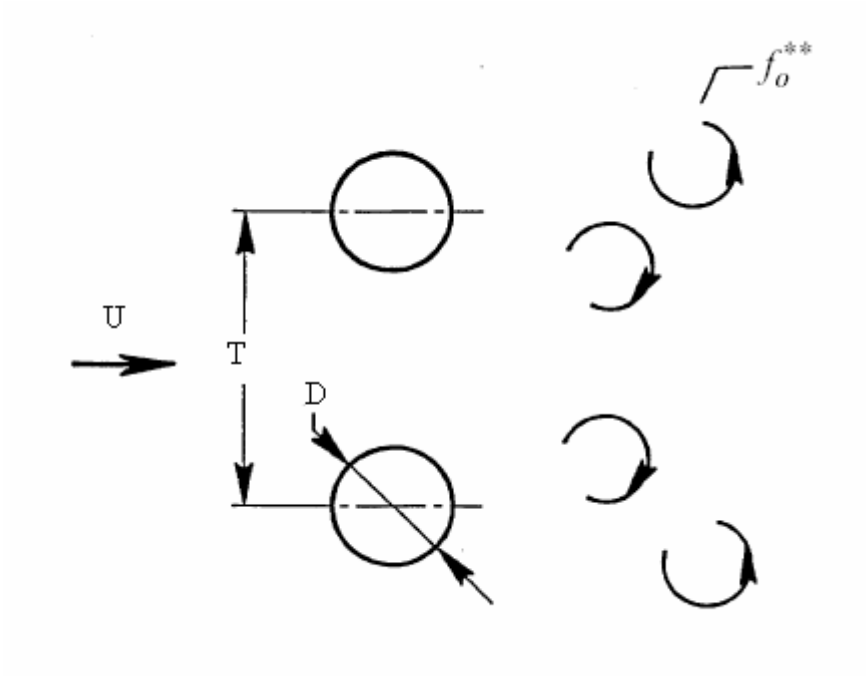

Figure 1.2. Anti-phase and in-phase vortex street synchronization.

1.3. Flopping Regime

The flowfields downstream of a single cylinder and a single plate have been studied in detail. However, studies of the flowfields downsream of cylinder arrays are less complete and studies of the flowfield downstream of plate arrays are even more scarce.Thus, the overall goal of the study presented here in is to extend the understanding of the flow downstream of cylinder and plate arrays and the variable concentraion field downstream of a plate array.

The flow pattern about a cylinder is characterized part, by the magnitude of the base pressure coefficient ($C_p=(P-P_\infty)$ / $(1/2\rho U^2_\infty)$, which always negative (hereafter, for simplicity, only the magnitude of C_p is used when geometries). Hence, the phrase "higher C_p" refers to a more negative C_p magnitude while the phrase "lower C_p" refers to a less negative C_p magnitude.

" Flopping " is first described by Bearman and Wadcock (1973) in a study of the transitition from multiple independent wakes to a single wake of a two-cylinder array positioned normal to the flow. Bearman and Wadcock (1973), observe a critical spacing in which unequal wake sizes are formed behind each cylinder of the two-cylinder array. They find that the relative positions behind the cylinders of the wide and narrow wake may switch spontaneously or may switch only after being forced by a large perturbation to the flow field. Kim and Durbin (1988) are the first to present measurements of the base pressure coefficient as a function of cylinder spacing, C_p, of each cylinder during flopping. They define "spontaneous flopping" to be the occurrence of a wake behind each cylinder that alternates between a wide wake with a low magnitude C_p and a narrow wake with a high magnitude C_p. They determine that the time duration between transitions has a Poisson distribution and decreases as velocity increases.

When the natural perturbations in the backround flow are not adequate to initiate spontaneous flopping at a particular spacing, it may be initiated by means of a large perturbation. At other spacings, a large perturbation may cause the C_p value to change and the corresponding wake size to switch positions, but fail to induce

spontaneous flopping, i.e. the wakes remain stable. The former behavior is defined as “forced flopping” and the latter is defined as quasi-stable behavior.

The time resolved variation of C_p and the velocity power spectra for arrays of two-,three- and four-cylinders aligned in a plane normal to the flow are presented. Also presented are the probability distributions of the time duration of flopping for two-and three-cylinder arrays. For the three cylinder array, depending on the spacing, spontaneous and forced flopping or quasi-stable behavior is observed. The hot-wire power spectra is observed to have three peaks that correspond to different Strouhal numbers. Each peak corresponds to a wake structure, i.e. a pattern of vortices behind the cylinder array. For the two-and three cylinders arrays, a pdf of the time of each period that each average C_p value remains relatively high or relatively low closely matches a zero event Poisson distribution as found by Kim and Durbin (1988). For the flopping period, which is defined as the time interval between one transition on from low to high C_p and the subsequent transition from low to high C_p value, a pdf does not match a one event Poisson process.Thus, flopping is not a Poisson process. For the four-cylinder array, at all spacings, only quasi-stable behaviour is observed and neither forced nor spontaneous flopping is observed.

Bearman and Wadcock (1973), for a two-cylinder array with same T/D range and with a Reynolds number (Re) based on cylinder diameter of 2.5×10^4, also find that the average C_p of each cylinder has two different values.In their study, the C_p of a cylinder may switch between relatively high and low values spontaneously, but sometimes may require forcing by either stopping and starting the flow or by causing a large flow perturbation. Thus, either spontaneous flopping or quasi-stable behavior is observed.

Previous studies of transition from multiple independent wakes to a single wake have shown that, within a critical spacing ratio ($0.1\leq T/D\leq1.3$), the average C_p of each cylinder varies in time and takes on two different values. Kim and Durbin (1988) describe this as the “ flopping regime.” They suggest that flopping occurs spontaneously when the wake behind the each cylinder alternates between a wide wake with a low magnitude C_p, and a narrow wake with a high C_p.

Since both flopping and quasi-stable behavior of the average C_p values have been observed in previous studies, it is useful to define terms that describe each of the three types of behavior: quasi-stable behavior, spontaneous flopping, and forced flopping. These behaviors can be explained as fallows.

- Quasi-stable behavior is the wake behavior observed downstream of the cylinders in which different C_p values exist behind each cylinder. The C_p values do not vary with time. A large amplitude flow perturbation can cause the average C_p values until another large perturbation is applied.
- Spontaneous flopping is the behavior observed downstream of the cylinders where the average C_p values are always observed to alternate over time between relatively high and low values, even when no large perturbation is applied to the flow field
- Forced flopping is the behavior observed downstream of the cylinders in which initially stable wakes exhibiting flopping as a result of a large, one time perturbation. After the initial large perturbation is applied and flopping occurs, there is no observable difference between forced and spontaneous flopping.

2. PREVIOUS STUDIES

2.1. Kelvin-Helmholtz and Karman Vortices

It is well known that the structure of the near- wake is remarkably complex, even from a stationary cylinder. When the Reynolds number based on cylinder diameter reaches a critical value, instabilities initiate from the end of the recirculation region, and eventually result in periodic vortex array, known as a Karman vortex street . The onset of this vortex pattern has been found to be the result of global (absolute) instabilitiy of the near-wake, as summarized by Huerre & Monkewitz (1990).

In addition, at a sufficiently high value of Reynolds number, so-called "transition waves" appear in the shear layer separating from the surface of cylinder. These waves are detectable in the region of the wake extending from the separation point on the body to the first appearance of the large-scale Karman vortex. When the value of Reynolds number is sufficiently high, then these transition waves take the form of train of Kelvin-Helmholtz vortices shown in Figure 2.1. In the bluff body community, these small-scale vortices are often referred to as Bloor-Gerrard vortices. The onset of "transition waves" is expected to be strong function of the disturbance level of the free stream, in view of the fact that they arise from a convective-type instability, as described by Ho and Huerre (1984). Bloor (1964) detected the small-scale vortices for the range of Reynolds number Re>1300, however, Ünal and Rockwell (1988) first noted these vortices at Re_d=1900. Wu et al. (1994b) discussed the possible influence of background disturbance levels and observed these waves over the range of Reynolds numbers $1000 \leq Re \leq 3000$.

Kelvin-Helmholtz vortices in the shear layer are an essential feature of the transition from a laminar to turbulent state. As a consequence of this transition process, the first Karman vortex formed from the cylinder at Re_d=5000 is essentially turbulent. Karman vortices from circular cylinder is shown in Figure 2.1.Bloor (1964) addressed the three-dimensional aspects of this transition process using point velocity measurements obtained from hot-wire anemometry. She observed that the

region of transition to turbulence moves upstream towards the cylinder with increasing Reynolds number.

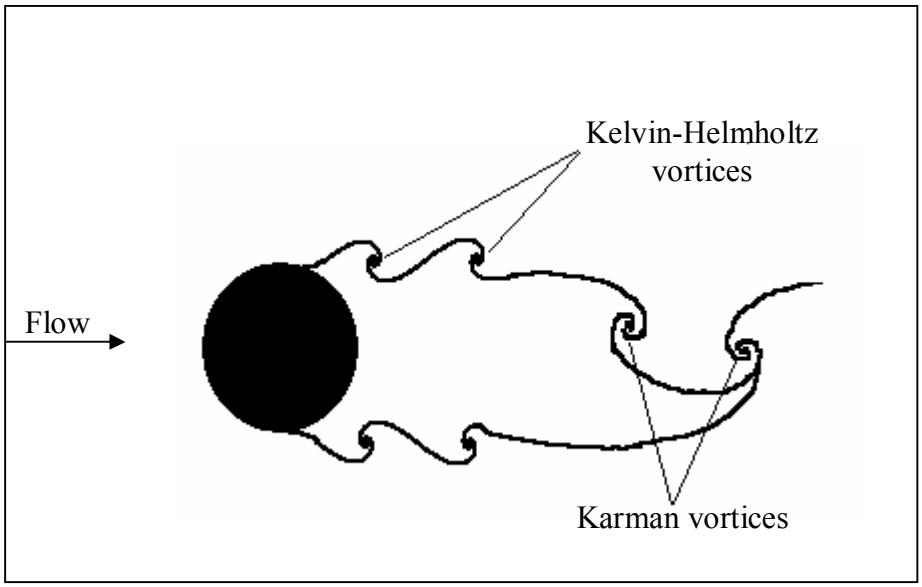

Figure 2.1. The Kelvin-Helmholtz (secondary) vortices and the Karman vortices from circular cylinder.

Gerrard (1978) claims that there is an interaction between the formation of the large-scale Karman vortices and transition waves in the Reynolds number range from 350-2000. His flow visualization photos show that in some cases the transition wave and the roll-up occur in such a fashion that the antisymmetrical formation of the large-scale Karman vortices is not altered. On the other hand, other photos suggest that the symmetrical formation of the transition waves (i.e., Kelvin-Helmholtz vortices) can actually inhibit the onset of the Karman vortices.

Wei and Smith (1986) addressed such waves, manifested in the form of discrete Kelvin-Helmholtz vortices, over the range of Reynolds number extending from Re_d=1200 to 11000 using both hydrogen-bubble flow visualization hot-wire anemometry. They pointed out that the Kelvin-Helmholtz or" secondary" vortices detected in the near wake of the cylinder are identical to the transition waves reported by Bloor (1964), because both phenomena occur immediately downstream of the separation point and appear to have similar unsteady characteristics. They

described the origin of the Kelvin-Helmholtz or secondary vortices as instability of the free shear layer separating from the surfaces of the cylinder.

Ünal and Rockwell (1988) examined the separated shear layer over the range of Reynolds number $440 \leq Re_d \leq 5040$ using combinations of hydrogen-bubble and dye injection visualization, along with hot-film measurements. They observed the onset the Kelvin-Helmholtz vortices are associated with a decrease of the formation length of the large-scale Karman vortices.

Chyu and Rockwell (1995) showed that relatively small amplitude perturbations at the fundamental frequency of the K-H instability and its subharmonics can lead either to a modulated or a phase-locked small-scale K-H instability.

As illustrated by Williamson (1996) and Chyu & Rockwell (1996), the Kelvin-Helmoholtz vortices can scale on the shear layer momentum thickness θ, and the features of this small-scale vortex formation, including the conditions for their onset, as well as their frequency and wavelength,is a function of Reynols number. Further studies carried out by Chyu and Rockwell (1995) confirmed that the formation of shear layer vortices is associated with enhanced values of Reynolds stress in the shear layer which, in turn, can influence the Reynolds number dependence of the formation length of the corresponding large-scale vortices.

2.2. Shallow Water

Investigation studies have been conducted in wind tunnels and water channels where the flow is considered deep and the aspect ratio is high. However, many turbulent shear flows exist in shallow environments.

Wolanski et al. (1984) investigated wakes flow behind Rattray Island in shallow coastal waters (figure 2.2.) The island is located in northeast Australia. Their results showed that the length of the wake in the lee of the island, as documented by aerial photographs and satellite imagine, appeared to equal that of wake behind a flat in two-dimensional flow at Reynolds number of 10.

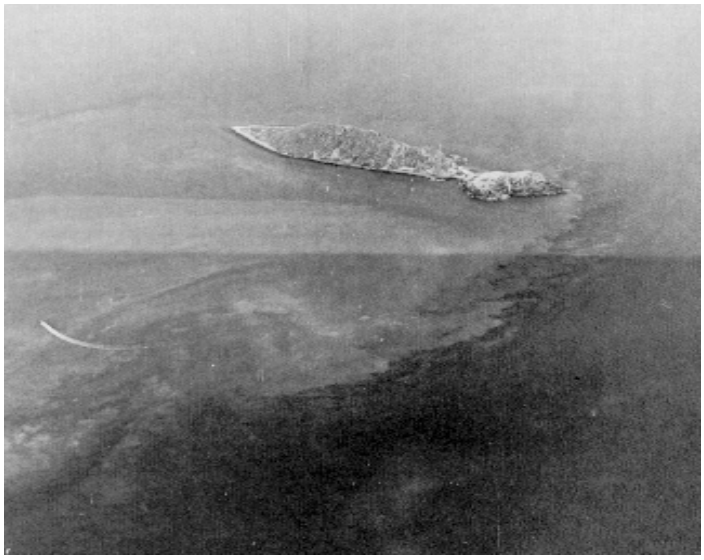

Figure 2.2. Rattray island.

Pattiaratchi et al. (1986) studied on island wakes and headland eddies in shallow coastal waters. Island wakes and headlines were identified from space borne and airborne remotely sensed imagery in the visible wavelengths. They gave some useful information for the wakes formed behind an obstacle at various Reynolds numbers and formed behind an island for various island wake parameters, P, defined by Wolanski et al. (1984).

$$P = \frac{Uh^2}{K_z D}$$

Where U = horizontal velocity of the current, h = water depth, K_z = vertical eddy viscosity coefficient and D = diameter of the island. P is based on a balance between the vorticity flux entering the eddy at the point of seperation and the vorticity flux extracted from the core region of the eddy, assuming the size of the eddy is of the order of the island width. For $P << 1$, friction dominates and potential flow results. For $P \sim 1$ a stable wake is present (as is the case with Rattray Island).When $P >> 1$, bottom frictional effects are negligible and the island wake can be expected to be similar to the flow around obstacles at large vales of Re in the laboratory, i.e. unsteady wake results.

Shear flows on the effect of bottom (bed) friction around an island were examined by ingram Ingram and Chu (1987). They observed two basic pattern of wake flow around the island. A vortex street wake was formed when transverse shear was large, as in flow around the small islands. On the other hand, for small transverse shear, as in flows around large islands, the shear layers were stabilized by bottom friction and, in that case, a clear water wake of low turbulence and low sediment concentration was observed. They made a laboratory demonstration of bottom friction influence on the turbulent wake in shallow water using shallow water table. A wake stability parameter was found for wake classification and for correlation of field and laboratory data. Their results showed that vortex street wakes were observed in nine out of 27 events when the wake was less than critical value. This result was consistent with the laboratory and numerical simulation results.

Chu et al. (1991) made a theoretical about the stability of shear flows in shallow open channels. He described a dimensionless stability number S also known as shallow wake parameter to account for the stabilizing effect of the bed friction and destabilizing effect of the transverse shear. The S parameter is $S = C_f D / h$ (denoted as "S_c") for the bluffbody. It is based on the ratio of the small-scale kinetic energy loss to the production of large-scale turbulence kinetic energy. Here, D is the diameter of cylinder, and h is the water depth and C_f is the friction coefficient.

Schar and Smith (1993) studied the global normal mode of instability for an inviscid flow as it passes an isolated topography. Their studies consisted of two parts. In the first part of their study, steady numerical solutions for flow past circular topography were obtained by imposing symmetrical conditions that essentially suppressed vortex shedding. In the second part, this symmetrical condition was relaxed in order to study the transition into vortex shedding regime. They used finite difference numerical simulations to derive the most unstable global normal mode leading to the break-up of the study wake into an oscillating Karman vortex street. The frequency of eddy shedding in their numerical simulations agreed well with that from observations of eddies behind mountainous islands.

Chen and Jirka (1995) performed experimental studies on the shallow two-dimensional turbulent wake flows on the large-scale water table. The “shallow wake “ was generated by vertical cylindrical bodies extending over the water depth. The ambient flow was characterized by two main features: one was the existence of a free surface and bottom by which the shallow water layer was bounded and the other was a fully developed turbulent boundary layer. Here, the transverse body dimension D greatly exceeds the water depth h (D/h >1). The wake Reynolds number $Re_d = U_\infty D/\nu$ was greater than 10^4, while the ambient flow Reynolds number that governs the shear flow in the transverse dimension $Re_h = U_\infty h/\nu$ was always larger than 1500. U_∞ is the depth-averaged ambient velocity and ν is the kinematic viscosity. Re_h is thus well above the transition value of about 500. Different types of bodies were investigated, including cylinders, flat plates and porous plates oriented transversely to the ambient flow. The flow patterns fell into three categories: vortex shedding, unsteady bubble and steady bubble as shown in figure 2.3 stability parameter $S = c_f D / h$ has been used to classify these three flow patterns.The friction coefficient of the water table c_f was estimated from the standart smooth-wall relation.

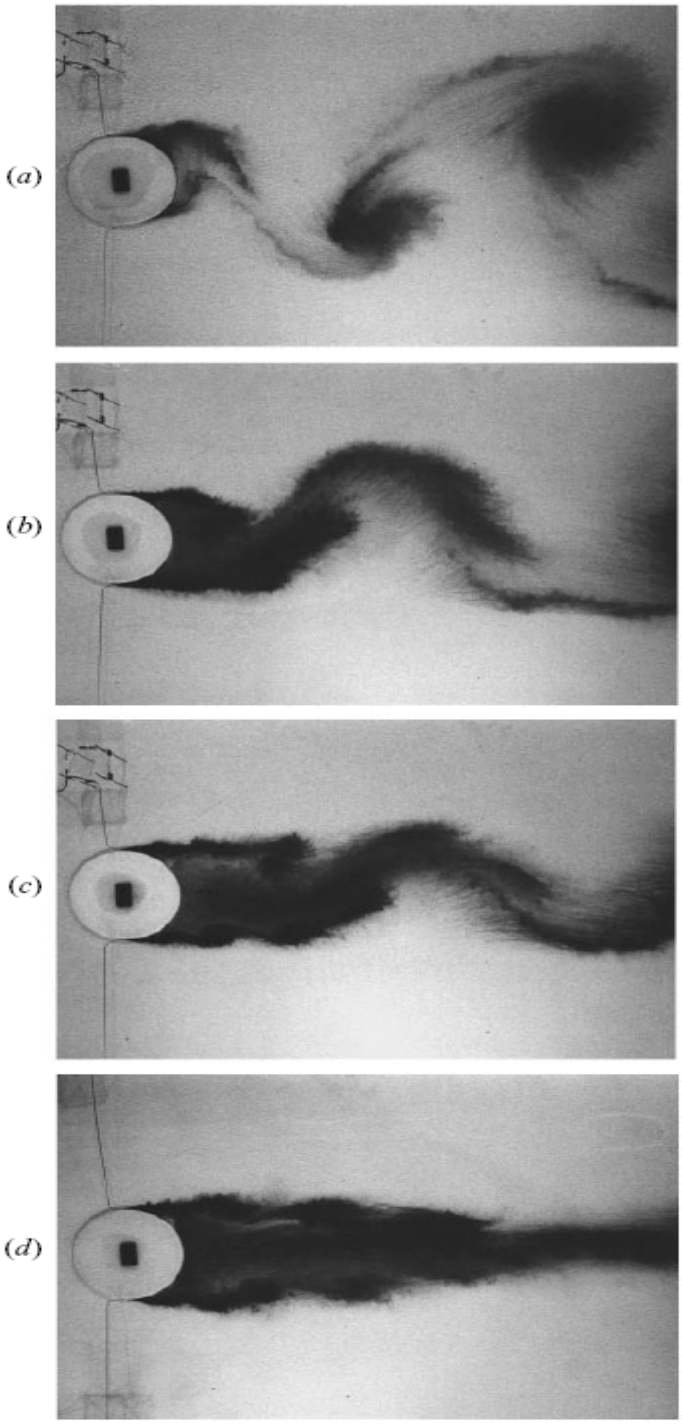

Figure 2.3. Schematic flow patterns of a shallow near wake produced by a D=62cm cylinder (adapted from figure 5 of Chen and Jirka 1995) a) vortex street pattern, S=0.19, Reh=5.900; b) unsteady bubble wake, S=0.27, Reh=3.810; c) unsteady bubble wake with weaker downsream instabilities, S=0.34, Reh=2.600 and d) steady bubble wake S=0.53, Reh=1.800.

Extensive experimental and numerical investigations were performed by Lloyd and Stansby (1997) in shallow wakes behind conical model islands with gentle slopes. Four islands were used with side shapes ranging from 8.0 to 33.1 degrees. For small values of the wake stability parameter, for example S< 0.2, the island wakes were characterized well-organized vortex shedding systems. The island side slope had a small effect on the wakes produced. With slope angles varying from 8.0 to 33.1 degrees, the basic mechanism generating the wake was found to be the same.

Chen and Jirka (1997) investigated the effect of bottom friction on absolute/convective and local/global stability characteristic of shallow wake flows by means of a linear stability analysis, and interpreted and compared it with the results of their previous experiments (1995). They also proposed critical values of S (denoted as S_c) to signify the onset of particular flow patterns.

In shallow flows, bed friction effects became very important and were quantified in terms of a friction length scale, which is usually defined as the ratio of depth of flow (h) to the skin friction coefficient (C_f). Balachandar et al. (1997) have defined a bed friction parameter ($S=C_fX/h$) as Chu et al (1991) to describe the influence of bed friction in shallow flows. Here, X is a horizontal length scale. It is clear that, the bed friction effects are expected to be minimized in deep flows.

Balachandar et al. (1999) developed a theoretical model to predict the spread of wake in shallow flows. They investigated the effects of flow depth and plate width on the spread of the wake. Some useful remarks on the wake stability parameter ($S_c=C_fD/h$) were presented therein. The range of velocities and the depths (10 mm ≤ h ≤ 80 mm) of flow considered in Balachandar et al. (1999) and Lloyd and Stansby (1997) studies are similar. However, the size of the wake generators used by Lloyd and Stansby (1997) are about 8 to 30 times larger than that used by Balachandar et al (1999). From careful visual observations and concentration measurements, it was found by Balachandar et al. (1999) that for $S_c \leq 0.008$ distinct and continuous Karman vortices were noted. For $S_c \approx 0.009$-0.018, weak and intermittent Karman vortices were observed, while the Karman vortex street was completely annihilated when $S_c \geq 0.021$. In fact, for a given velocity and cylinder of plate width, no significant difference between the nature of the Karman vortex street

and the development (or spread) of the wake was observed for h ≥ 30 mm. Based on these observations, shallow wakes were reclassified into shallow-wakes and deep-shallow wakes. Given the significant difference in the reported values of the critical wake stability parameter, an alternate measure using the wake velocity data may be more appropriate. In the study reported by Balachandar et al. (1999), only an intermittent Karman vortex street was observed at a flow depth of 20 mm in the wakes generated by a 20 mm and a 40 mm wide flat plate.

Balachandar et al. (2000) searched characteristics of shallow turbulence near wakes at low Reynolds numbers. Reynolds number based on the test body width was maintained nearly constant (Re ≈ 4.000). Velocity and the concentration in the near region of shallow turbulent wakes were measured using a LDA and video-imaging techniques. A 40 mm wide flat plate placed normal to the flow was used as a wake generator. It was concluded that the wake stability parameter pointed out earlier was not quite approximate to characterize the relative effects of transverse and bed friction. In their study, a new definition as a transverse parameter was proposed to characterize wake stability. It was reported that the wake velocity defect data collapsed fairly onto a single curve and were independent of the measurement location and depth of the flow. The wake half-width data based on the concentration profiles show a higher spread compared with the velocity data.

Tachie and Balachandar (2001) searched behaviour of the shallow turbulent wakes generated on smooth and rough surfaces. They used a flat plate as the wake generator placed normal to the flow. The wakes were generated on two types of surfaces: i) a hydraulically smooth surface (brass channel bottom) and ii) a rough surface created using wire mesh. The mesh was made of a 0.6 mm diameter wire with 7.0 mm centerline spacing. The wire was 1.8 m long and 0.45 m wide and fixed to the channel bottom by means of a double-sided tape. They measured mean and turbulence intensity to understand shallow wakes generated on smooth and rough surfaces. Using the local minimum and maximum velocity at any axial location to define velocity scale, the velocity profiles across the wake generated on smooth and rough surfaces collapsed onto a single curve. Their study indicates that for x/d ≤ 5.0 (d is the plate width), the width of the wake increases from the wake generator with

increasing axial distance, attains a maximum value at about x/d=2.0 and decreases to a minimum value at x/d=5.0. It was found that at similar Re_d the spread rate of the wake on rough surface was significantly lower than observed for a smooth surface due to a stronger bed friction effect.

Balachandar and Tachie (2001) searched the interaction between the boundary layer on a horizontal floor of a shallow open channel flow and the wake of a thin flat plate mounted vertically on the floor of a channel. They used LDA technique to measure the velocity of the flow. Measurements were obtained upstream and downstream of a smooth flat plate wake generator. They used plates are two having different aspect ratios. Their results showed that the profiles in the near wake region were quite distorted and the recovery of the boundary layer to the upstream condition was slow. They stated that the inner region appeared to develop more quickly than the outer region of the boundary layer. When compared with the approaching flow, the stream wise turbulence intensity values increased in the near wake region followed by a gradual but slow decrease with increasing axial distance.

Akıllı and Rockwell (2002) searched the near wake of a vertical, circular cylinder in shallow water using a combination of a visualization marker and particle image velocimetry technique. They located laser sheets parallel to the bed of the water channel at different heights to investigate the flow characteristics at the bed and at the various locations above it. At the bed, the time averaged streamline topology downstream of the base of the cylinder took on a form known as an owl face of the first kind, which was originally defined for a completely different exterior flow. Immediately adjacent to the base of the cylinder, an additional system of saddle points was located at either end of a nodal line. At locations above the bed, one of the two principle saddle points of the owl face of the first kind disappeared and the principle foci were transformed from a stable to an unstable state.

Kahraman et al. (2002) searched vortex formation of a vertical cylinder in shallow water and the control technique of these vortices. In order to control vortex formation behind a cylinder, a narrow transverse strip of roughness elements having different heights was placed behind the cylinder on the bottom surface channel. They employed a technique of high-image-density particle image velocimetry (PIV) to

obtain global, instantaneous representations of the flow patterns, which lead to phase- and time-averaged patterns of streamline topology, velocity, vorticity and Reynolds stress on planes above the bed.

Fu and Rockwell (2005) reported that instability of the horseshoe vortices emanating from the upstream of the vertical cylinder in shallow water flow activates the instability of the wake flow region. Fu and Rockwell (2005) studied the control of vortex formation in the near wake of shallow water flow downstream of the vertical cylinder using a base water bleed through a very narrow slot. They concluded that a water bleed through this very small gap alters the flow data in upstream and downstream of the cylinder base.

Akilli, et al. (2005), revealed that a detached splitter plate located at various stations downstream of the vertical cylinder in shallow water flow has a drastic effect on the suppression of the vortex shedding for the gap ratio between 0.0 and 1.75D.

2.3.Turbulent wakes generated by side-by-side cylinders in deep water

Biermann and Herrnstein (1933) found that the base-bleed flow downstream of two circular cylinders was bi-stable as the gap ratio was bellow 2.25. Deflection of the base-bleed flow changed the width of the wake, hence the vortex shedding frequency of the wake downstream of each bluff body in two-body arrangement.

Zdravkovich (1968) conducted a smoke visualization of laminar wake behind the three cylinders in various triangular configurations. He observed that multiple Karman vortex streets could co-exist. However, the vortices decayed very quickly and an entirely new single vortex street was formed.

Palmer and Keffer (1972) measured an asymmetric turbulent wake generated by two side-by-side of unequal diameter at different downstream distances from the cylinders. Their aim was to create and investigate the region of turbulent " energy reversal" where the turbulent kinetic energy production turns negative. However, these studies did not focus on the interaction between the individual wakes.

Andreopoulos (1972) found that the interaction between two or more gap flows leads the wake behavior to be even more complicated.

Bradshaw (1973) proposed a superposition scheme. According to their hypothesis, when two simple shear layers merged from a complex shear layer, the characteristics of the complex shear layer could be deduced from the individual simple shear layer providing the interaction effects were weak on the turbulence structures. In other words, the turbulence fields of the two simple shear layers could be superimposed to from the turbulence field of the complex shear layer. It is well known that the non-linear Navier-Stokes equations forbid the superposition of two or more turbulence fields. However, this hypothesis seemed to be quite valid for those flows that were formed by interactions of shear layers. They demonstrated that, based on the hypothesis, a fully developed duct flow could be well predicted by a calculation method by using empirical data obtained from isolated fully developed boundary layers.

Weir et al. (1981) carried out some calculations for a plane jet using the data of two mixing layers that originated at the two lips of the jet nozzle. They found that there was fairly good agreement between calculations and measurements, except for triple velocity products near centerline. The validity of the superposition hypothesis was further substantiated by the calculation of a turbulent near-wake of a flat plate using the data of the two shear layers developed on opposite sides of the plate (Andreopoulos and Bradshaw, 1980).

Fabris (1984) studied the interaction of two turbulent wakes generated by a pair of cylinders in side-by-side arrangement. The ratio was set at 8 and his measurements were carried out in the far field of the cylinder arrangements. From this brief review, it is evident that the near field interactions in the near field of simple wakes generated by individual circular cylinders and attempts to provide a reliable documentation for the Reynolds stresses and heat fluxes, which are important for developing and fine-tuning turbulence models.

Kumada et al. (1984) measured the pressure distributions and vortex shedding frequencies of the wake behind a three side-by-side circular cylinder at the Reynolds number $Re=(1.0\sim3.2)\times10^4$, He identified four typical flow regimes. When T/D was between 1.0 and 1.125, the three cylinders behaved like a single bluff body and one vortex street occurred. For T/D=1.125~1.35, both gap flows between the cylinders

deflected towards one side, thus forming narrow and wide wakes. For T/D=1.35~2.225, the two gap flows were deflected towards the free-stream, respectively. Consequently, two narrow wakes occurred behind the two outer cylinders and one wide wake behind the central one; the narrow and wide wakes are associated with high and low dominant vortex frequencies, respectively. The two outer cylinders also had large drag, compared with the central cylinder. One distinct difference of the three-cylinder flow from that of two cylinders was that the gap flow was generally quasi-stable, unless near T/D=2.225 where the gap flow deflection might change its direction. For T/D=2.225~3.75, three separate vortex streets were observed. The flow behind three side-by-side plates behaved quite similarly.

Williamson (1985) visualized a laminar wake with a Reynolds number ($R_e=U_\infty D / \nu$) of 100-200 behind a pair of side-by-side cylinders in the range from T/D=1.85 to 4.0. Here, U_∞ is the free-stream velocity, D is the diameter of the cylinders, ν is the fluid kinematic viscosity and T is the distance between the cylinder axes. He noted that, as a result of interaction, the wakes of the two cylinders could amalgamate to form a single wake. On the other hand, quantitative data on simple wake interactions is scare. He came to the conclusion that low-frequency vortex shedding occurred as a result of narrow wake. He also reported the first visualization of quasi-stable behavior for a two-cylinder array for T/D = 2.0 and $50 \leq Re \leq 200$. Streamline topology of the flow shows a relatively narrow and short wake behind one of the cylinders and a relatively wide and long wake behind the other cylinder. Because, the size and shape of the wakes remain stable, this flow behavior is taken to correspond to quasi-stable behavior.

Cheng and Moretti (1988) reported the mean velocity and turbulent intensity profiles, measured by Pitot tubes, Kiel probes and hot-wires, up to 4.5d downstream of a single tube row with a T/D =1.3.

Wei and Chang (1999) studied turbulence effect on the interaction of wake and base-bleed flow downstream of two circular cylinders arranged side-by-side. They found that free stream turbulence had an effect of changing the relation between the

gap ratio and the wake behavior. However, the biasing characteristic of the gap flow was not substantially affected by free stream turbulence.

Guillaume and LaRue (1999) observed for the Reynolds number of 2500, three quasi-stable modes for T/D=1.338~1.730, one quasi-stable mode with forced flopping for T/D=1.730~1.850, and only one quasi-stable mode for T/D=1.850~2.202.

Sumner et al. (1999) investigated the flow in the ranges of T/D=0~5 and Re=500-3000, and then identified three basic wake patterns that were insensitive to the Reynolds number: single bluff-body vortex shedding at small gap spacings ($0 \leq T/D < 0.2$), biased flow with synchronized vortex shedding at intermediate spacings ($0.2 \leq T/D < 1.2$), and symmetric flow with synchronized vortex shedding at larger spacings ($1.2 \leq T/D < 3.5$).

Zhou et al. (2000) measured the velocity and temperature the velocity and temperature fluctuations at Re=1800 in the two- and three-cylinder case. They observed that the cross-stream distributions of the Reynolds stresses and heat flux varied significantly, which were ascribed to different flow patterns, as T/d reduced from 3.0 to 1.5.

Sumner et al. (2000) measured the flow patterns of two cylinders in a staggered arrangement. They observed nine flow patterns and found that vortex shedding frequencies were more properly associated with individual shear layers rather than with cylinders.

2.4.Flopping Regime

Bearman and Wadcock (1973) are the first scientists to study quasi-stable behavior and flopping for a two-cylinder array as a function of cylinder spacing. Their specific goal was to locate the critical spacing where the wakes downstream of the two cylinders stopped behaving as individual cylinder wakes and combined to form a single wake. They showed that, when dimensionless distance (T/D) between cylinder centers was greater than 5 or equal to 5, the cylinder wakes did not interact until after a significant distance downstream. The cylinders had to nearly be touching

for a single wake to be formed. In the intermediate range of spacing ($1.1 \leq T/D \leq 2.0$) and at a Reynolds number of 2.5×10^4, they found that either quasi-stable behavior or flopping could be induced by stopping and starting the wind tunnel. Thus, they observed forced flopping, not spontaneous flopping. They further found that each mode generated peaks at different frequencies in the velocity power spectra, and therefore each mode had different and multiple Strouhal numbers. In addition, they reported quasi-stable behavior in the flow downstream of two parallel flat plates for $1.1 \leq T/D \leq 3.0$ at $Re = 4.4\times10^4$ where d was the thickness of the plate in the direction normal to the flow.

Ishigai and Nishikawa (1975) also observed quasi-stable behavior for five-cylinder arrays. They found quasi-stable behavior when the five cylinders were aligned in a plane normal to the flow with $0.2 \leq T/D \leq 1.5$, over a Reynolds number range of 3.3×10^4~4.0×10^4. They did not observe forced or spontaneous flopping. They argued that the different average C_p values of the various cylinders were a result of Coanda effect, which deflected the wakes.

Zdravkovich (1977) reviewed both the Ishigai and Nishikawa (1975) and Bearman and Wadcock's (1973) studies. Zdravkovich stated that, in order for forced or spontaneous flopping to be a result of the Coanda effect, flopping must be related to the movement of the separation point on the cylinders. However, since the separation positions on plates were not affected by the Coanda effect, Bearman and Wadcock (1973) showed flopping with an array of two-flat plates, quasi-stable behavior could not be explained by the Coanda effect.

Kiya et al. (1980) for the cases of $1.4 \leq T/D \leq 2.0$ and $Re = 1.58 \times 10^4$, found flopping when the plane of a two-cylinder array was aligned perpendicular to the flow. When the array was ten or more degrees out of alignment, no flopping was found. They did not explicitly state whether the flopping was forced or spontaneous.

Eastop and Turner (1982) observed the flow behavior downstream of a three-cylinder array with $2.2 \leq T/D \leq 3.6$ and $4.5\times10^4 \leq Re \leq 1.11\times10^5$ placed normal and parallel to the free stream flow. Pressure distributions on the cylinders and

downstream of the center cylinder were presented. They only observed quasi-stable behavior when T/D = 2.375. Neither spontaneous nor forced flopping was observed.

The first visulation of quasi-stable behaviour for a two cylinder array is reported By Williamson (1985) for s/d=1.0 and $50 \leq Re \leq 200$. His streakline photograps show a relatively narrow and short wake behind one of the cylinder. Because the size and shape of the wakes remain stable, this flow behavior is taken to correspond to quasi-stable behavior.

Kim and Durbin (1988) also studied flopping behaviour behind two side-by-side arranged circular cylinders. For their study, T/D ratio was varied between 1.1 and 2 and the Reynolds number was varied between 2.2×10^3 and 6.2×10^3. Only spontaneous flopping was observed. They presented the first statistical analysis of the time interval for each period that the average C_p value remained relatively high combined with the time for each period that the average C_p value remained relatively low. Specifically, for a Reynolds number of 200, they estimated that the average time interval between flops would be on the order of hours. As pointed out by Kim and Durbin (1988), this may explain why Williamson (1985) did not observe spontaneous flopping.

Zdravkovich and Stonebanks (1990) observed quasi-stable and forced flopping with seven- and eleven-cylinder arrays with $2.1 \leq T/D \leq 2.75$ and $3.7\times10^4 \leq Re \leq 7.4\times10^4$. The forced flopping they produced by increasing the velocity rapidly from the rest stopped after 10-20 min. Pressure distributions and velocity power spectra are presented.

Le Gal et al. (1990) performed studies using two cylinder having gaps between $1 \leq T/D \leq 7.5$ and Re=110 and found wake interaction at ratio as high as 5.5. Probably because of their low Reynolds number value, they stated that flopping was really difficult to observe. However, they did observe quasi-stable behavior and perform a flow visualization study, which was in agreement with the large-wake, small-wake model of Williamson (1985).

Mizushima and Takemoto (1996) numerically solve and experimentally visualize the flow pattern downstream or an array of square bars. For $1.2 \leq s/d \leq 2.6$ (d

in this case is the length of a side) and 80≤ Re ≤320, flow visualization shows that at specific Reynolds number and s/d combinations, both spontaneous flopping and quasi-stable bahavior can exist downstream of the array.

Peschard and Le Gal (1996) observed with flow visualization and numerically modeled the interaction of wakes downstream of a two-cylinder array with 2≤ T /D ≤ 7 and 90≤ Re ≤ 150. Although they successfully model quasi-stable behavior, no spontaneous or forced flopping was observed.

Akıllı, Akar and Karakus (2004) searched the flow around two and three side-by-side circular cylinders of equal diameter in shallow water using the Particle Image Velocimetry (PIV) technique, over a transverse gap ratio in the range of G/D = 1.3-3.0 with an increment of 0.25. For two side-by-side cylinder case, it was found that the flow structure behind the cylinders is asymmetrical at small gap ratios as a result of jet-like flow between the cylinders. The jet-like flow tends to deflect toward the narrow wake region that has higher vortex shedding frequency.In the case of three cylinders, both an asymmetrical flow structure at small gap ratio (G/D = 1.25) and a symmetrical flow structure at intermediate gap ratios (1.5≤G/D≤2.0) were observed. Bistable wake regions were obtained for the asymmetrical cases. The Reynold stress ($u^{'} v^{'}$) downsteam of the upper cylinder was significantly attenuated for G/D = 1.25 where the jet-like flow is more effective for both two and three circular cylinder arrangements.

3. MATERIAL and METHOD

3.1.Experimental Arrangement

3.1.1 Water Channel System

Experiments were performed in a large-scale water channel located in the Fluid Mechanics Laboratory at Çukurova University,TURKEY,shown in Figure 3.1. The water channel test section was constructed of transparent plexiglass with upstream and downstream fiberglass reservoirs,Which have the following dimensions : a length of 8000 mm, width of 1000 mm, and a depth of 750 mm. A honeycomb screen system is located at the entrance of the contraction.These reservoirs and honeycomb screen arrangements are used to maintain the turbulence intensity below 0.5 %. An axial flow pump controlled the water flow speed,Which provide reliable test flow speeds.

Figure 3.1. Picture of the water channel

3.1.2. Experimental Model

An overview of the experimental system is given in Figure 3.2. The water level were (H) maintained at the depth of 10mm, 20mm and 40mm.The value of Reynolds number based on the cylinder diameter was Re = 5000.

During the experiments the cylinders used was made of plexiglas material and Its diameter was D:40mm.The experiments were conducted in the water tunnel examined two cylinder confiqurations with T/D varied from 1.25 to 1.75 ,depth of water 20 mm. And varied from 1.25 to 1.5 ,depth of water 10mm, 40mm and also three cylinders configurations with T/D = 1.25 to 1.5 depth of water 10mm, 20 mm and 40mm with the spacing incremented by 0.25 in each case.All experiment were included 3000 instantaneous images.

The flow was illuminated with a double pulsed system consisting of two Nd: Yag pulsed laser sources of a wavelength of 532nm, each with a maximum energy output of 120 mJ. The optimal thickness of the laser sheet in the field of view was generated by combination of spherical and cylindrical lenses.The flow was seeded with 12 μm, metallic-coated hollow plastic spheres. The movement of the particles was recorded by using a CCD camera with a resolution of 1024x 1024 pixels.The camera was equipped with a 55 mm focal-length lens. Dantec flow grabber digital PIV software employing frame-to-frame cross-correlation technique was employed to calculate the raw displacement vector field from the particle image velocity data.

The different laser sheet orientations were used. For the plan view, the laser sheet was located parallel to the bed of the water channel at heights.

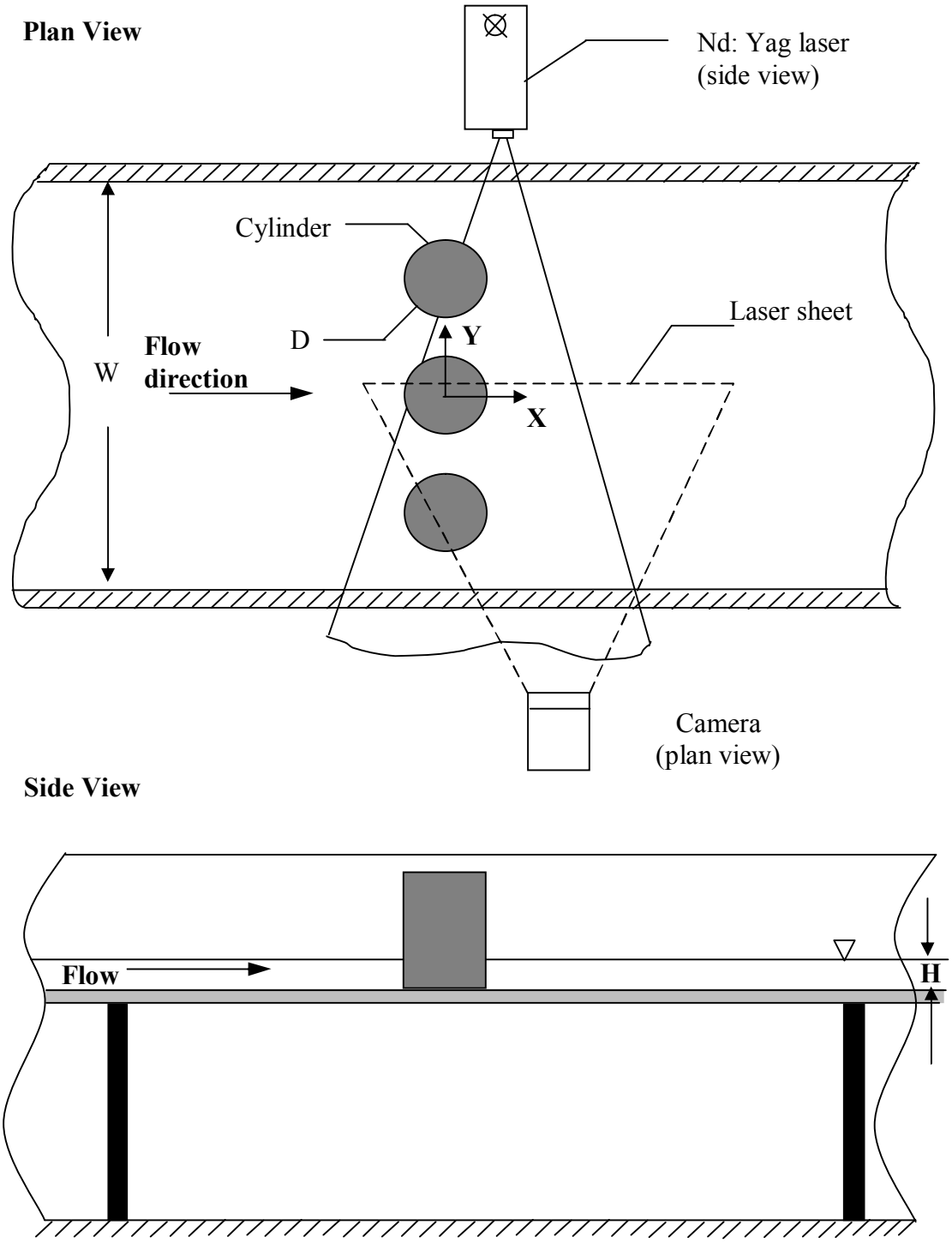

Figure 3.2. Overview of a vertical cylinder in shallow water.

3.2. Measurement Techniques

3.2.1. Particle Imaging Techniques

Local measurements of the velocity field (i.e., individual points) are now measured using Hot-Wire (HW) and Laser Doppler Velocimetry (LDV). However, many flow fields such as coherent structures in shear flows flows or wake flows,are highly unsteady.HW or LDV data of such flows are difficult to interpret,as both spatial and temporal information of the entire flow field are required,and these methods are commanly limited to simultaneous measurement at only a few spatial locations.Particle Image Velocimetry (PIV) technique can measure the velocity of entire 2-D or 3-D flow fields instantaneously, without disturbing the flow and thereby reveal the quantitative, global structure of an unsteady turbulent flow field.

Figure 3.3 briefly explains a typical set up for PIV recording. Particle Image Velocimetry (PIV) is determined the velocities at many points in a fluid flow is a non-instrusive measurement technique. The technique involves seeding the flow field, illuminating the region under investigation and capturing two images of that region in rapid succession. From the displacement of the tracer particles, provided that the time interval between image captures is known, a velocity vector map can be calculated in the flow field.

The theory of PIV was introduced by Adrian (1988) in the late 1980s with the first experimental implementations following shortly afterwards (Kean et al. 1990 and Kean et al. 1991). At the stage, due to hardware limitations, a single photographic frame was multiply exposed and analysed using an auto-correlation technique. However, improved speed of photographic recording soon allowed images to be captured on separate frames for analysis by cross-correlation (Kean et al. 1992). The introduction of digital camera technology to PIV enabled the direct recording of particle images (Willert et al. 1991), at the expense of reduced resolution, resulting in the development of digital PIV (DPIV)(Westerweel, 1997). As well as these hardware advances, many new algorithms have been developed in the last decade, increasing the accuracy and speed of PIV analysis.

The technique of PIV can be considered as consisting of two stages; image acqustion and image evaluation (Figure 3.4). The general principle of PIV is to illuminate tracer particles in the flow field of interest with a plane sheet of light, and acquire two images of the flow field with a known time separation. When a digital CCD camera is used for image acquisition, one uses the acronym DPIV. The displacement field is determined from the motion of the tracer particles between the two images, and by dividing this with the known time separation one obtains the velocity field. The problem in PIV is to determine the displacement field. The time separation is assumed to be known with sufficient accuracy.

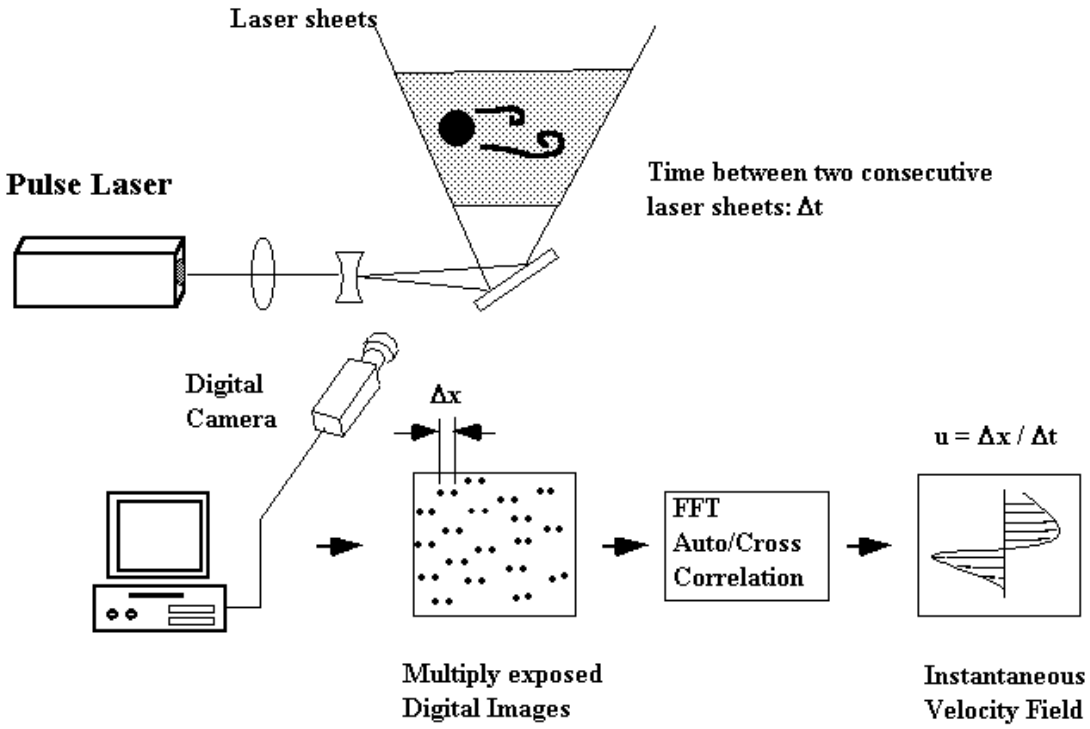

Figure 3.3. A typical PIV experimental set-up

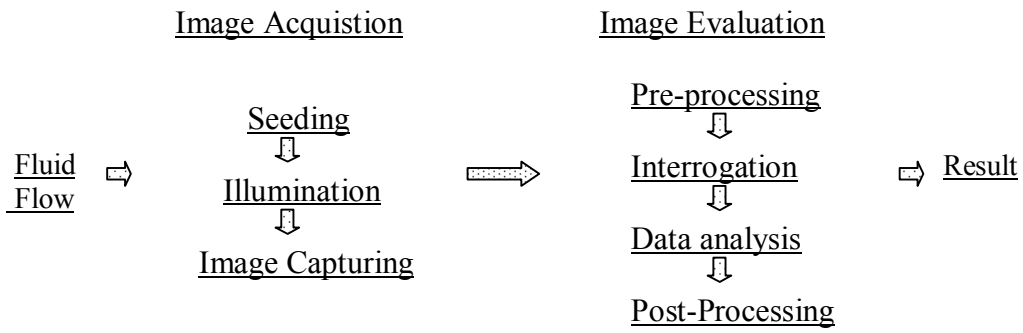

Figure 3.4. General PIV process

3.2.2. Image Acquisition

Tracer particles are added to flow under investigation.These are illuminated by laser sheet and images of the illuminated flow field are captured and stored for later analysis. Figure 3.5. Shows a typical experimental arrangement for carrying out PIV measurements.

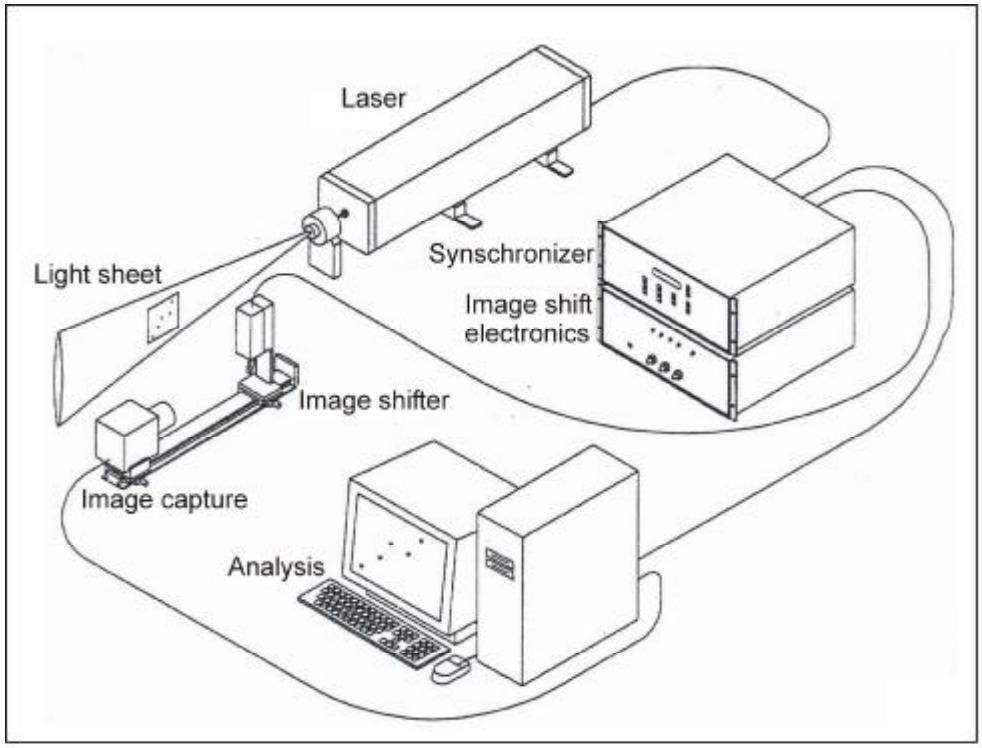

Figure 3.5. Schematic of experimental apparatus and digital PIV instrumentation

3.2.2.1. Seeding

The application of optical flow measurement techniques to gas and liquid flows usually requires artifical seeding of the flow. Tracer particles must have different extra features to fulfill different requirements.Based on the optical configuration and the overall conditions. If the selection of the seeding material is right, the results can be as wanted.

Factors that have to be considered are:

- Flow medium (air/water)
- Volume to be seeded
- Flow velocity
- Light scattering
- Particle image size
- Safety considerations (ingestion, risk of explosion)
- Cost

Recording both light pulses in the same image frame to track to movements of the particles gives a clear visual sense of the flow structure.İn air flows, the seeeding particles are typically oil drops in the range 1 μm to 5 μm. For water applications, the seeding is typically polystyrene, polyamide or hollow glass spheres in the range 5 μm to 100 μm. Any particle that follows the flow satisfactorily and scatters enough light to be captured by the CCD camera can be used.The number of particles in the flow is important to obtain a good signal peak in the cross-correlation.As a rule of thumb,10 to 25 particles should be seen in each interrogation area.

3.2.2.2. Illumination

For applications is gas flows a high power light source for illumination is required in order that the light scattered by the tiny tracer particles will expose the photographic film or the video sensor. However, the need to utilize larger particles because of their better light scattering efficiency is in contradiction to the demand to

have as small particles as possible in order that they follow the flow faithfully. In most applications a compromise has to be found. In liquid flows larger particles can usually be accepted which scatter much more light. Thus, light sources of considerably lower peak power can be used here.

In order to efficiently illuminate the seeding particles a high intensity light source,normally a laser, must be used.To study the flow in 2-dimensions, a combination of different lenses is used to generate a thin sheet of high intensity light from the source beam.(Raffel,M.Willert,C.,Kompenhans,J.,)

For the illumination, it is preferable to use a laser, since the laser beam is easy to form into a sheet by a cylindrical lens. A pulsed laser is to prefer, since one obtains a high light energy during a very short time interval (typically 5 ns for a YAG-laser), which means that the particle images will be practically frozen even for high velocities (> 100 m/s). The repetition rate of a YAG-laser is typically 10-30 Hz, which is too low except for very low velocities (< 1 cm/s). One therefore needs two lasers to get full freedom in terms of time separation between the pulses. Special PIV YAG-lasers are available that combine two laser cavities with a common beam outlet.

3.2.2.3. Image Capturing

To be able to acquire two single exposed images with a time separation of the order of microseconds, one uses a so-called full-frame interline transfer progressive scan CCD camera, also called a cross-correlation CCD-camera. The basic idea is that the image exposed by the first laser pulse is transferred very rapidly to light-hidden areas on the CCD-chip. This is done on a pixel-by-pixel basis, i.e. each pixel has its own storage site in immediate vicinity of the light sensitive pixel area. After the second exposure, both images are transferred to the computer. Since a lot of data has to be transferred, it is only possible to take a few double-images per second. The temporal resolution of the flow is thus in general very poor with this technique.

Seeding of the flow with tracer particles is a very important issue for obtaining accurate PIV measurements. The particles should be as small as possible, but on the

other hand they may not be too small.Because then very small particles will produce too weak images and will not scatter enough light.

3.2.3. Image Evaluation

Since the introduction of the first PIV image evaluation methods, alternative analysis algorithms have been developed as well as error correction and post-processing procedures designed to improve speed and accuracy of the PIV method. However, the classical PIV analysis method is still the most frequently used and forms the basis of many other algorithms. (Figure3.6).

a)

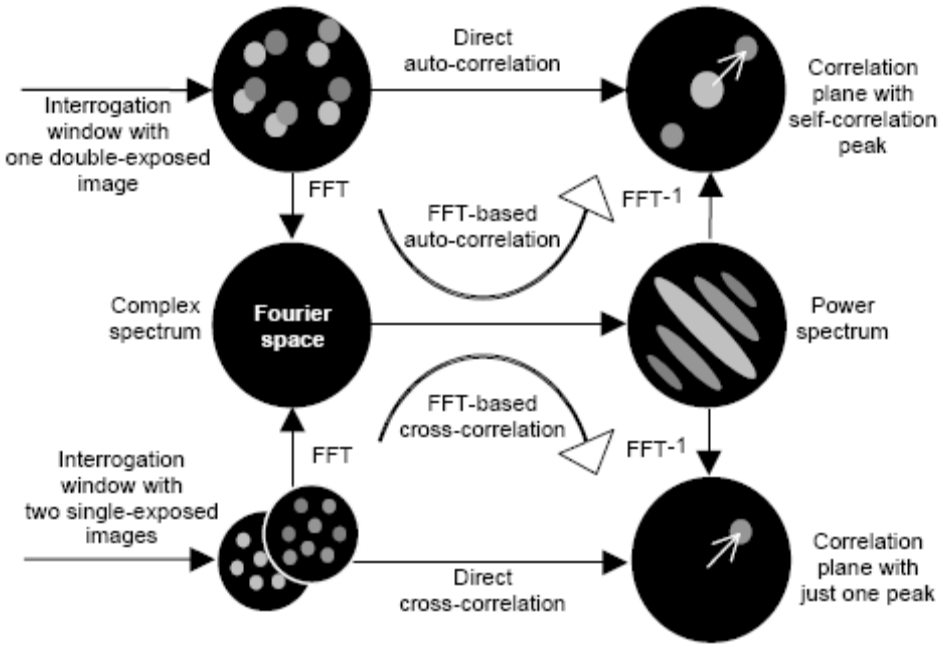

b)

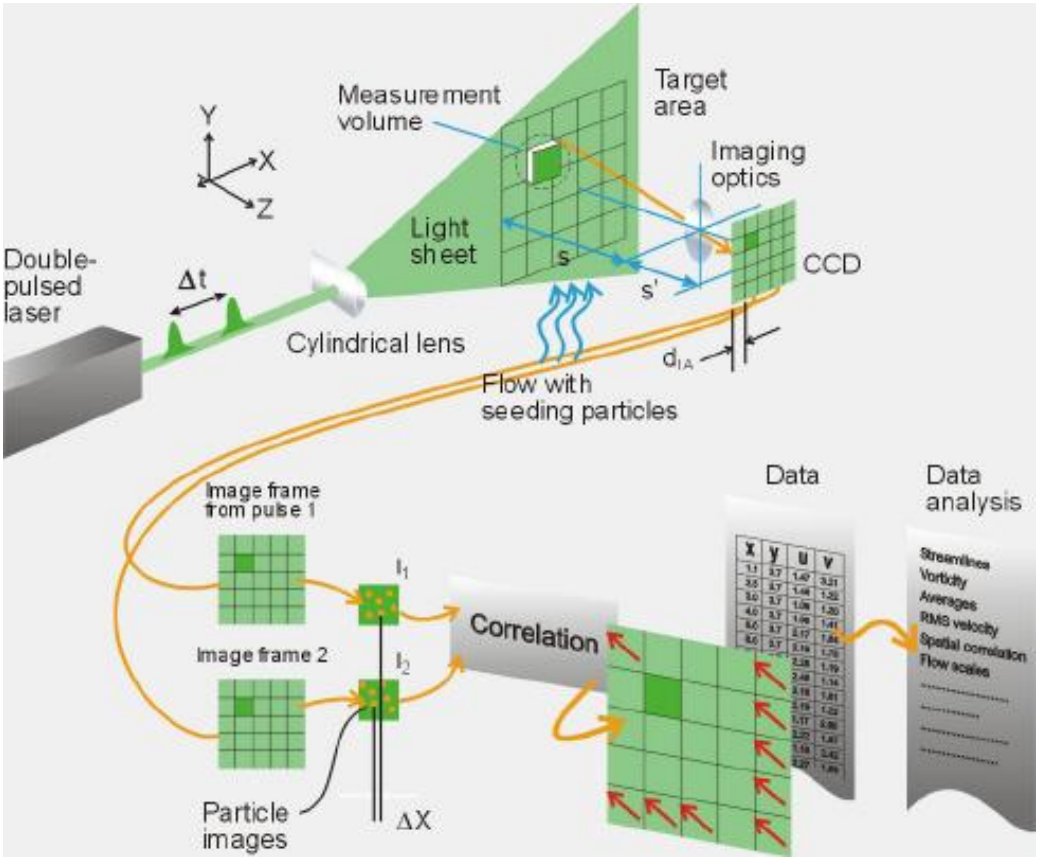

Figure 3.6. Basic PIV analysis process

The heart of the PIV analysis is the correlation of regions of the input images (known as interrogation areas) with each other to determine the displacement vector of the flow in that part. Knowing the time interval between the image captures enables a velocity vector to be calculated from the displacement vector. The correlation technique can be used for a single frame multiply exposed (auto-correlation) or multiple frames singly exposed (cross-correlation). To speed up the convolution process, correlation of each pair of interrogation areas is carried out in Fourier space. After interrogating the images in this way and generating the vector map, post-processing is carried out to validate the data and to improve the vector map resolution and accuracy. Using this vector map, vorticity and Reynolds stress contours and streamline topology can be obtained.

3.3. Cross-Correaltion Process

Particle Image Velocimetry processing basically determines the distance that the particles have moved in the time between laser illuminations in photographic based or laser pulses in digital PIV. The most common methods to determine this distance are particle tracking or correlation. Here, correlation method which can be auto-correlation, one-frame cross-correlation and two-frame correlation will be explained briefly. The differences in these correlation techniques are the image window areas for the first and second images. In the auto-correlation, the same image window is used for both first and second images window. In the one-frame cross-correlation, the second image window is offset in the flow direction from the first image on the same window. The processing of the one-frame cross-correlation depends on the amount of overlap between the first and second image windows. In two-frame cross-correlation, the first image window located on the first frame and the second image window is located on the second frame. Both interrogation windows in time delay have the same coordinate.

The correlation field shows the dominant distance between each particle and every other particle within the interrogation spot. The maximum intensity spot, which represent the correlation of each particle image itself, is located in the center. A second peak, called the positive displacement peak that correspond to the dominant particle spacing. The auto-correlation function is symmetrical so that each displacement peak has a peak of equal size in the opposite direction. One peak represents the distance between the first and second particle images forward velocity, the other is distance between the second and first particle images in the reserve velocity. If there are no negative velocities in the flow field, image shifting by means of an oscillating bias mirror is used to resolve the directional ambiguity in based the photographic PIV.

The main advantages of the cross-correlation approach over the auto-correlation are:

- The displacement is obtained without any directional ambiguity

- The correlation peak signal carries more signal strength, and thus is more immune to noise

The main disadvantages of the cross-correlation approach are:

- The computation is more expensive in time, as three two-dimensional Fourier transforms are required instead of two for the auto-correlation
- The image acquisition system (camera) must cope with the necessity of acquiring two images frames in quick succession in synchronization with the laser illumination pulses and register the frame position with respect to the flow with absolute precision.

In this study, cross-correlation technique was used to determine the distance when particle move in the period of a specified time of two laser illuminations.

3.4. Image Post-Processing

Images were received from CCD camera (See Figure 3.7) that has resolution 1008 pixels × 1016 pixels at a rate of 15 frames per second. The time delay changes from 2 ms and 3 ms between frames. Digital image was analyzed using FLOWMAP software. The image was recorded on a CDD array. A Frame Grabber in the computer read the camera image from CCD camera and stored it as the digital image file format (TIFF) in the RAM. This digital image was processed and analyzed using the FLOWMAP software. During each continuous run, a total 200 images were taken. In order to determine the velocity field, a cross- correlation technique, with 32×32-interrogation window, was employed, with an overlap of % 50. The magnification factor of lens was 1:19.022.

Figure 3.7. Picture of CCD camera

The resulting vector field obtained from FLOWMAP software and corresponding boundaries of objects were then viewed using program V3 (Kahraman, 2002) to determine incorrect vectors from interrogation. These type of vectors can result when an incorrect particle correlation is made near boundaries or within shadow regions, when the particle images are too widely spaced for interrogation window side specified, pr the power of laser sheet is poor (Kahraman, 2002).

Vector validation software called CLEANVEC was used to remove incorrect vectors. The software CLEANVEC contains four statistical filters designed for incorrect vectors removal:

- Absolute Range Filter
- RMS Tolerance Filter
- Magnitude Difference Filter
- Quality Filter

Three of these four filters were used for the purposes of eliminating incorrect vectors. Here the Quality Filter requires a correlated data, which are supposed to be done by interrogation and this data, was not provided by this software.

In the Absolute Range Filter, all u and v velocity components that lie outside of given range were removed. With this filtering method, one can identify a moving reference frame in order to save real vectors that are numerically specified and eliminated incorrect vectors on the main frame. Although very trivial, this filter

might be very useful in removing the most tedious incorrect vectors, and hence improves the performance of the other filtering tools.

The RMS Tolerance Filter removes incorrect vectors those lay outside of given range. This filter must be applied to a velocity field in a reference frame moving with the mean velocity components in both directions, since it is involved with the fluctuating components only.The detailed procedures of post processing handled in this research are summerized in Figüre 3.8.

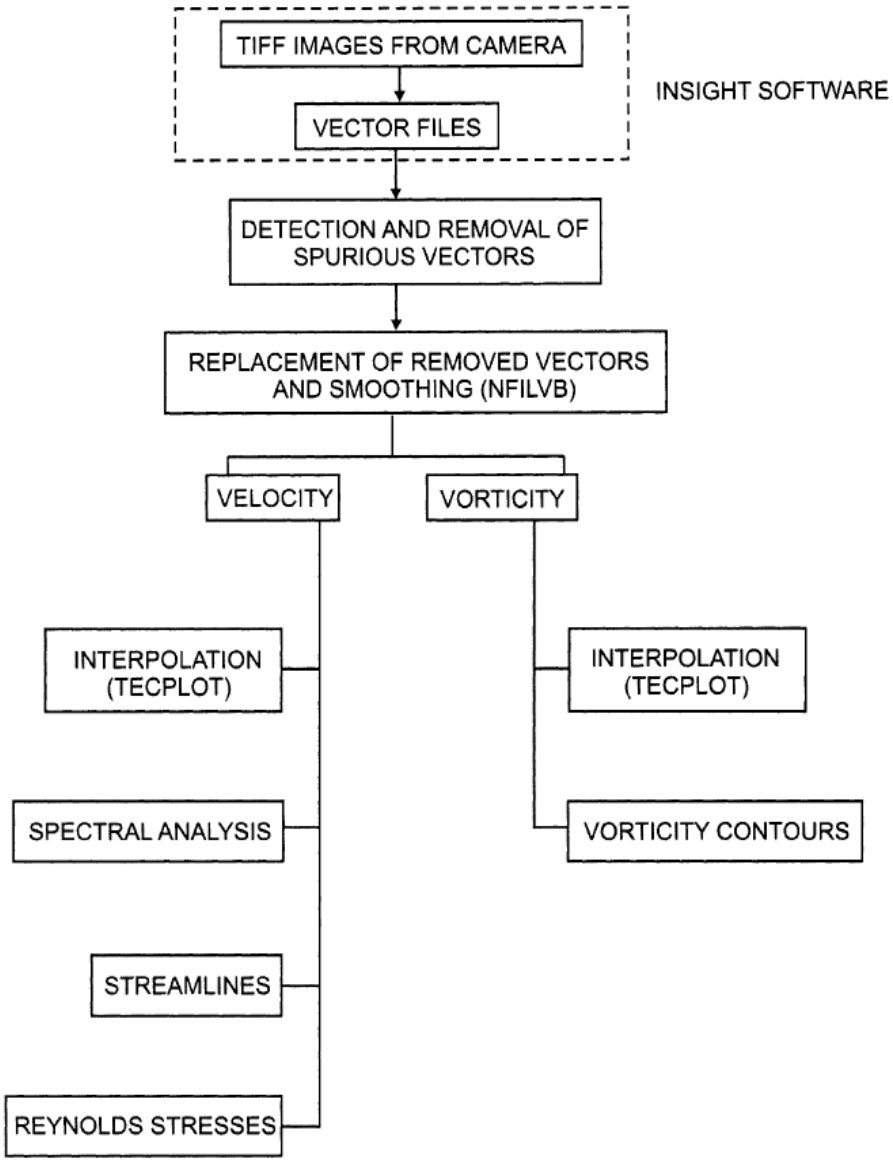

Figure 3.8. Summary of post processing

Finally, the Magnitude Difference tool removes unnecessary vectors based on the difference in magnitude between a vector and its neighborhood median. This is the local-median test defined by Westerweel (1994). This filter is the most effective among the available filters, as indicate by Westerweel (1994). However, it should be handled carefully, because it may lead to an excessive vector in a certain type of flows.

4. RESULTS AND DISCUSSION

4.1. Two and Three Circular Cylinders at Pitch Ratios (T/D), from 1.25 to 1.5 and (H/D), from 0.25 to 1.0

Figure 4.1. shows time-averaged velocity vector field, streamline topology and corresponding vorticity contours for two side-by-side cylinder case. For the vorticity contours, solid lines represent positive vorticity (counter clockwise) layers and dashed lines show negative vorticity (clockwise) layers. In the first row, the gap between cylinders is equal to 10mm, which corresponds to T/D=1.25 and the height of the shallow water is 10mm, which corresponds to H/D=0.25. The second row depicts the flow characteristics for T/D=1.5 and H/D=0.25 case.

Time-averaged flow characteristics were obtained from averaging 3000 images which were acquired at 2 Hz frequency. Namely, two images were taken in one second an done set of experiment takes approximately 25 minutes. The free stream velocity is uniform and equal to 133 mm/sec. Velocity vector field demonstrates two separate wake regions downstream of each cylinder. Time-averaged flow characteristics show similar behavior for both gap ratios. Symmetrical flow structures were obtained downstream of two cylinders. However, wake region of the cylinder placed right hand side extends longer distance in free stream direction for T/D=1.5 case. This flow structure could also be seen from the streamline topology. Saddle point for the right side cylinder was obtained further downstream location compared to the saddle point of left side cylinder. Streamline topology shows clearly that four foci which were located in the wake region of the cylinders and two saddle points were observed downstream of the cylinders. However, streamline topology of T/D=1.25 case shows an interesting structure, such that, tow foci points were located in the wake region and other two foci were located downstream of the wake region. This kind of flow structure is probably obtained due to the flopping regime of the flow or water height. In terms of vorticity contours, vorticity layers placed outside of the cylinder elongate in free stream direction and have bigger magnitude compared to inner side vorticity layers. Moreover, outer

vorticity layers do not orientate towards the wake region, but extends streamwise direction. Vorticity layers very close to the gap between cylinders orientate towards the outer vorticity layers. When, gap ratio is increased from T/D=1.25 to T/D=1.5, inner vorticity layers elongates slightly in streamwise and spanwise direction. Velocity vector fields also show the jet-like flow between two cylinders.

Even though, symmetrical flow structures were obtained from the averaging of instantaneous flow field, flow visualizations showed that an unsteady flow occurred downstream of the cylinders. This unsteadiness occurs due to the flopping behavior of the flow downstream of the cylinders. Instantaneous velocity vector field and other flow data indicate the flopping; the wake behind each cylinder alternates between a wide wake and a narrow wake, clearly. The flow does not remain deflected towards the same cylinder at all times. Sometimes, deflection occurs towards the one cylinder and sometimes to other cylinder without changing any parameter that could affect the flow structure.

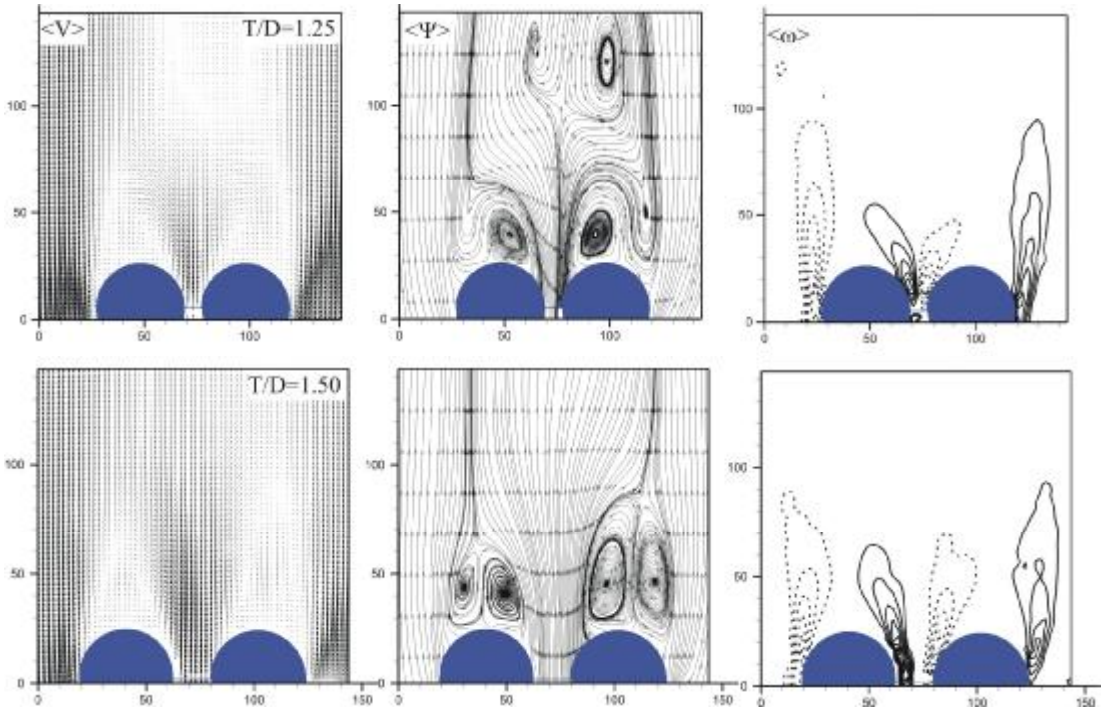

Figure 4.1. Average velocity vector field, vorticity contours and corresponding streamline topology for two side-by-side cylinders, H/D=0.25; T/D=1.25; T/D=1.50

Figure 4.2. shows the flow characteristics such as time-averaged velocity vector field, streamline topology and corresponding vorticity contours for various gap ratios, T/D=1.25, 1.5 and 1.75 at H/D=0.5 case. Again, symmetrical flow structures were observed in these cases similar to H/D=0.25 case. However, the elongation of the vorticity layers is bigger for H/D=0.5 case compared to H/D=0.25 case. At T/D=1.75 it seams that both cylinder wakes do not affected from each other.

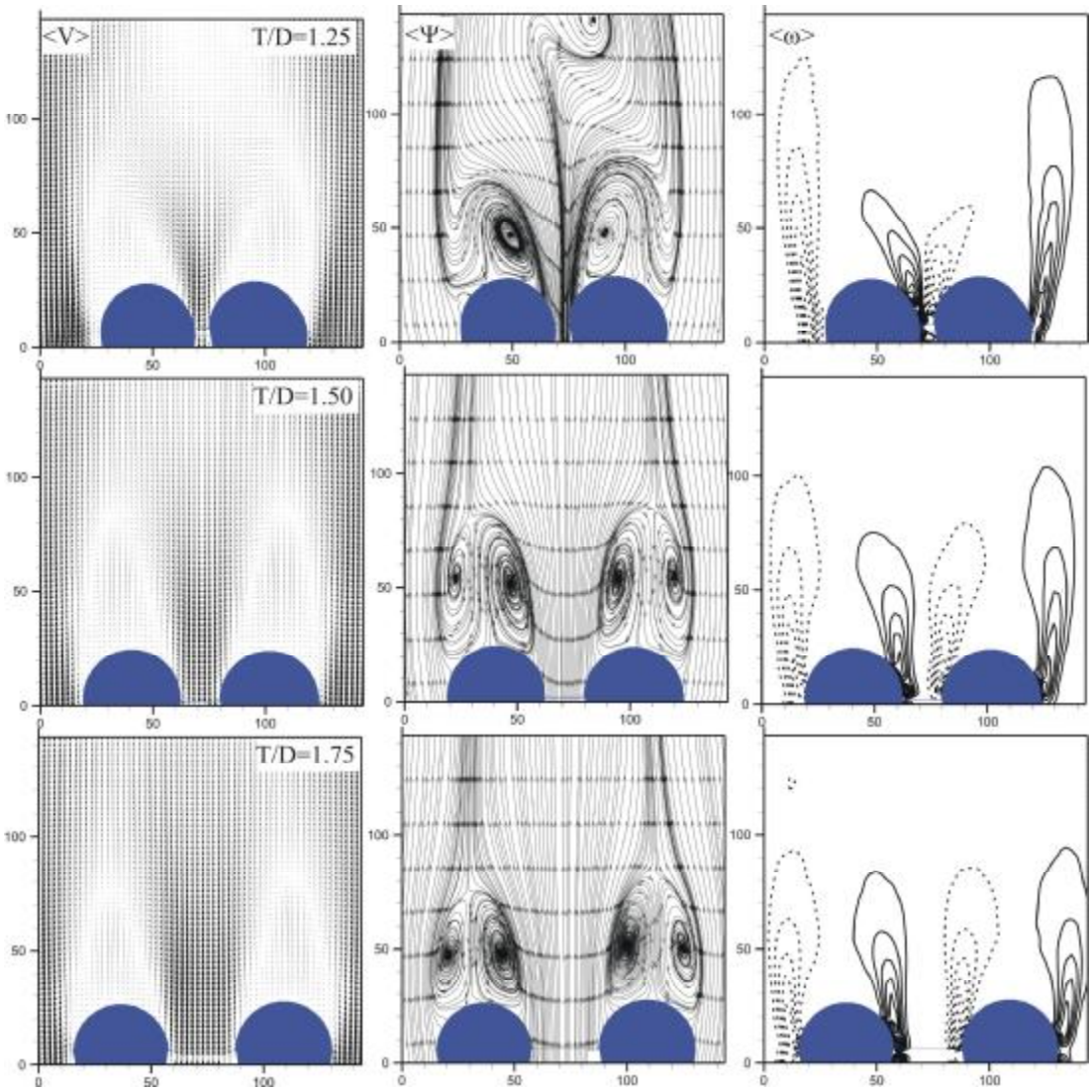

Figure 4.2. Average velocity vector field, vorticity contours and corresponding streamline topology for two side-by-side cylinders, H/D=0.50; T/D=1.25; T/D=1.50; T/D=1.75

Figure 4.3. demonstrates time-averaged velocity vector field, streamline topology and corresponding vorticity contours for T/D=1.25 and 1.5 at H/D=1.0 case. Flow characteristics at this water height were slightly different from other two water height cases. Unsymmetrical flow structures were obtained at this water height. One of the wake regions is wider and it deflects towards the narrow wake region.

Four foci points were obtained for T/D=1.25 and three foci were obtained for T/D=1.5 case.

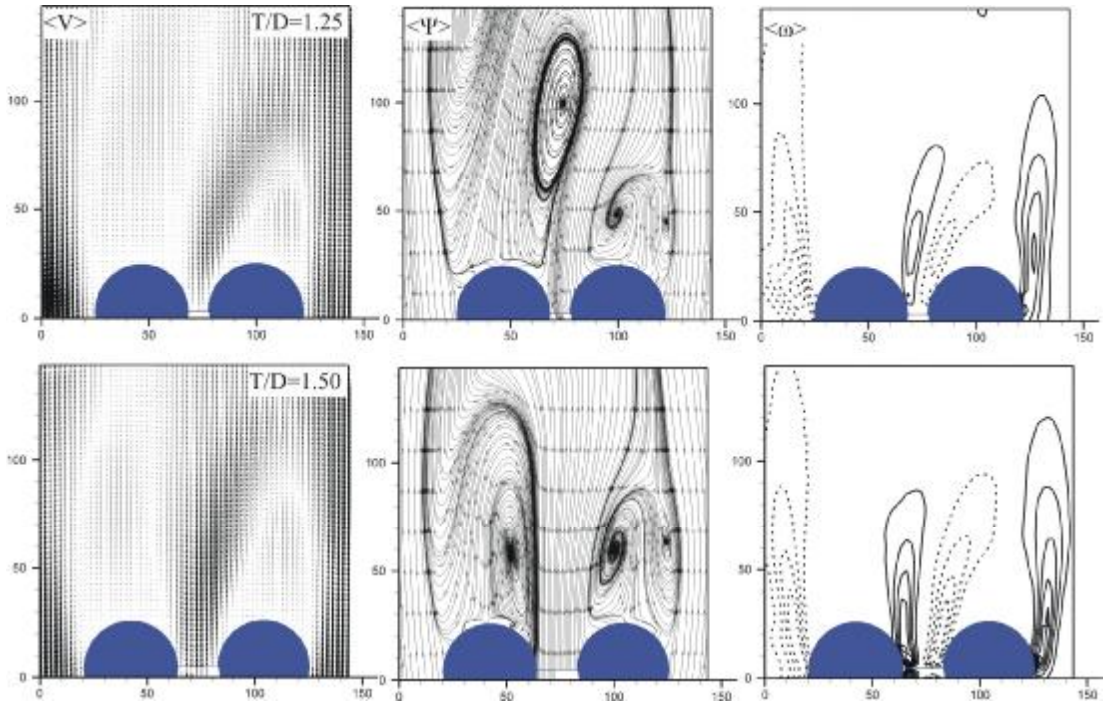

Figure 4.3 Average velocity vector field, vorticity contours and corresponding streamline topology for two side-by-side cylinders, H/D=1.00; T/D=1.25; T/D=1.50

Figure 4.4. shows the time-averaged velocity vector field, streamline topology and corresponding vorticity contours for the case of three side-by-side circular cylinders. Here, the water height is H/D=0.25 and gap ratios are T/D=1.25 and 1.5. Similar results are obtained for both gap ratios. A narrow wake downstream of the center cylinder and two wide wakes downstream of side cylinders were obtained. Almost a symmetrical flow structure is observed.

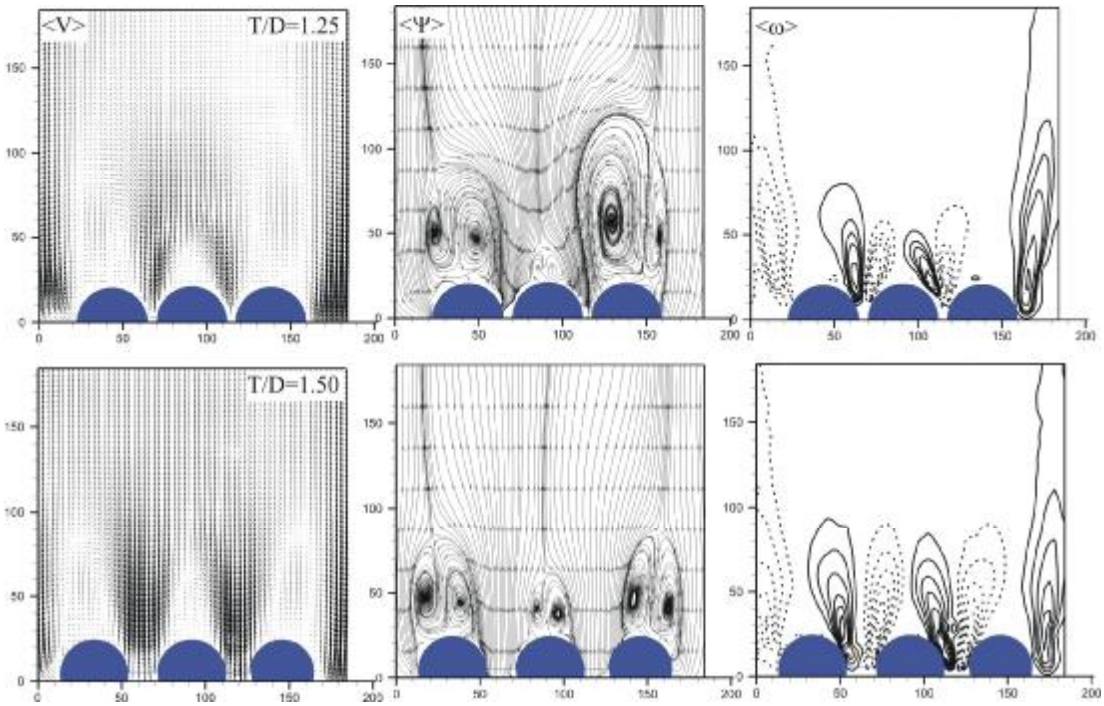

Figure 4.4. Average velocity vector field, vorticity contours and corresponding streamline topology for three side-by-side cylinders, H/D=0.25; T/D=1.25; T/D=1.50

Figure 4.5. indicates time-averaged velocity vector field, streamline topology and corresponding vorticity contours downstream of three side-by-side cylinders for H/D=0.5 and T/D=1.25 and 1.5. Two large wake region and one very narrow wake region is evident from both velocity vector field and streamline topology for T/D=1.25 case. Streamline topology also shows unsymmetrical flow structure downstream of the cylinder. However, flow structure is symmetrical for T/D=1.5 case. The wake region of central cylinder is wider for this case compared to T/D=1.25 case.

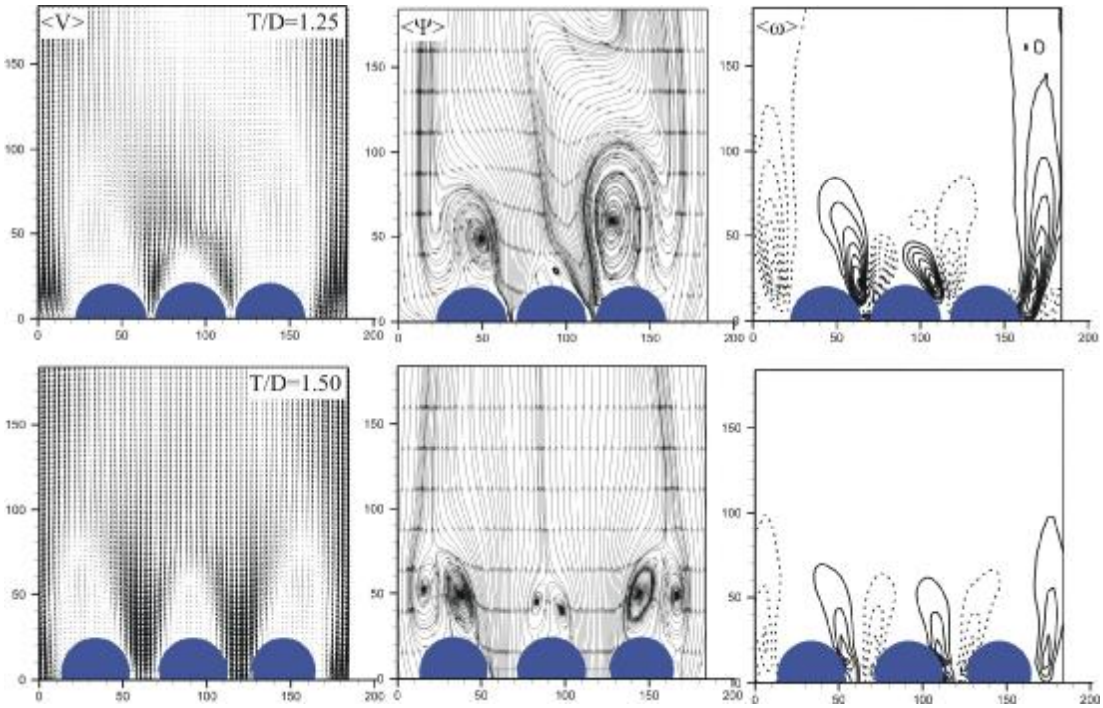

Figure 4.5. Average velocity vector field, vorticity contours and corresponding streamline topology for three side-by-side cylinders, H/D=0.50; T/D=1.25; T/D=1.50

Figure 4.6. shows time-averaged velocity vector field, streamline topology and corresponding vorticity contours for three side-by-side cylinder at H/D=1.0 and T/D=1.25 and 1.5. For T/D=1.25 case similar velocity vector field is obtained as found other water height cases. However, velocity vector field for T/D=1.5 case is remarkably different compared to other water height cases. A very wide wake is obtained downstream of the cylinder and narrow wakes are obtained downstream of side cylinders. Jet like flow could be clearly seen from velocity vector field. Streamline topology also shows this wide wake region with two foci far away from base of the cylinders.

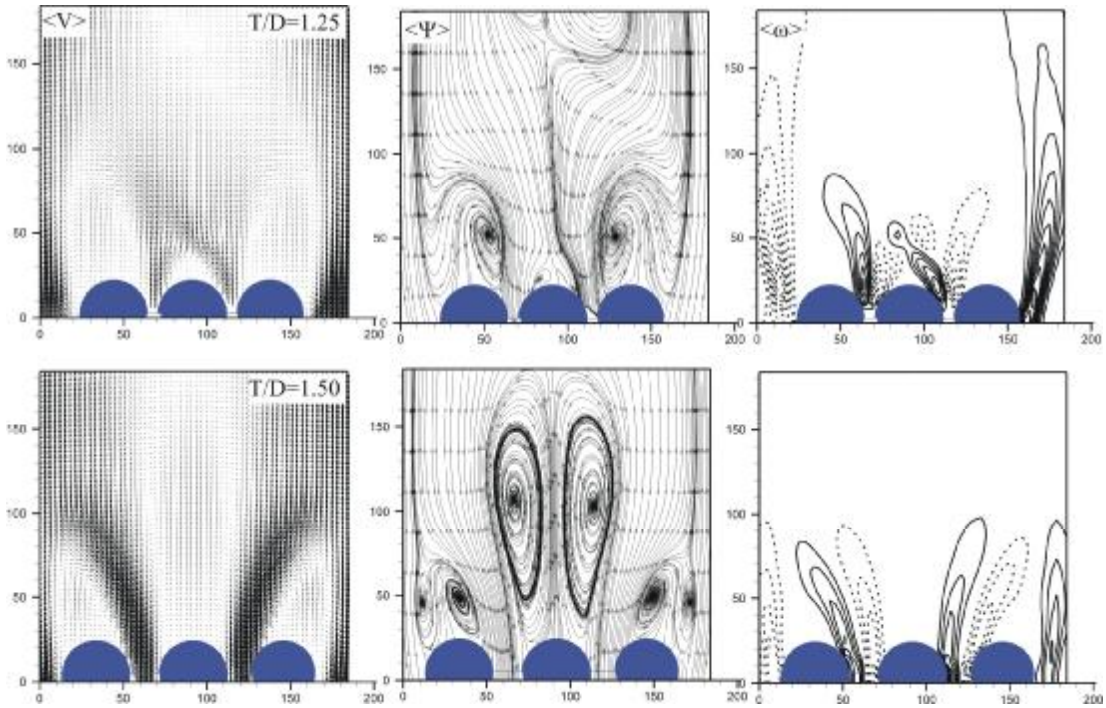

Figure 4.6. Average velocity vector field, vorticity contours and corresponding streamline topology for three side-by-side cylinders, H/D=1.00; T/D=1.25; T/D=1.50

4.2.Two Side-by-Side Circular Cylinders with H/D=0.25 and T/D=1.25

Figure 4.7. and 4.8. indicates simultaneous time histories of streamwise velocity component, u, behind two side-by-side circular cylinders for H/D=0.25 and T/D=1.25. Streamwise velocities were taken at point having coordinates of (61.56mm, 66.61mm). Flopping occurs 44 times during 720 seconds. Some of the flopping regimes are shown in figure 7. The term “right dominant” seen in figure 7 means that the wake region downstream of the right cylinder is wider and dominant compared to left one. The flopping times are easily obtained from these graphs. For example, first flopping occurs at t=10.5 and the second one occurs at t=35. The length of time between transitions appears to be random. Figure 4.9. also indicates time history of streamwise velocity component at points (87.01, 66.61) respectively for two side-by-side cylinders at H/D=0.25 and T/D=1.25. Transitions could also be seen from these two figures clearly.

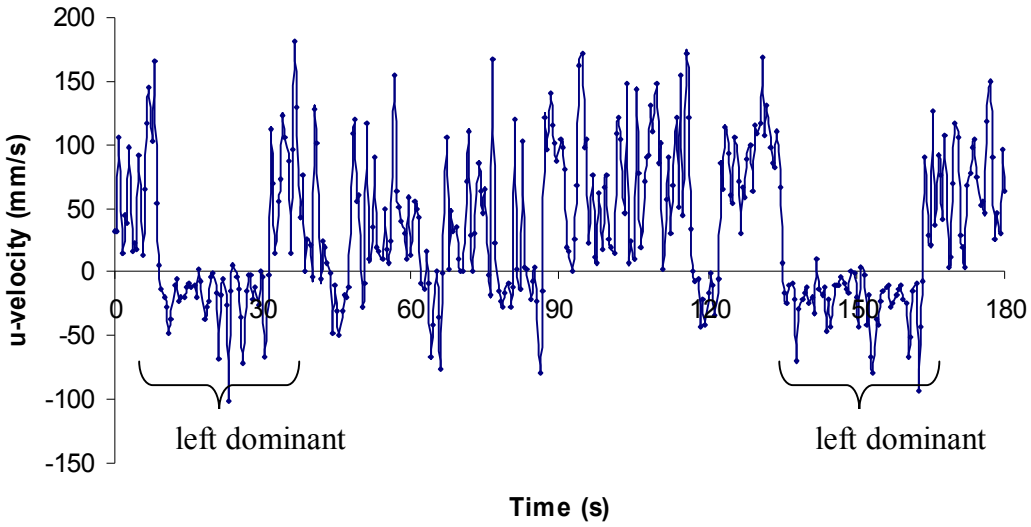
200
150
100
50
0
-50
-100
-150
0
30
60
90
120
150
180
u-velocity (mm/s)
left dominant
left dominant
Time (s)

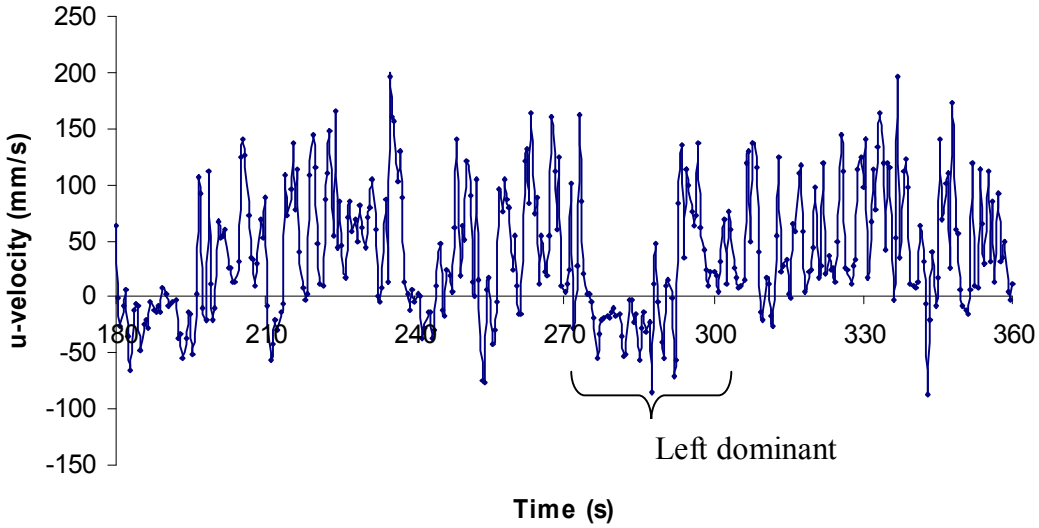
250
200
150
100
50
0
-50
-100
-150
180
210
240
270
300
330
360
u-velocity (mm/s)
Left dominant
Time (s)

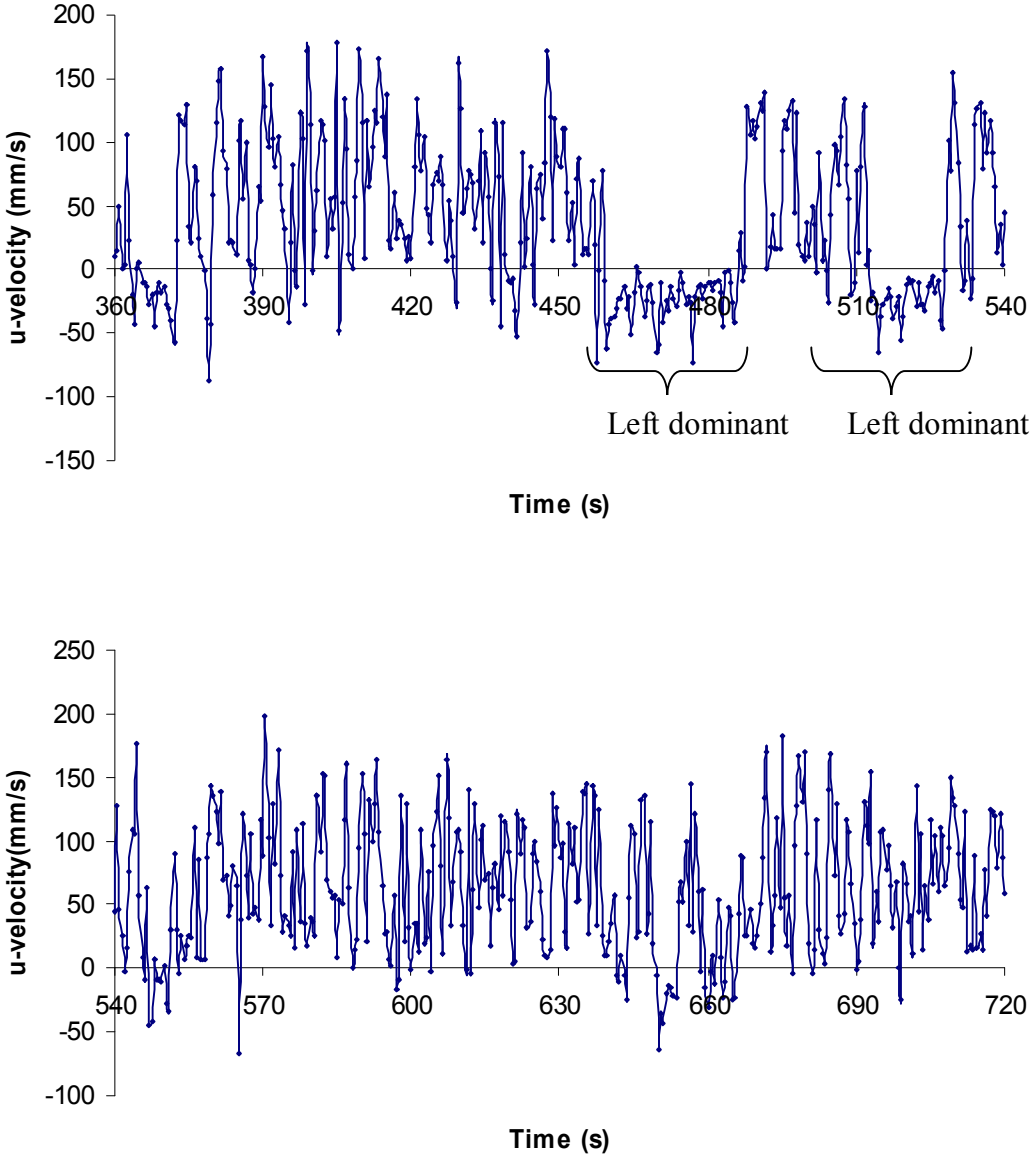

Figure 4.7 Instantaneous stream-wise velocity component for two side-by-side cylinders at x : 61.56mm, y : 66.61mm for H/D = 0.25, T/D = 1.25

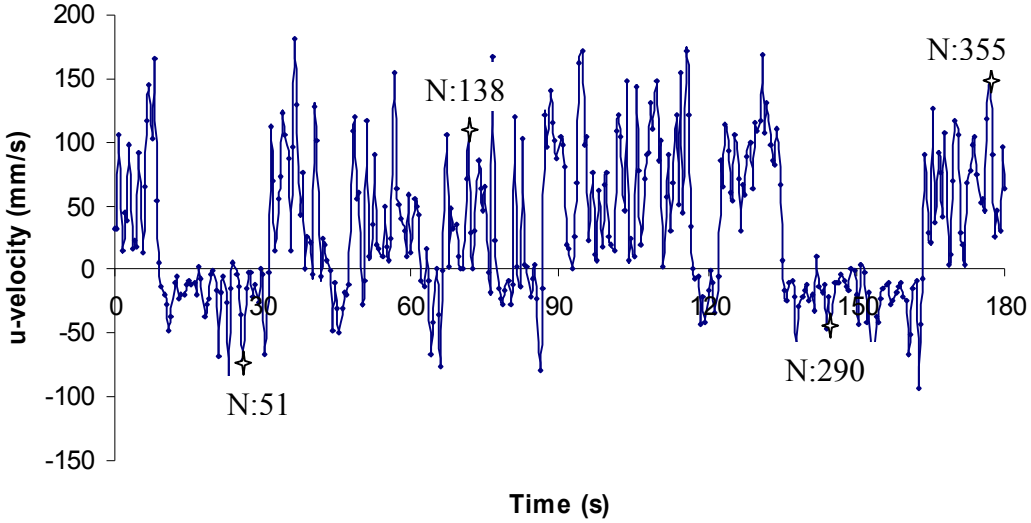
200
150
100
50
0
-50
-100
-150
u-velocity (mm/s)
0
30
60
90
120
150
180
Time (s)
N:51
N:138
N:290
N:355

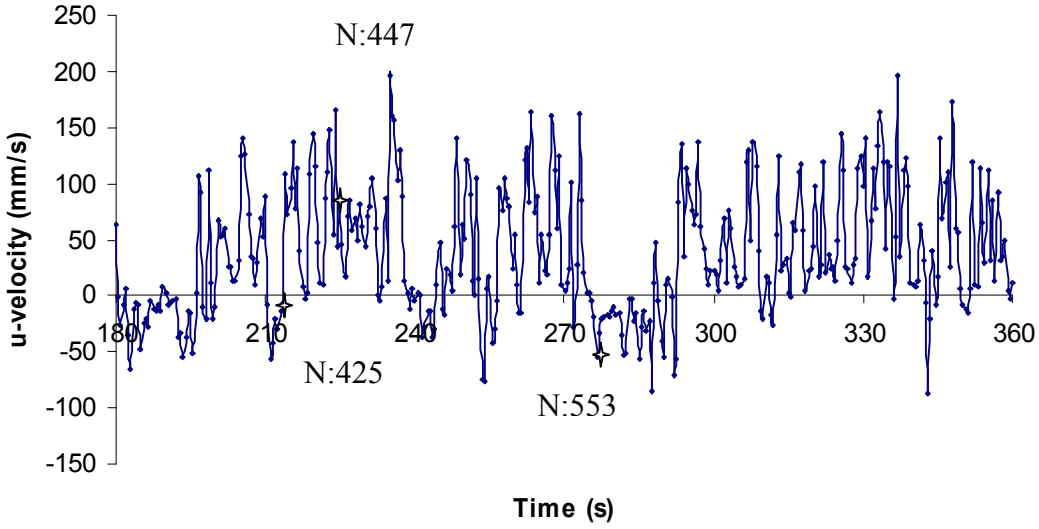
250
200
150
100
50
0
-50
-100
-150
u-velocity (mm/s)
180
210
240
270
300
330
360
Time (s)
N:425
N:447
N:553

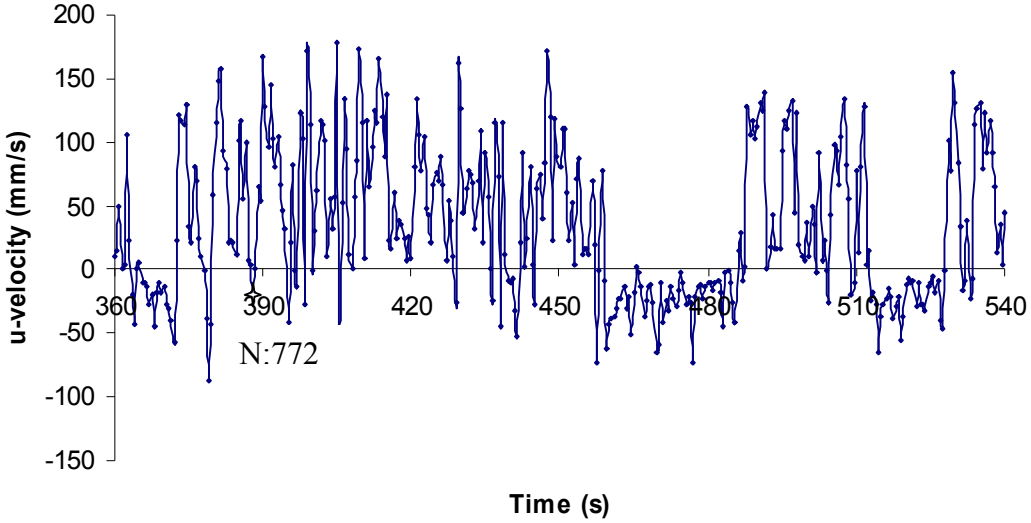

Figure 4.8 Instantaneous stream-wise velocity component for two side-by-side cylinders at x : 61.56mm, y : 66.61mm for H/D = 0.25, T/D = 1.25

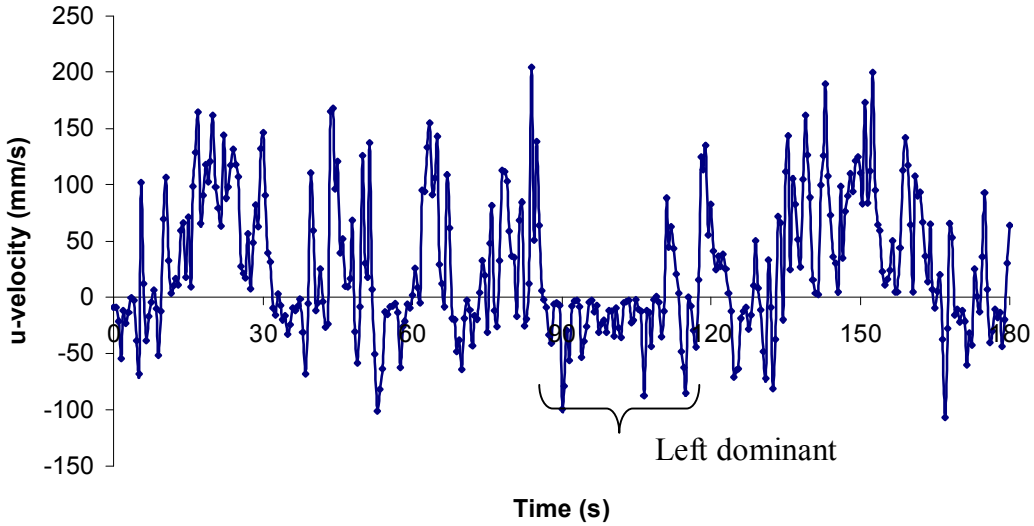

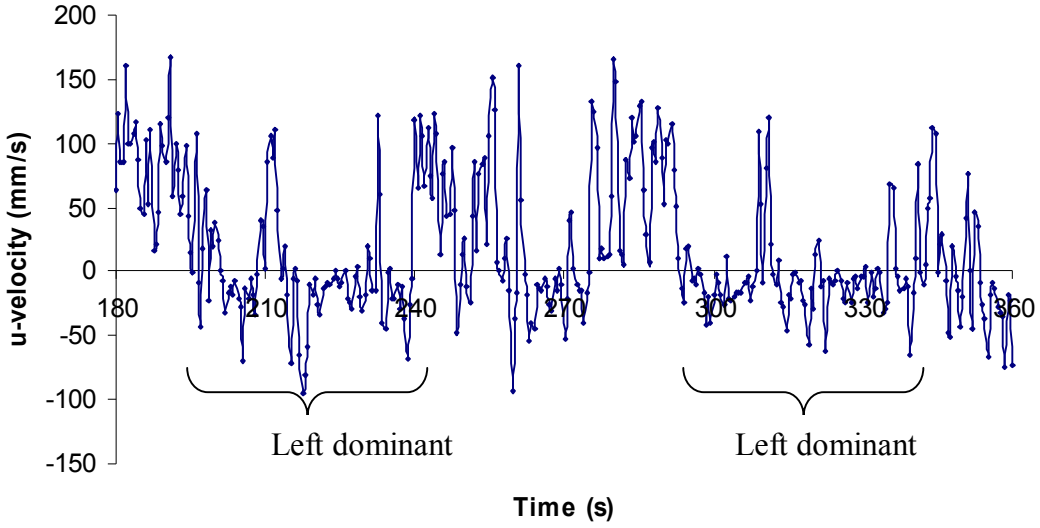
200
150
100
50
0
-50
-100
-150
u-velocity (mm/s)
180
210
240
270
300
330
360
Left dominant
Left dominant
Time (s)

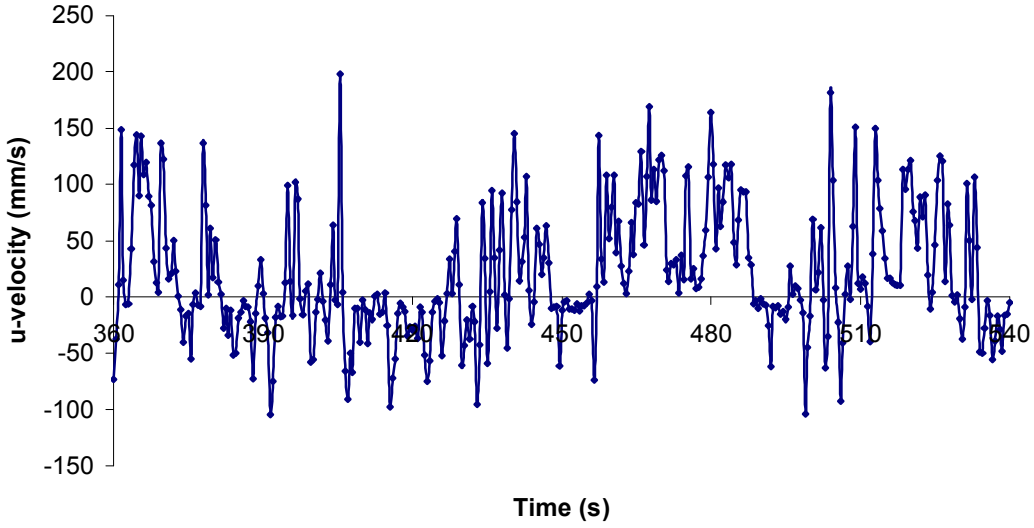
250
200
150
100
50
0
-50
-100
-150
u-velocity (mm/s)
360
390
420
450
480
510
540
Time (s)

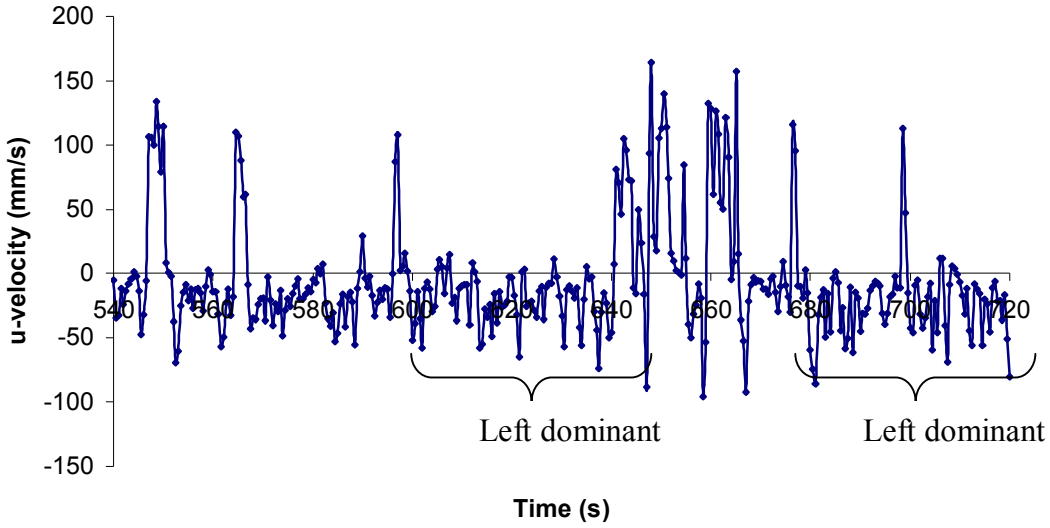

Figure 4.9. Instantaneous stream-wise velocity component for two side-by-side cylinders at x : 87.01mm, y : 66.61mm for H/D = 0.25, T/D = 1.25

Figure 4.10. shows eight different instantaneous velocity vector fields, streamline topologies and corresponding vorticity contours downstream of two side-by-side circular cylinders at various times and regimes at H/D=0.25 and T/D=1.25 case. Here, N shows the image number. The first image shows the flow characteristics at t=25.5 second (N=51) and it is clear from velocity vector field that the wake region of left cylinder is wider and deflected towards the narrow wake region of the right cylinder. The length of the narrow wake region in streamwise direction is approximately 1.2 cylinder diameter from the base of the cylinder. This value sometimes decreases to one cylinder diameter. Deflection of the wake region is also seen from the corresponding vorticity layers. Inner vortices deflect towards the wake region of right cylinder. Jet-like flow region between the two cylinders separate wake regions from each other. Deflection angle of jet-like flow is approximately 45 degrees from the free stream direction. The second image of figure 10 indicates the instantaneous flow characteristics at t=69 second (N=138). This time flopping occurs and wide wake region moves to the right cylinder and the wake region of left cylinder gets smaller. The deflection angle of jet-like flow between cylinders is

approximately the same. As can be seen from figure 4.10, the switching process occurs at different times. Streamline topologies in figure 4.10 also indicates that larger circulation regions occur in the wide wake region. At least three foci points could be seen from instantaneous streamline topology clearly. Besides these, elongated vorticity layers were evident at the outer sides of the cylinders. The magnitude of the vorticity layers in the wake regions close to the base of both cylinders is negligibly small.

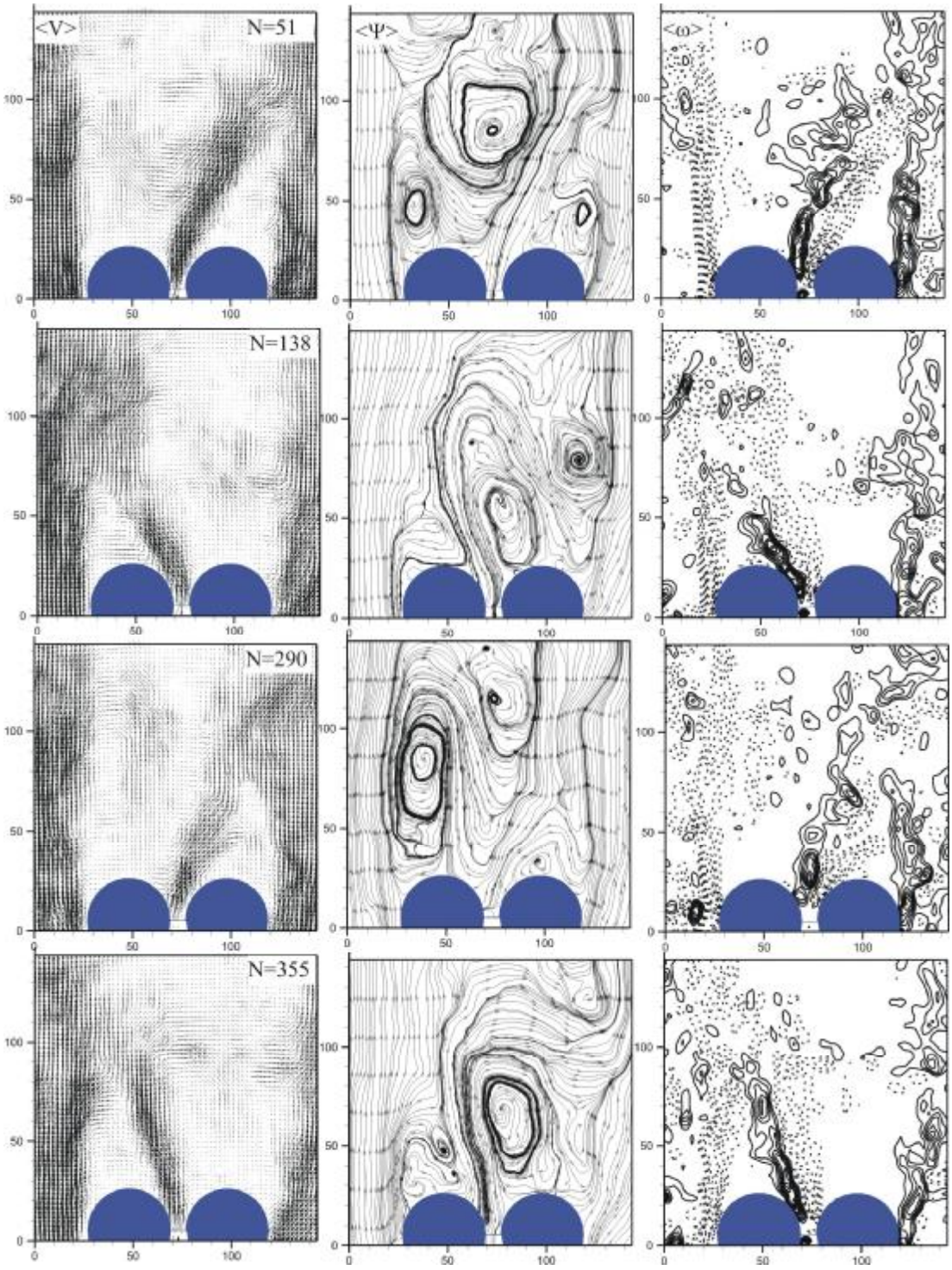
<V>
N=51
<Ψ>
<ω>
N=138
N=290
N=355

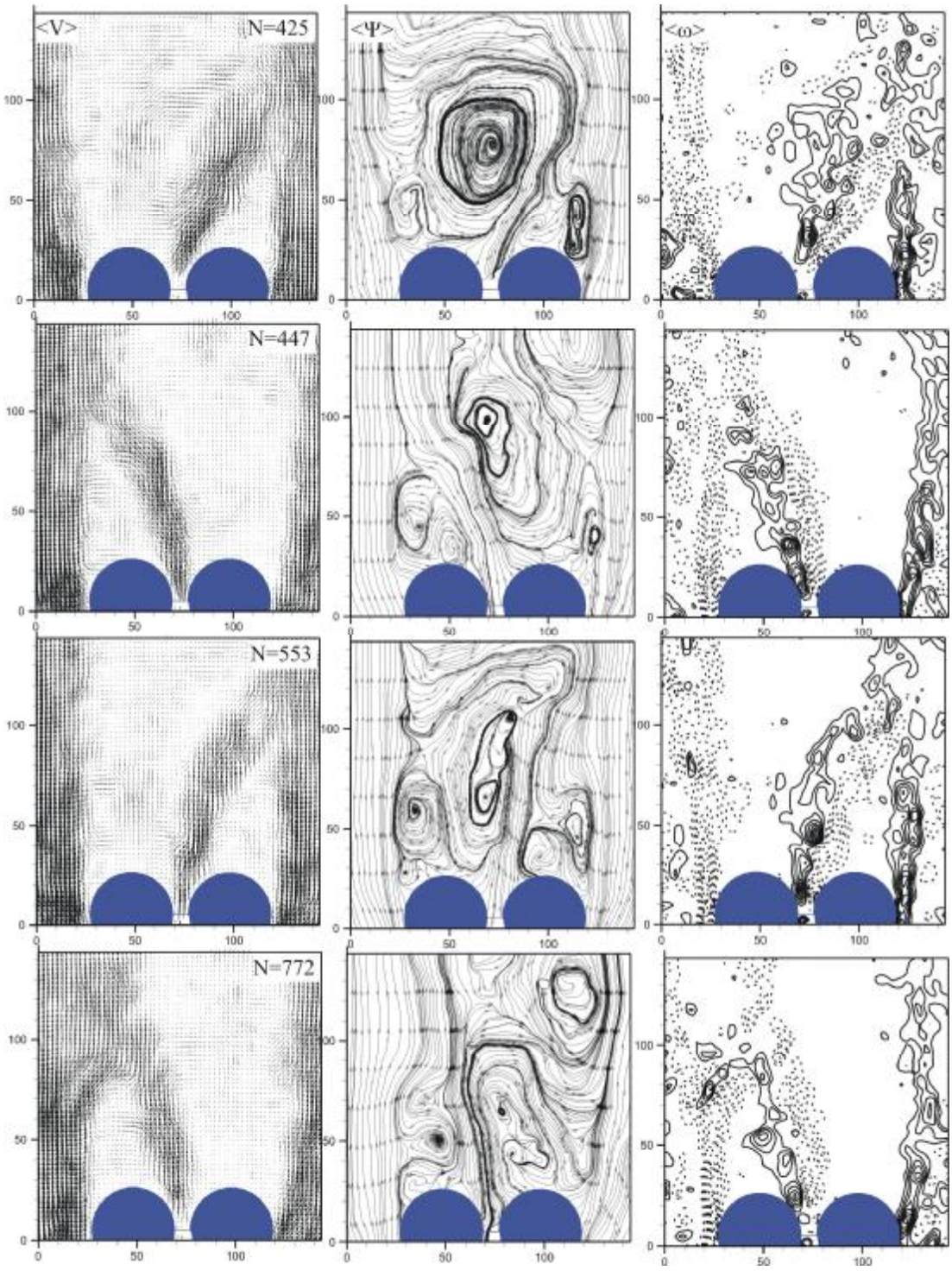

Figure 4.10. Instantaneous velocity vector field, vorticity contours and corresponding streamline topology for two side-by-side cylinders, H/D=0.25, T/D=1.25

Figure 4.11 shows Fast Fourier Transformation of time history of stream-wise velocity at specified location (x=61.56mm and y=66.61mm) for H/D=0.25 and T/D=1.25. As can be seen from this figure, there is no dominant frequency observed for the flopping regime of the wake region. There are high magnitude regions on this figure, but, it is believed that they occur due to noise in the experiments.

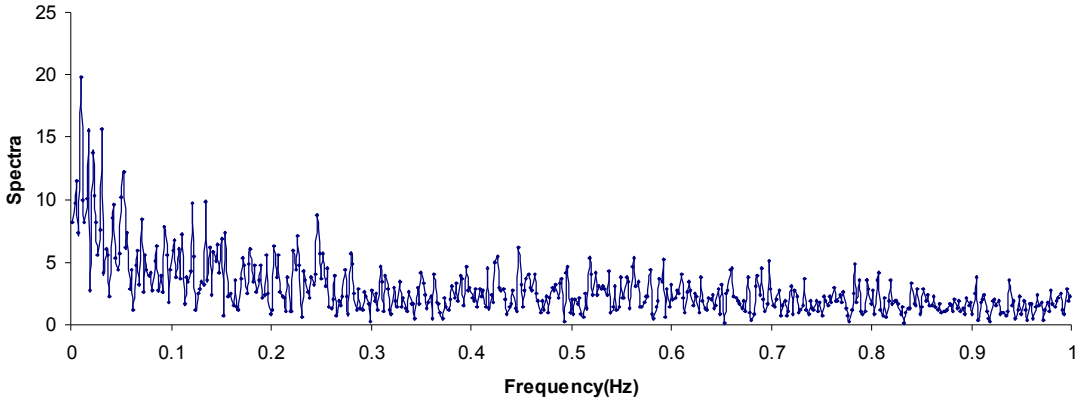

Figure 4.11. Spectra of stream-wise velocity component at x=61.56mm and y=66.61mm

4.3. Two Side-by-Side Circular Cylinders with H/D=0.25 and T/D=1.50

Figure 4.12. shows simultaneous time histories of streamwise velocity component, u, behind two side-by-side circular cylinders for H/D=0.25 and T/D=1.5 at point (103.7 mm, 65.68mm). Flopping occurs 13 times during first 180 seconds. Again, the length of time between transitions appears to be random during first 360 seconds. However, streamwise velocity values from 360 second to 540 second look like a sinusoidal signal which means they have a certain period and frequency. Image numbers shown on the time history indicates the number of instantaneous images given in figure 4.13. Figure 4.13 instantaneous velocity vector fields, streamline

topologies and corresponding vorticity contours downstream of two side-by-side circular cylinders at various times and flopping regimes at H/D=0.25 and T/D=1.5 case. Since the gap between two cylinders gets larger compared to T/D=1.25 case, jet like flow looses its magnitude and the deflection angle decreases. However, a wide wake and a narrow wake is still observed from instantaneous velocity vector fields. The streamwise extend of the narrow wake reaches up to 1.2 cylinder diameter from the base of the cylinders. Instantaneous velocity vector field also shows that the spanwise extend of the wider wake gets smaller compared to T/D=1.25 case.

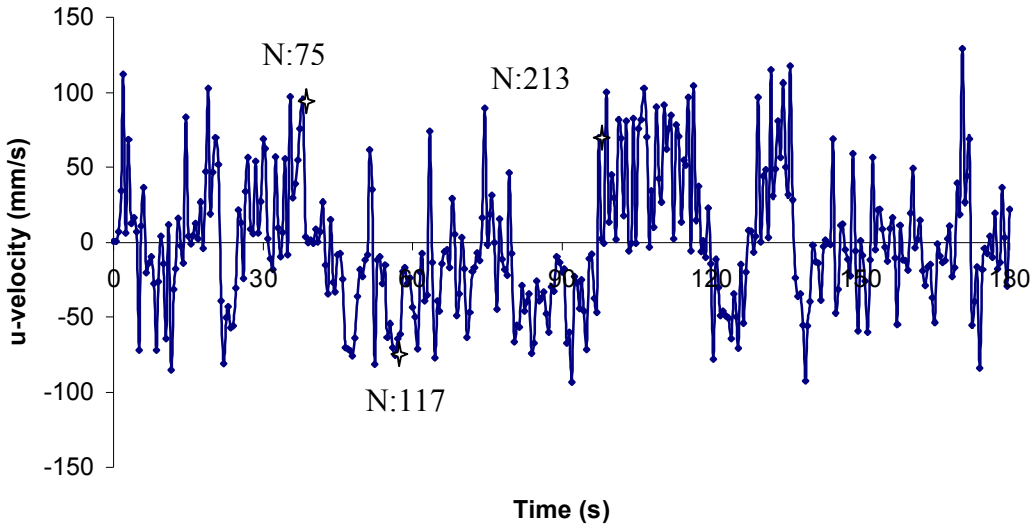

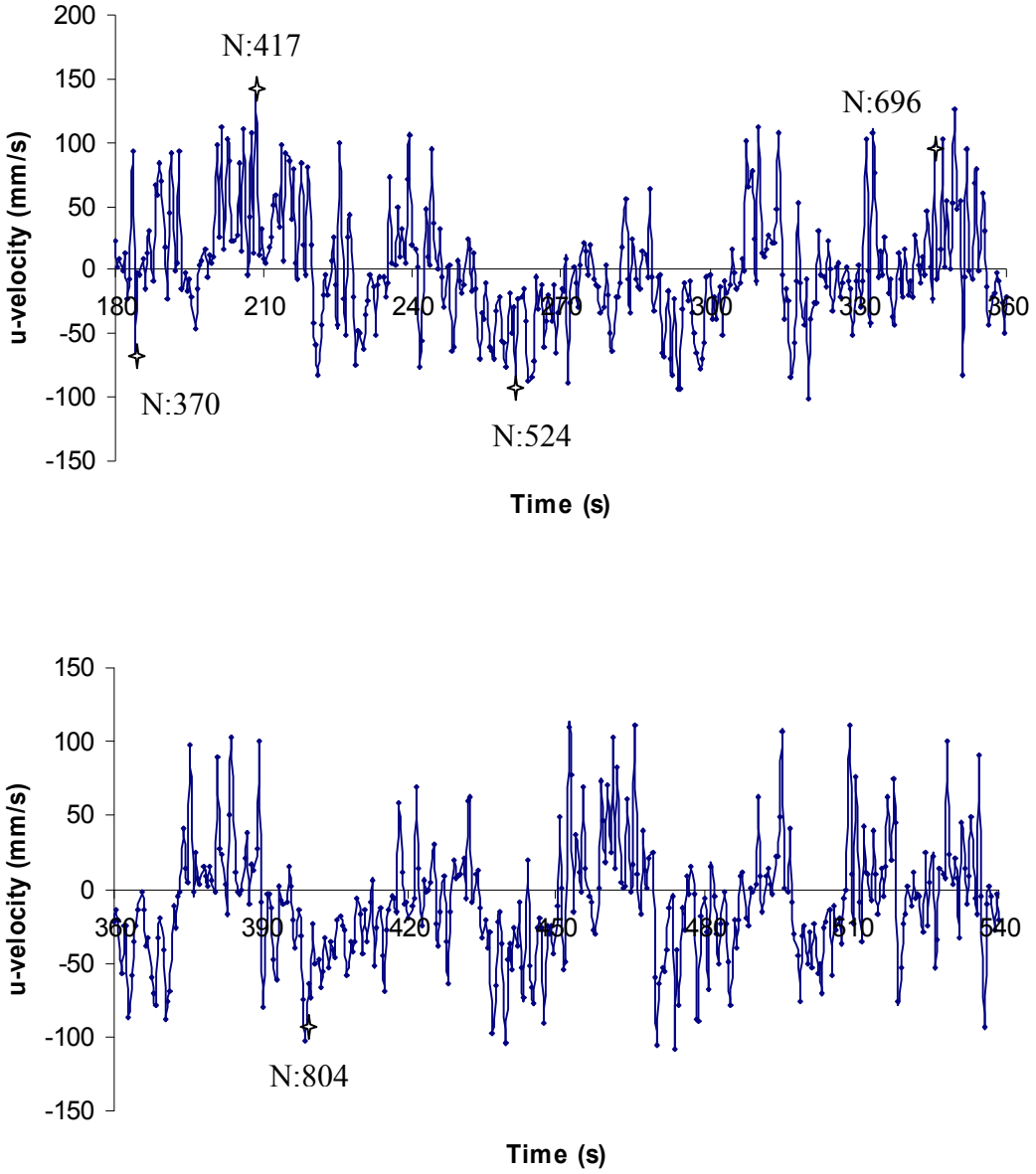

Figure 4.12 Instantaneous stream-wise velocity component for two side-by-side cylinders at x: 103.70mm, y : 65.68mm for H/D = 0.25, T/D = 1.50

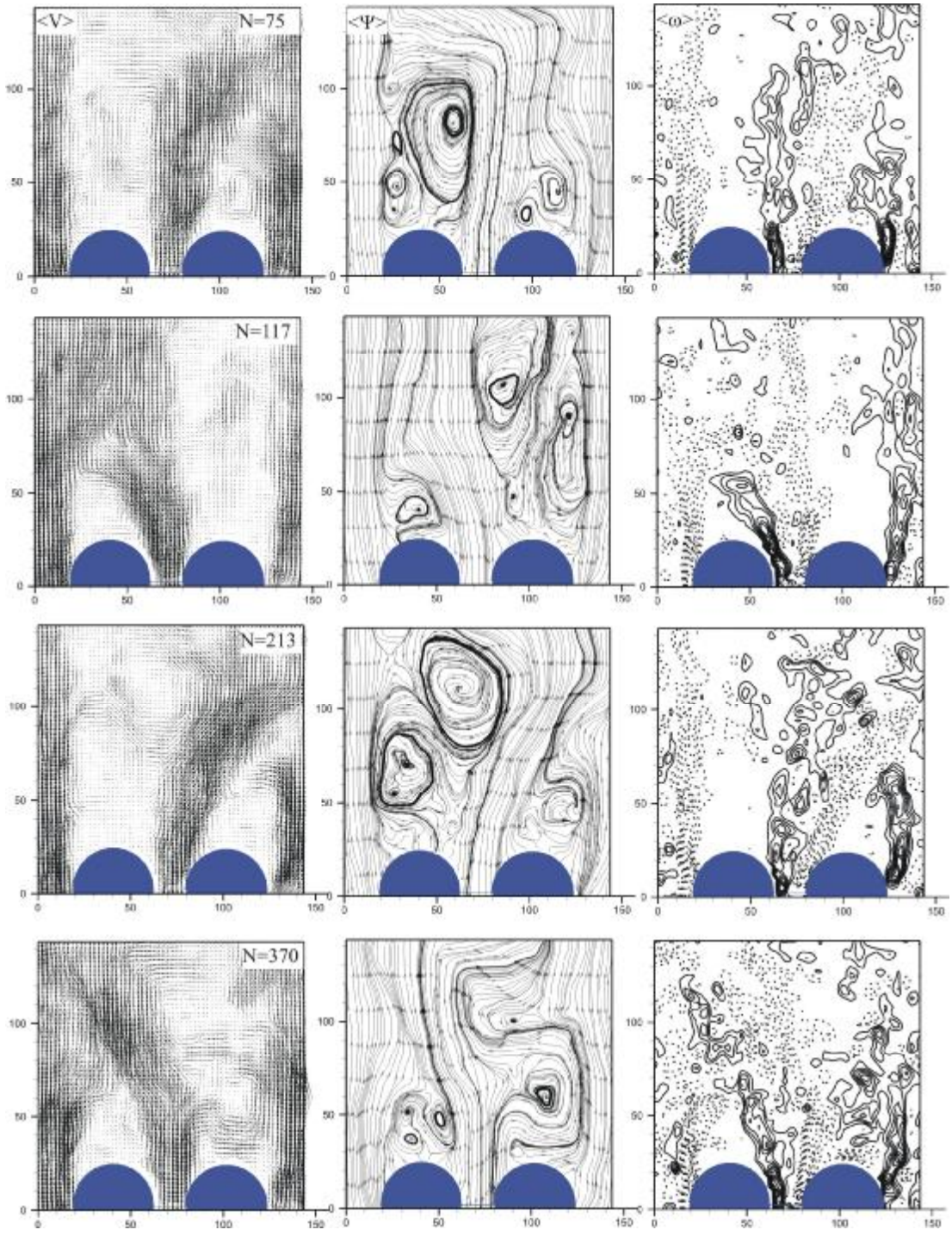
<V>
N=75
<Ψ>
<ω>
N=117
N=213
N=370

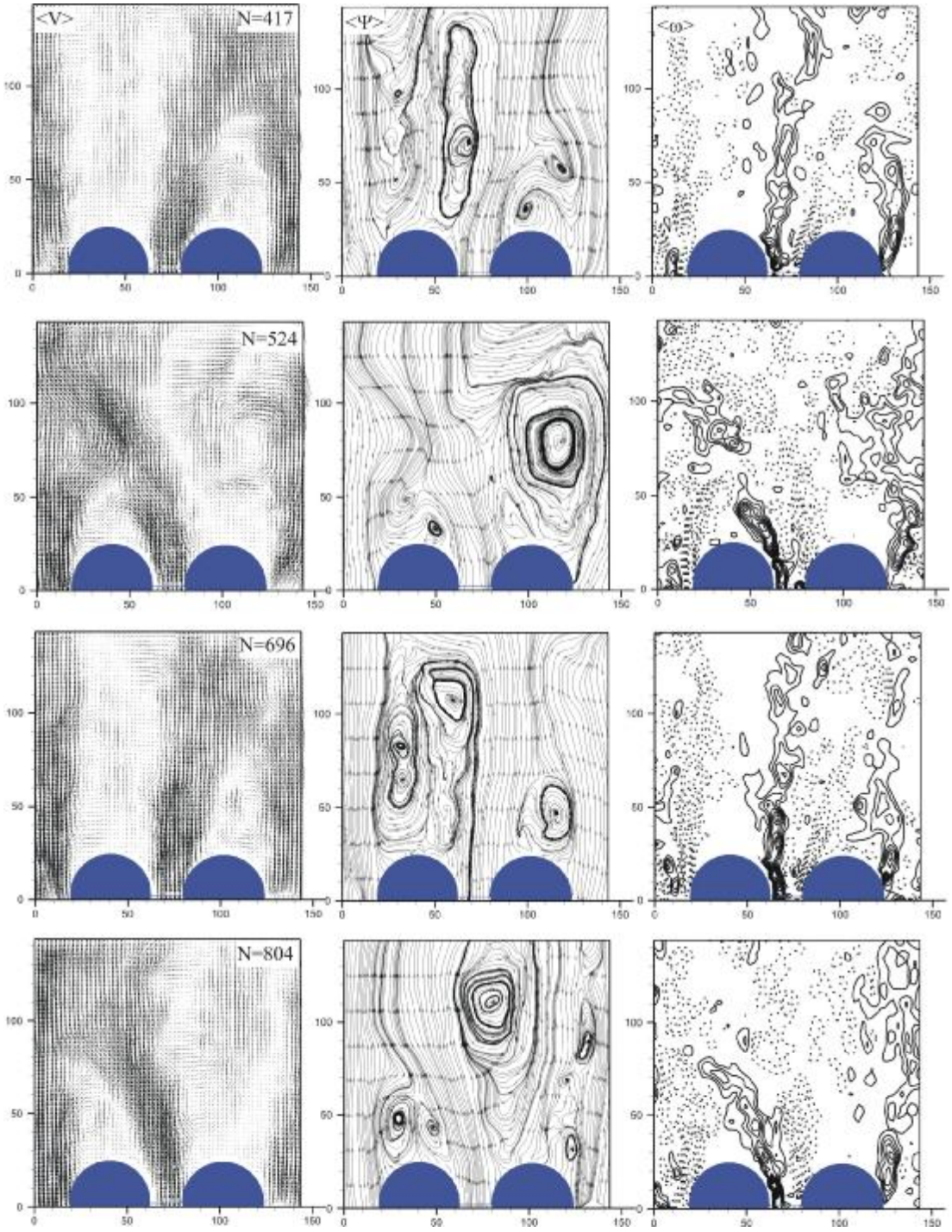

Figure 4.13. Instantaneous velocity vector field, vorticity contours and corresponding streamline topology for two side-by-side cylinders, H/D=0.25, T/D=1.50

Figure 4.14. shows Fast Fourier Transformation of time history of stream-wise velocity at specified location (x=103.7mm and y=65.68mm) for H/D=0.25 and T/D=1. 5. No dominant frequency observed for the flopping regime of the wake region.

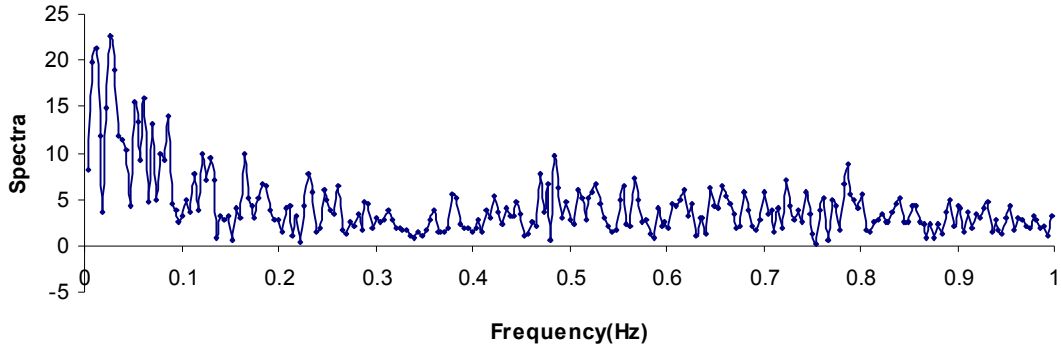

Figure 4.14. Spectra of stream-wise velocity component at x=103.7mm and y=65.68mm

4.4. Two Side-by-Side Circular Cylinders with H/D=0. 5 and T/D=1.25

Figure 4.15. indicates simultaneous time histories of stream-wise velocity component, u, behind two side-by-side circular cylinders for H/D=0. 5 and T/D=1.25 at point (42.02 mm, 68.07mm). Flopping occurs 11 times during first 180 seconds. Again, the length of time between transitions appears to be random during first 720 seconds. During the first 180 seconds, the wake region of left cylinder is wider most of the time, however, during the second 180 seconds the wake of the right cylinder is mostly wider.

Figure 4.16. instantaneous velocity vector fields, streamline topologies and corresponding vorticity contours downstream of two side-by-side circular cylinders at different times and flopping regimes at H/D=0. 5 and T/D=1.25 case. A wide wake and a narrow wake downstream of side-by-side cylinders are observed from instantaneous velocity vector fields (first column). The stream-wise extend of the

narrow wake reaches up to 1.2 cylinder diameter from the base of the cylinders. Since the distance between cylinders is small, a strong jet-like flow occurs between cylinders. Small scale vorticity clusters are evident from vorticity contours seen in the third column of figure 4.16.

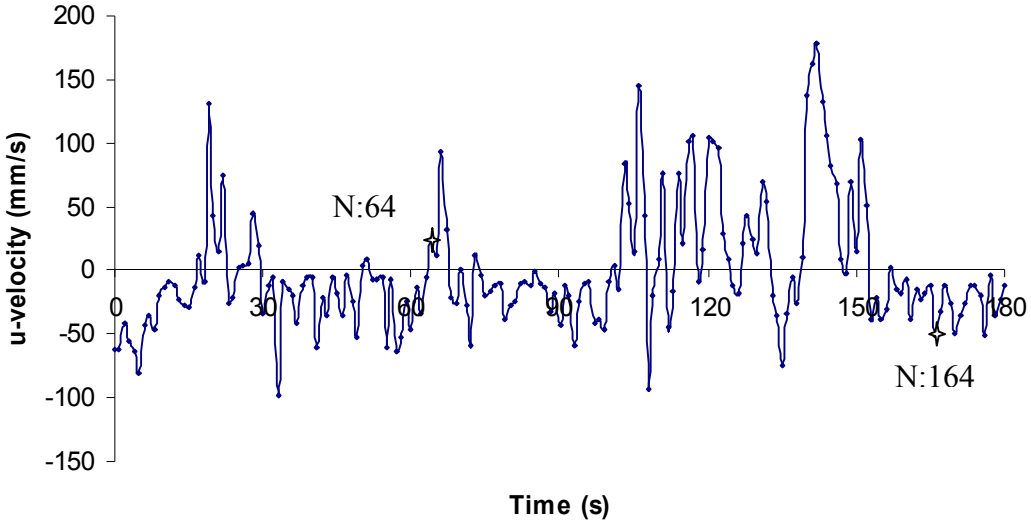

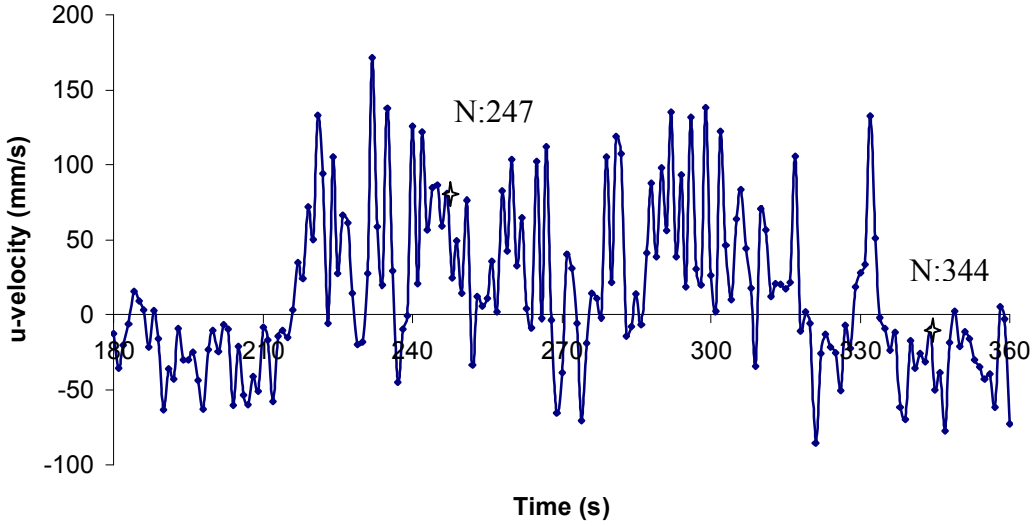

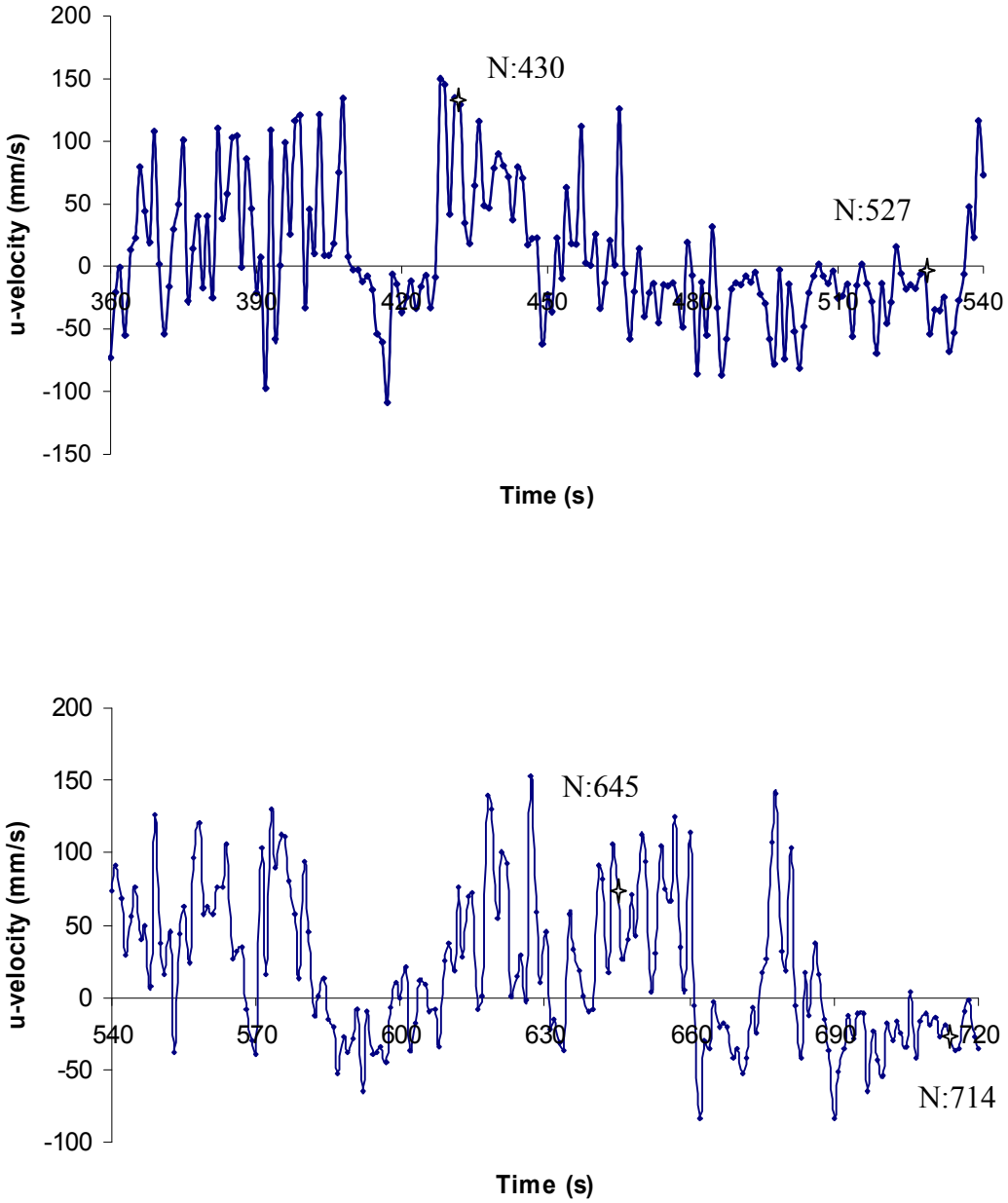

Figure 4.15 Instantaneous stream-wise velocity component for two side-by-side cylinders at x: 42.02mm, y: 68.07mm for H/D = 0.50, T/D = 1.25

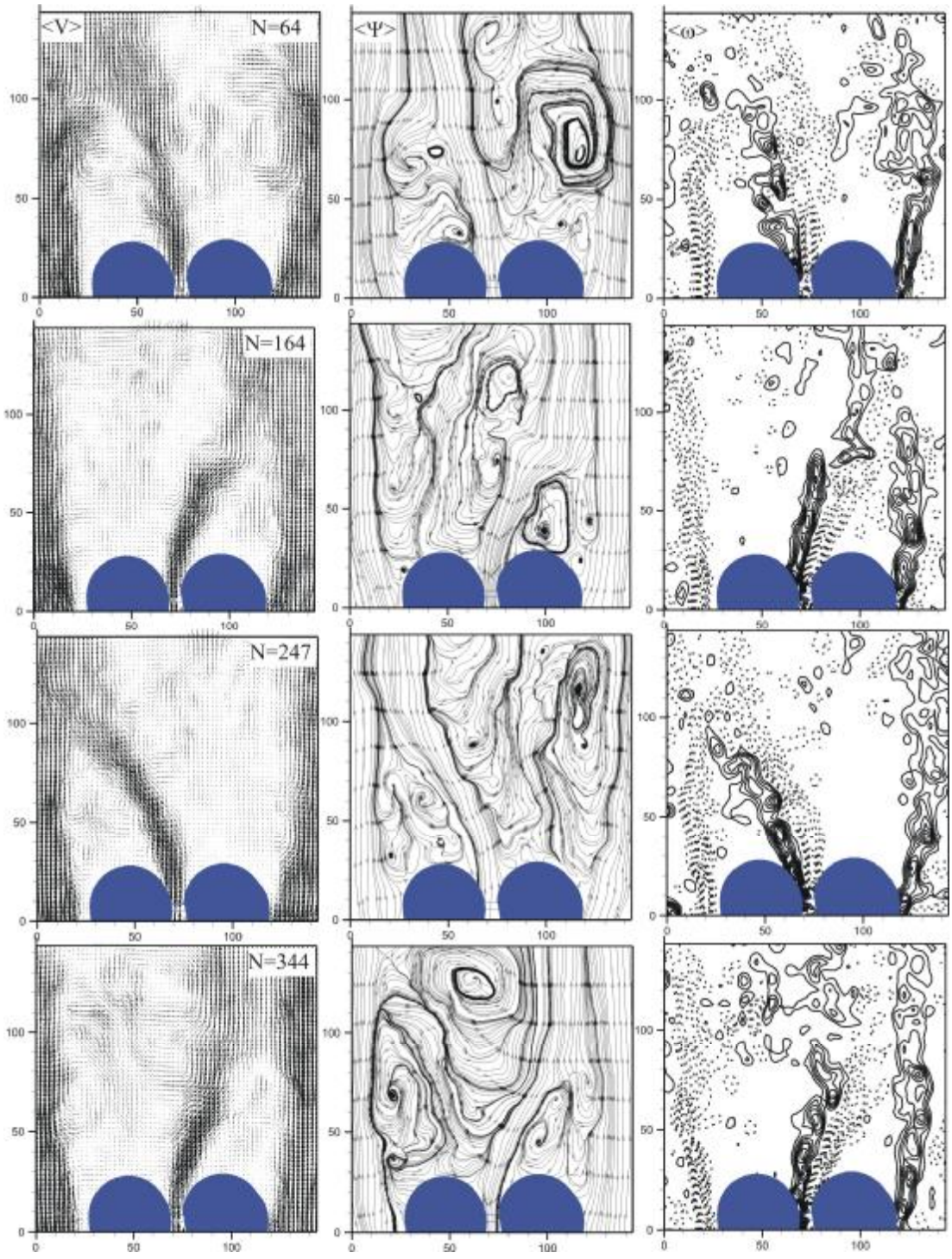
<V>
N=64
<Ψ>
<ω>
N=164
N=247
N=344

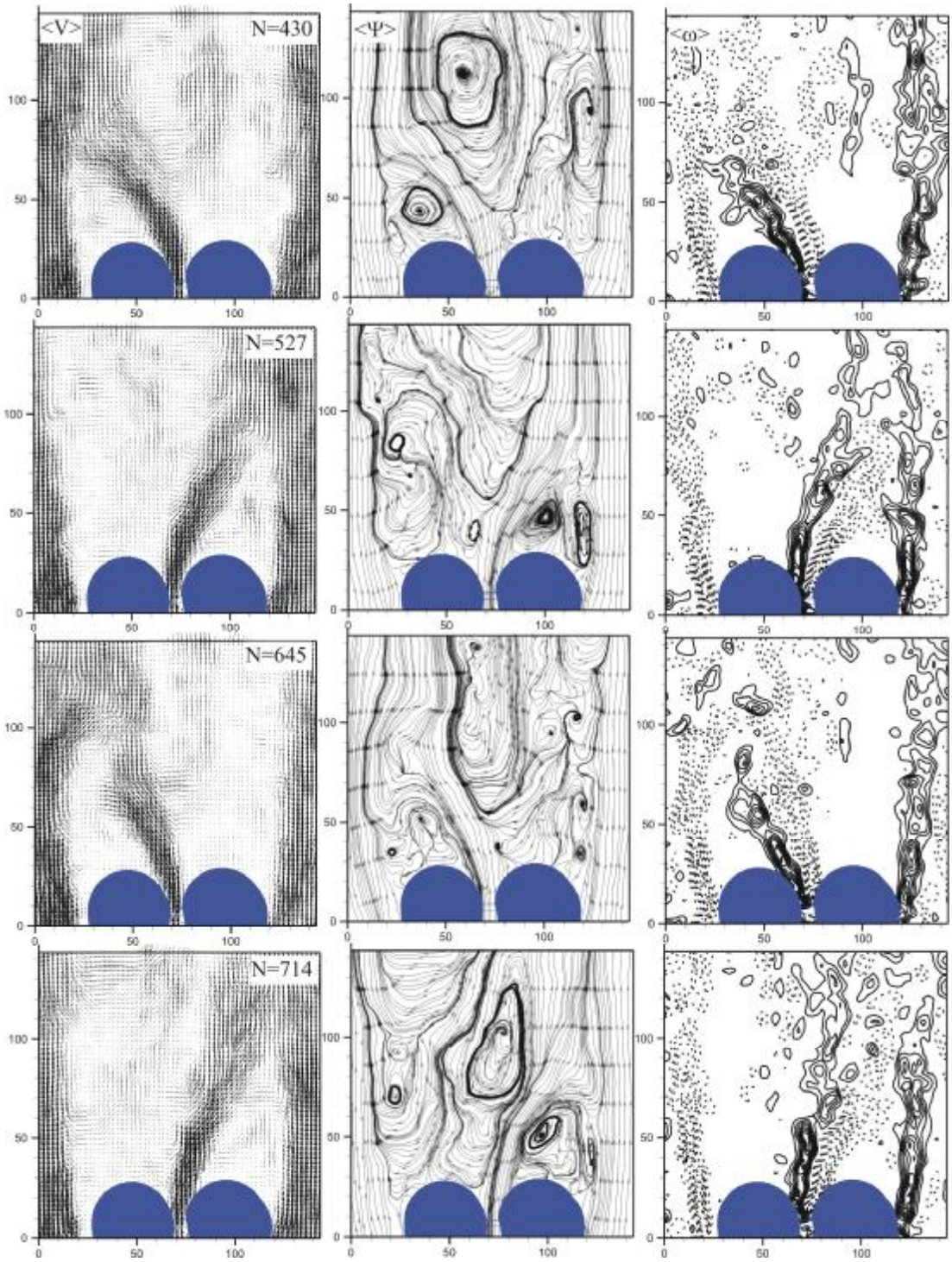

Figure 4.16. Instantaneous velocity vector field, vorticity contours and corresponding streamline topology for two side-by-side cylinders, H/D=0.50, T/D=1.25

Figure 4.17. shows spectra of stream-wise velocity at x=42.02 mm and y=68.07 mm for H/D=0.5 and T/D=1.25. This figure indicates the presence of a peak at approximately 0.03 Hz. This value corresponds to a period of approximately 33 seconds.

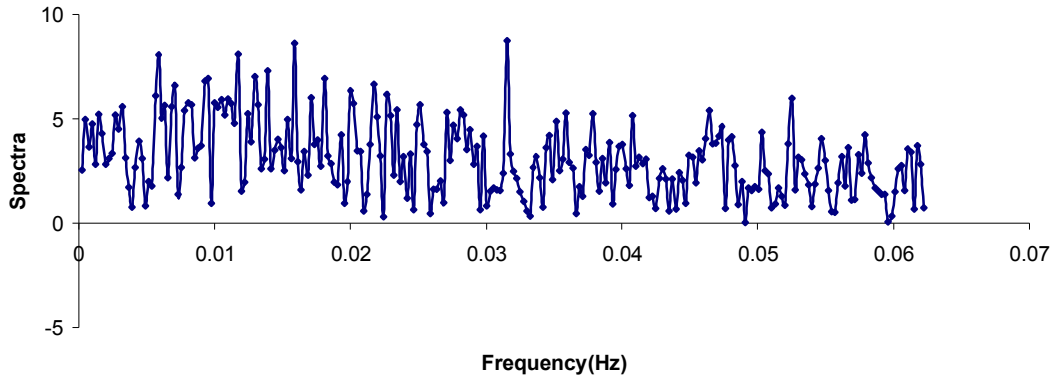

Figure 4.17. Spectra of stream-wise velocity component at x=42.02mm and y=68.07mm

4.5. Two Side-by-Side Circular Cylinders with H/D=0. 5 and T/D=1.5

Figure 4.18. shows simultaneous time histories of stream-wise velocity component, u, behind two side-by-side circular cylinders for H/D=0.5 and T/D=1.5 at point (44.97 mm, 65.52mm). Flopping occurs 10 times during first 180 seconds. The length of time between transitions appears to be random during first 720 seconds. The sudden and dramatic changes in velocity indicate the occurrence of flopping regime of the flow structure downstream of two side-by-side circular cylinders.

Figure 4.19 instantaneous velocity vector fields, streamline topologies and corresponding vorticity contours downstream of two side-by-side circular cylinders at various times and flopping regimes at H/D=0.5 and T/D=1.5 case. Since the gap between two cylinders gets larger compared to T/D=1.25 case, jet like flow looses its magnitude and the deflection angle decreases. However, a wide wake and a narrow

wake are still observed from instantaneous velocity vector fields. Instantaneous velocity vector field also shows that the span-wise extend of the wider wake gets smaller compared to T/D=1.25 case.

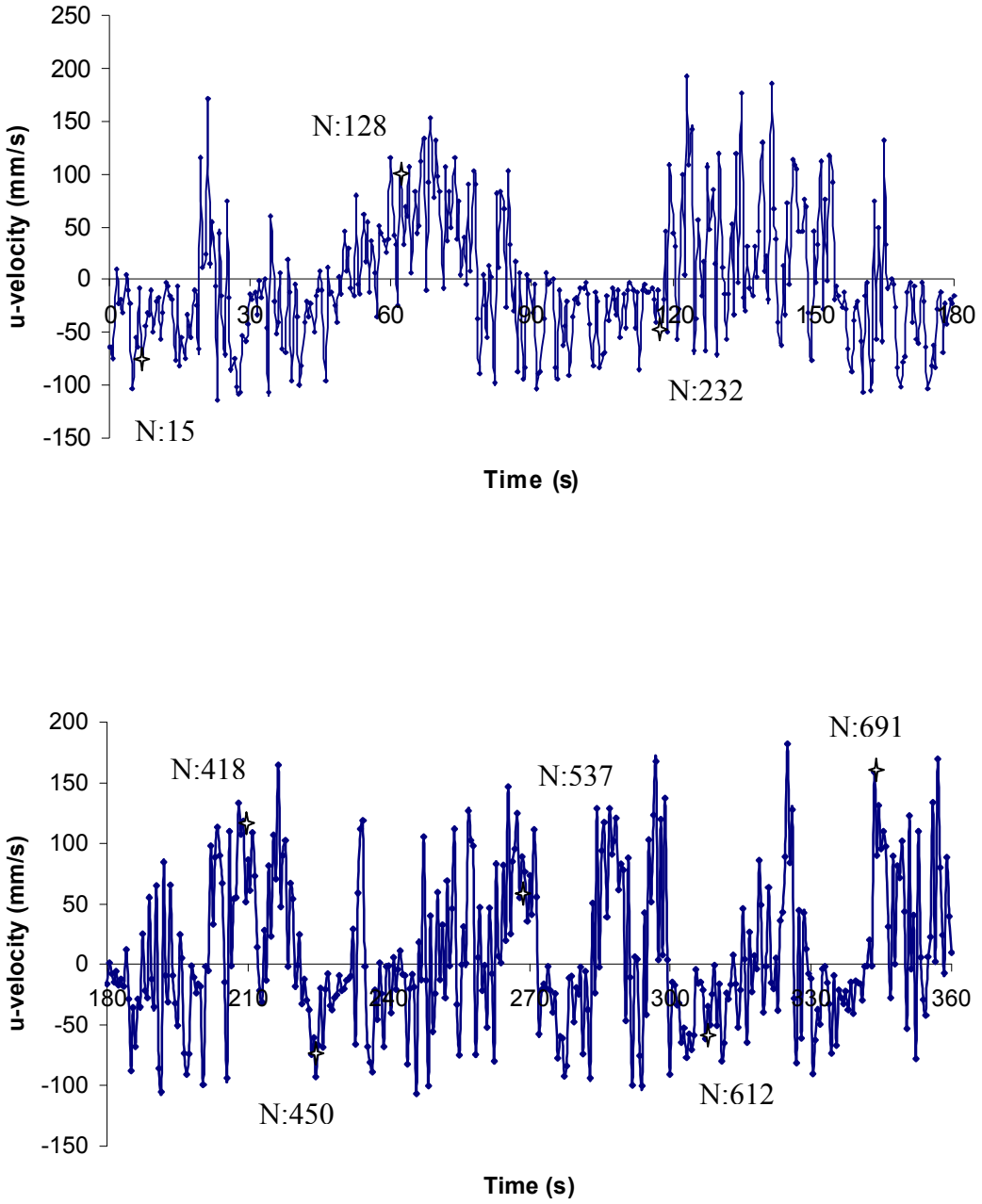

Figure 4.18. Instantaneous stream-wise velocity component for two side-by-side cylinders at x: 44.97mm, y : 65.52mm for H/D = 0.50, T/D = 1.50

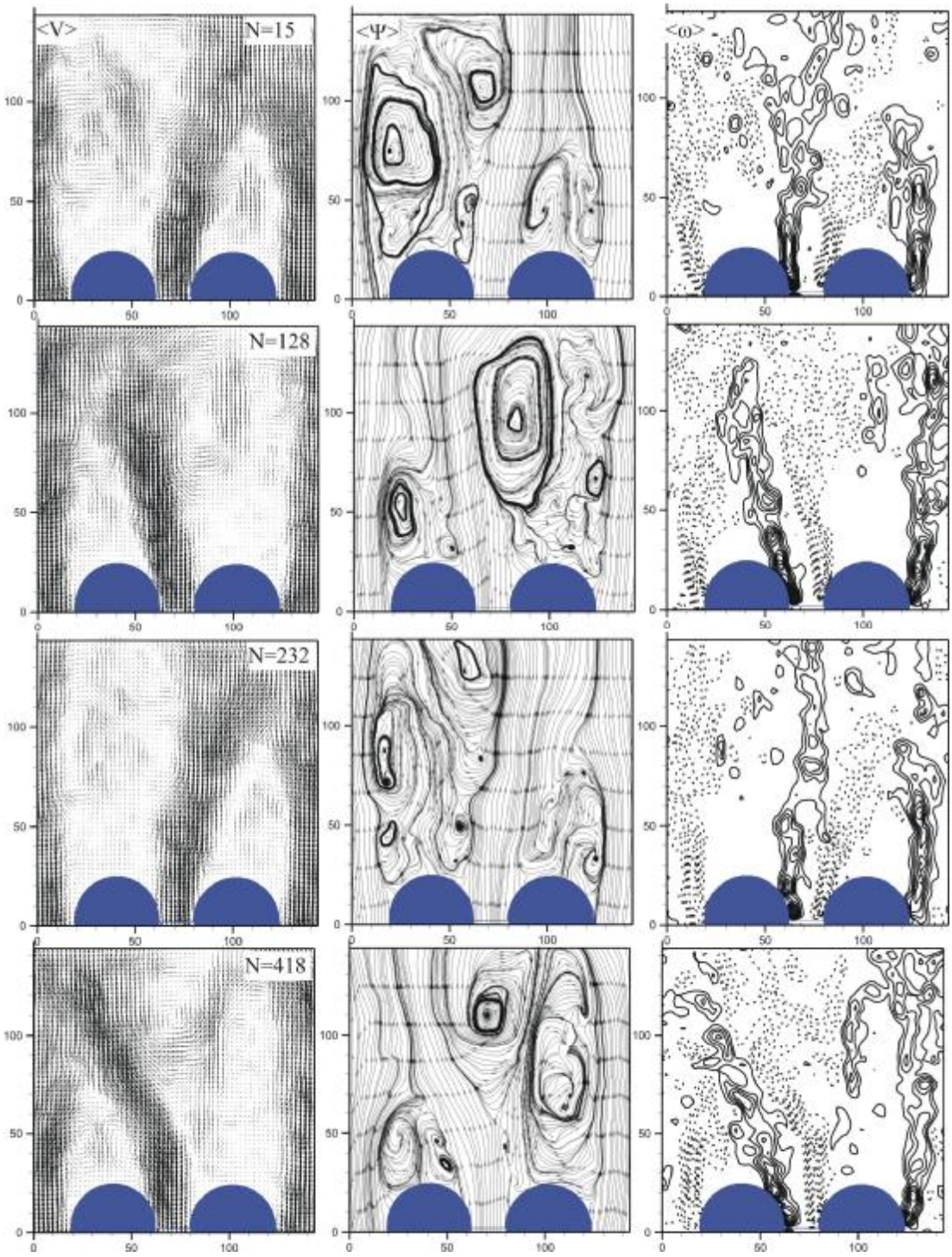
<V>
<Ψ>
<ω>
N=15
N=128
N=232
N=418

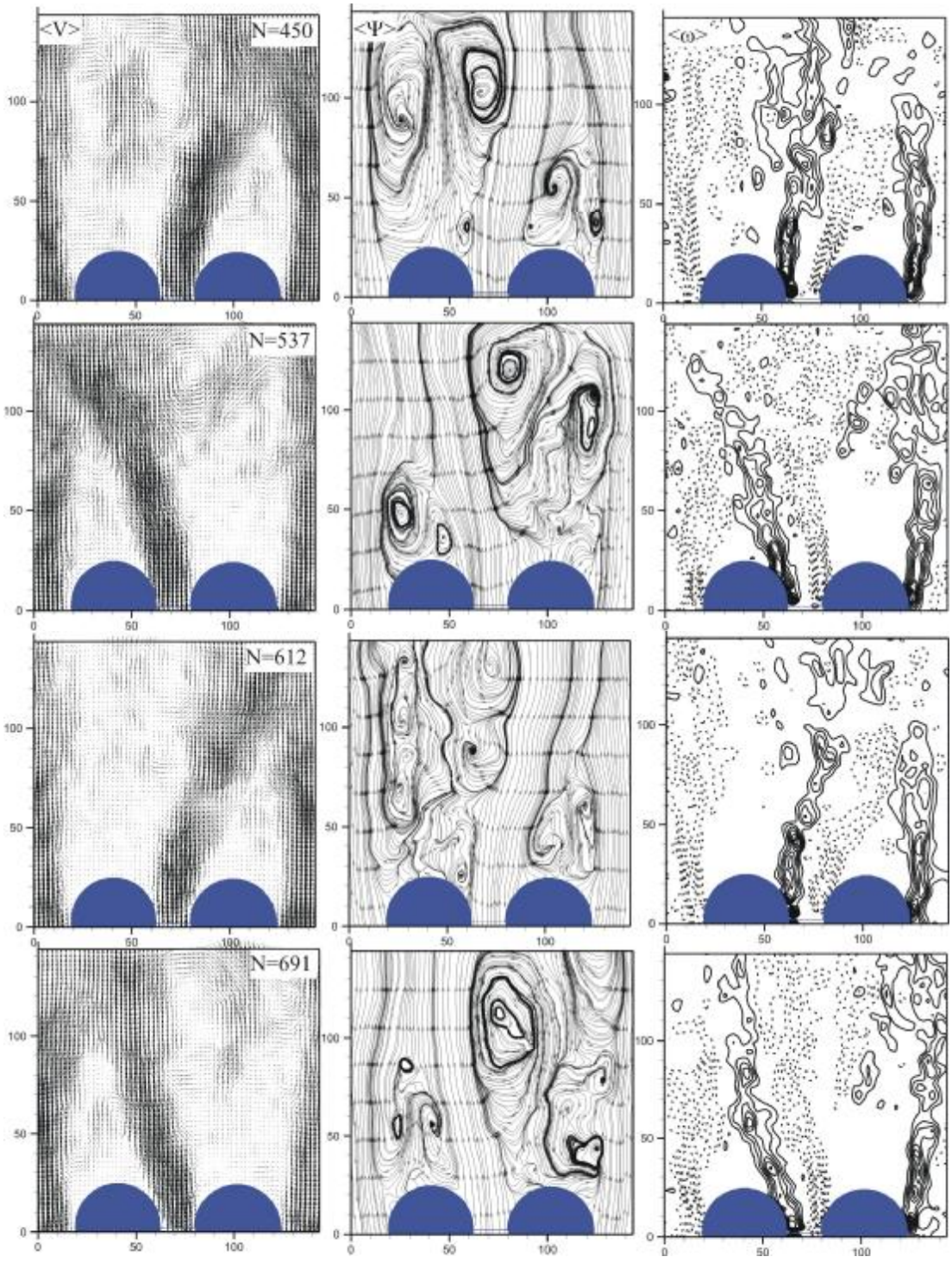

Figure 4.19. Instantaneous velocity vector field, vorticity contours and corresponding streamline topology for two side-by-side cylinders, H/D=0.50, T/D=1.50

Figure 4.20. shows spectra of stream-wise velocity component at x=44.97 mm and y=65.52 mm for H/D=0.5 and T/D=1. 5. This figure indicates the presence of a peak at approximately 0.015 Hz. This value corresponds to a period of approximately 66 seconds.

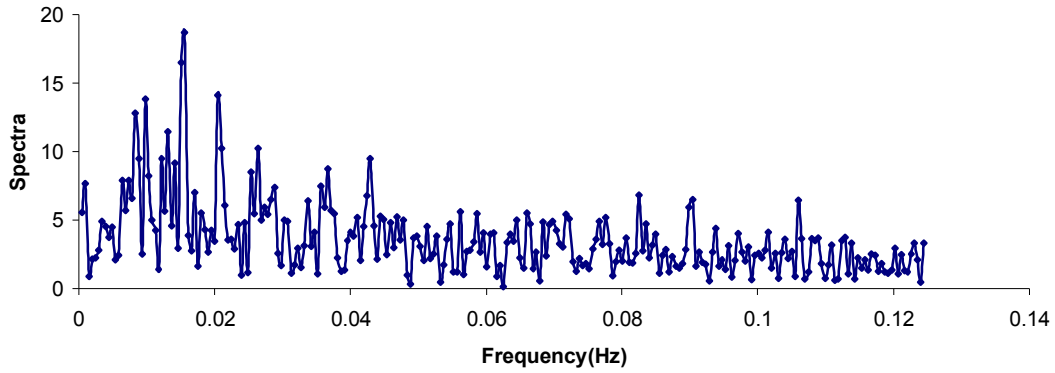

Figure 4.20. Spectra of stream-wise velocity component at x=44.97mm and y=65.52mm

4.6. Two Side-by-Side Circular Cylinders with H/D=0. 5 and T/D=1.75

Figure 4.21. shows simultaneous time histories of stream-wise velocity component, u, behind two side-by-side circular cylinders for H/D=0.5 and T/D=1.75 at point (95.50 mm, 67.71mm). The length of time between transitions appears to be random during first 720 seconds. As can be seen from time history, the wake of right cylinder was wider and dominant. However, flopping regime occurs 14 times during first 180 seconds. When the wider wake moves to right cylinder, flopping occurs immediately and the dominancy of the wake of left cylinder takes place again. This kind of flow behavior is also apparent for other two time sequences (between 180 seconds and 540 seconds).

Figure 4.22 instantaneous velocity vector fields, streamline topologies and corresponding vorticity contours downstream of two side-by-side circular cylinders at various times and flopping regimes at H/D=0.5 and T/D=1.75 case. Since the gap between two cylinders gets larger compared to T/D=1.25 case, jet like flow looses most of its magnitude and the deflection angle decreases to very small angles. This flow behavior can also be seen from instantaneous vorticity contours. However, a wide wake and a narrow wake are still observed from instantaneous velocity vector fields. Instantaneous velocity vector field also shows that the span-wise extend of the wider wake gets smaller compared to T/D=1.25 and 1.5 cases. The number of foci points is less for T/D=1.75 case compared to other two gap ratios (T/D=1.25 and 1.5).

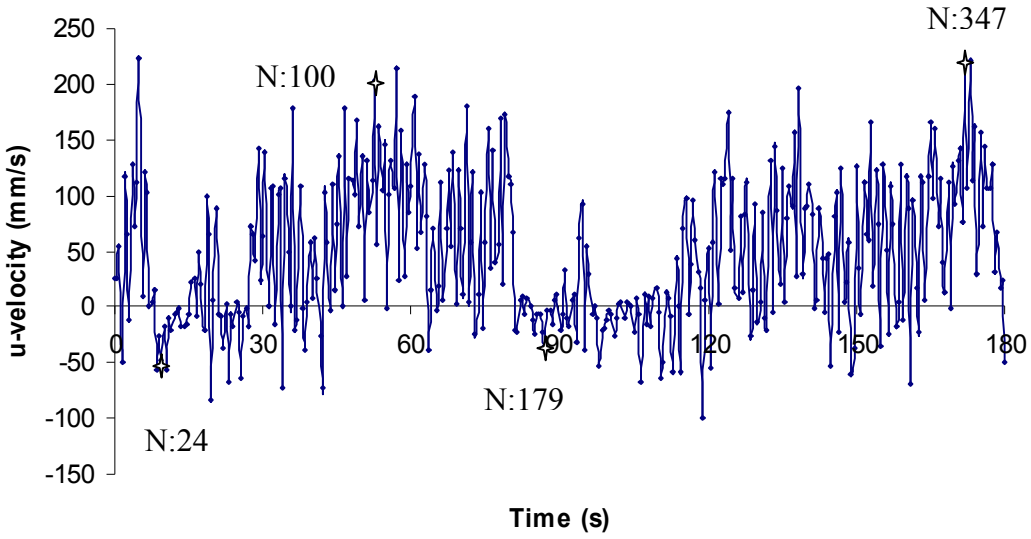

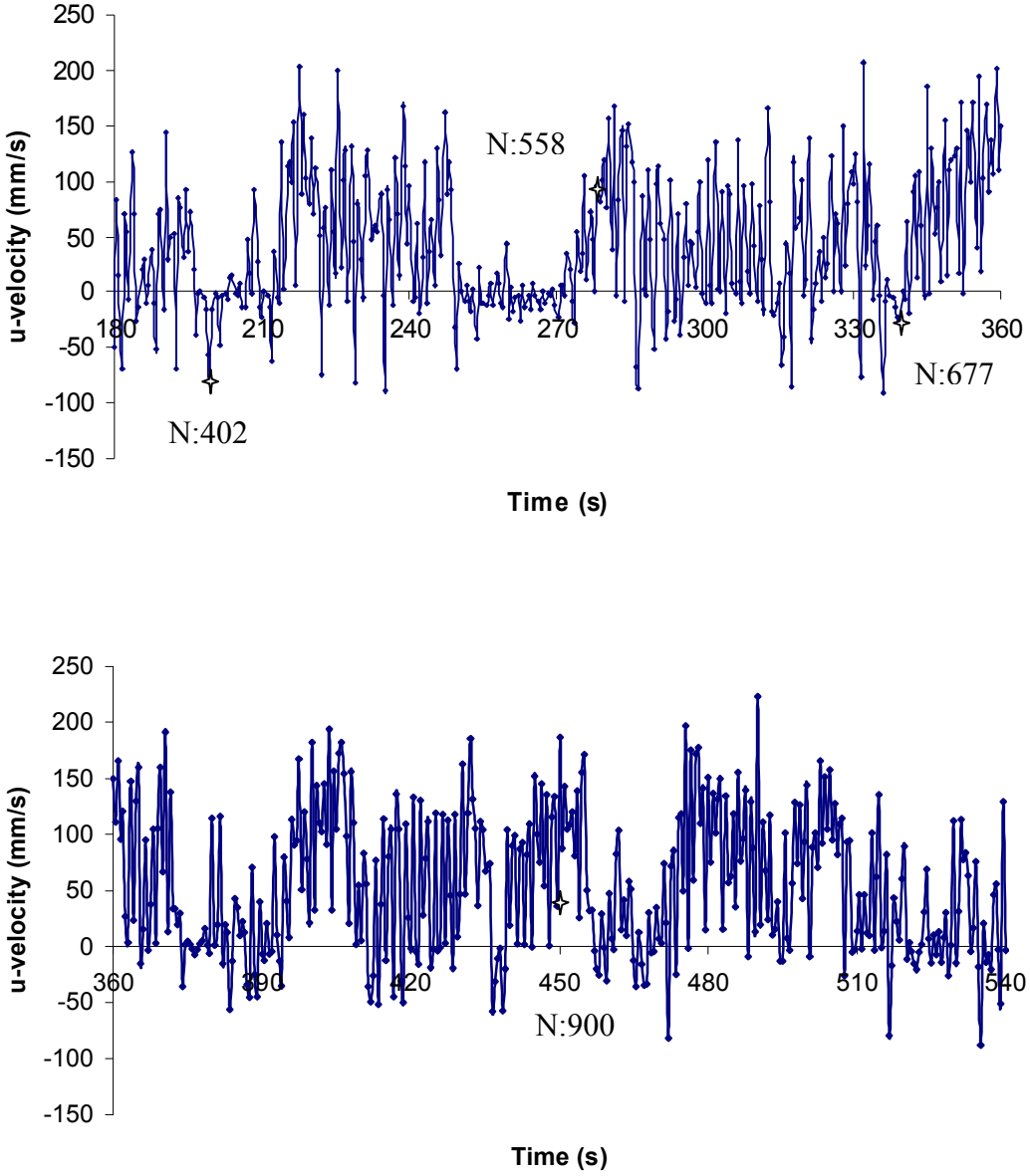

Figure 4.21. Instantaneous stream-wise velocity component for two side-by-side cylinders at x: 95.50mm, y : 67.71mm for H/D = 0.50, T/D = 1.75

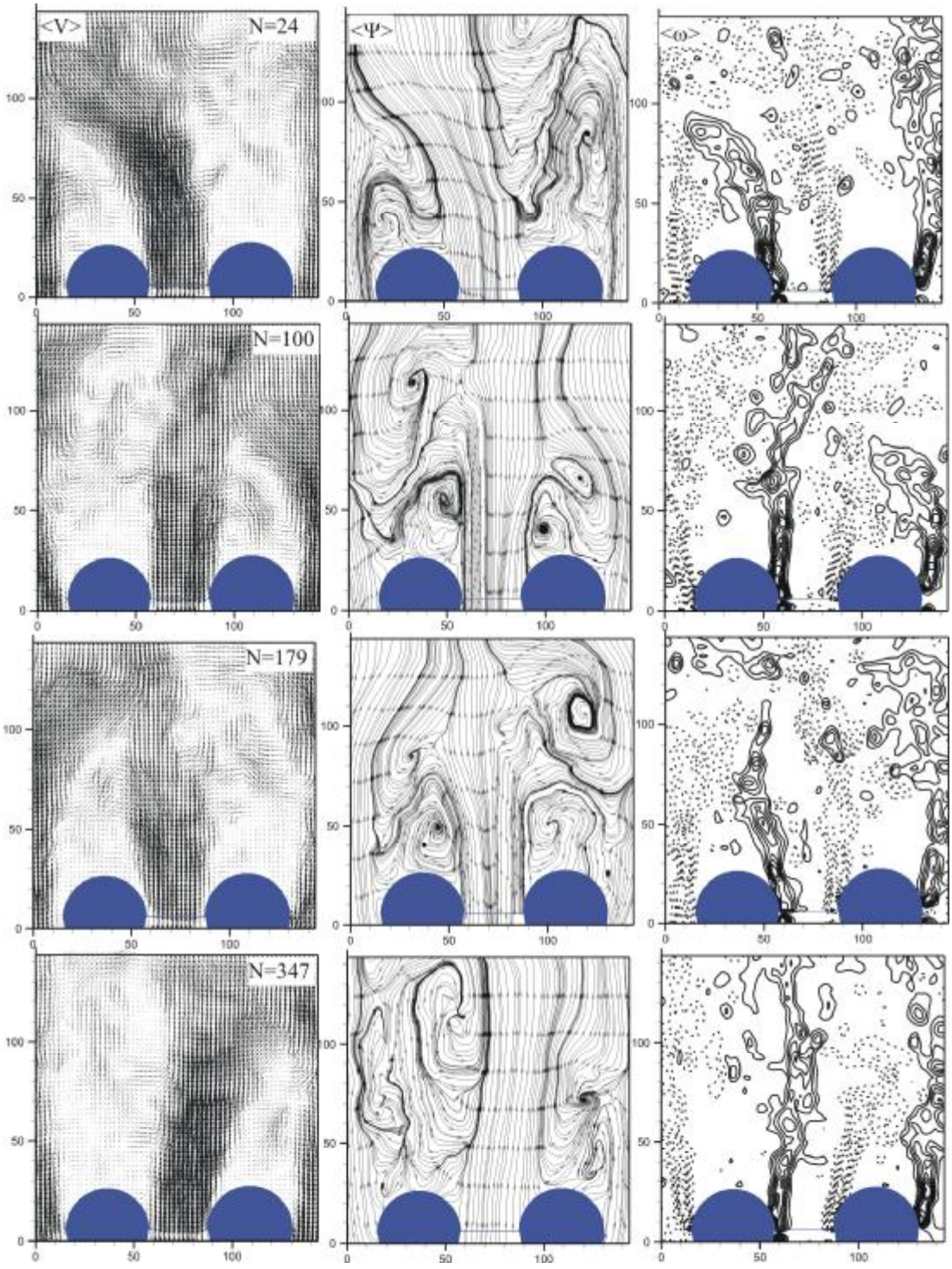
<V>
N=24
<Ψ>
<ω>
N=100
N=179
N=347

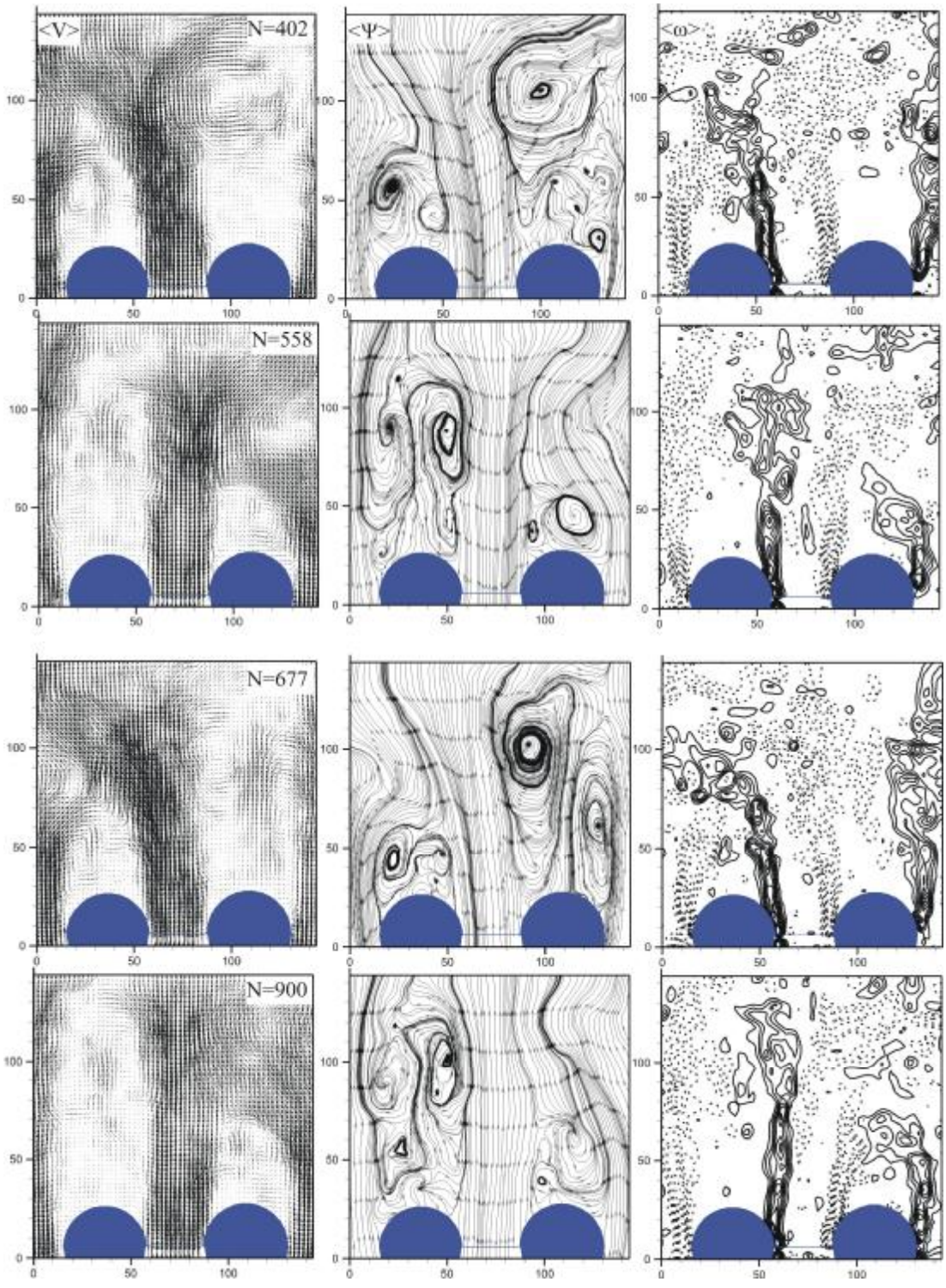

Figure 4.22. Instantaneous velocity vector field, vorticity contours and corresponding streamline topology for two side-by-side cylinders, H/D=0.50, T/D=1.75

Figure 4.23. shows the spectra of stream-wise velocity component at point 95.50 mm, 67.71 mm. This figure indicates the presence of a peak at approximately 0.02 Hz. However, this peak is not a clear and dominant peak. This frequency value corresponds to a period of approximately 50 seconds.

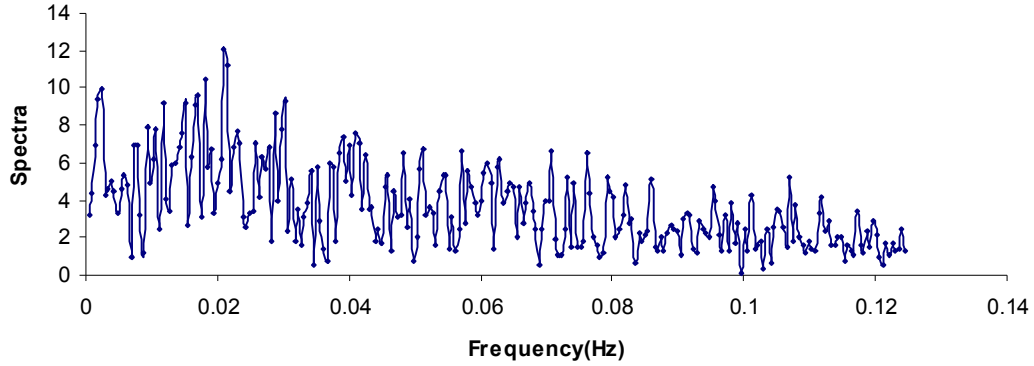

Figure 4.23. Spectra of stream-wise velocity component at point 95.50mm, 67.71mm

4.7. Two Side-by-Side Circular Cylinders with H/D=1.0 and T/D=1.25

In this case, the water height was adjusted to 40mm which is the diameter of the cylinder. The distance between side-by-side cylinders is 10mm which corresponds to the gap ratio of T/D=1.25. Figure 4.24. shows simultaneous time histories of stream-wise velocity component, u, behind two side-by-side circular cylinders at point (73.00 mm, 65.52 mm). The length of time between transitions appears to be random during first 720 seconds. As can be seen from time history, the wake of left cylinder was wider and dominant. The number of flopping is less than those obtained for other water heights.

Figure 4.25. instantaneous velocity vector fields, streamline topologies and corresponding vorticity contours downstream of two side-by-side circular cylinders at various times and flopping regimes for H/D=1 and T/D=1.25 case. Velocity vector fields seen in the first column clearly show that the wake region of left cylinder is wider for most of the images. The length of both wake regions is approximately the

same for image numbers N=122, 234, 525 and 722. However, wider wake region of right cylinder was not seen from instantaneous velocity vector field.

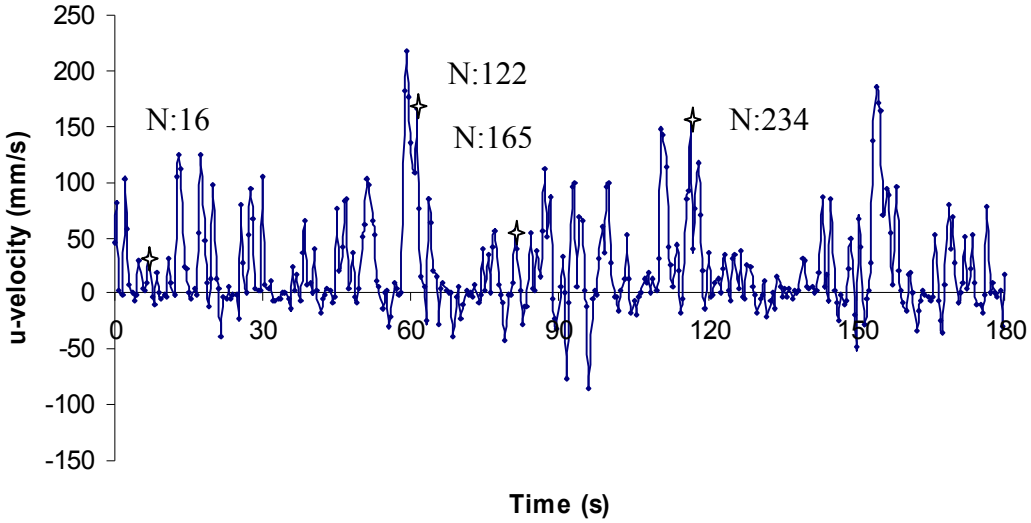

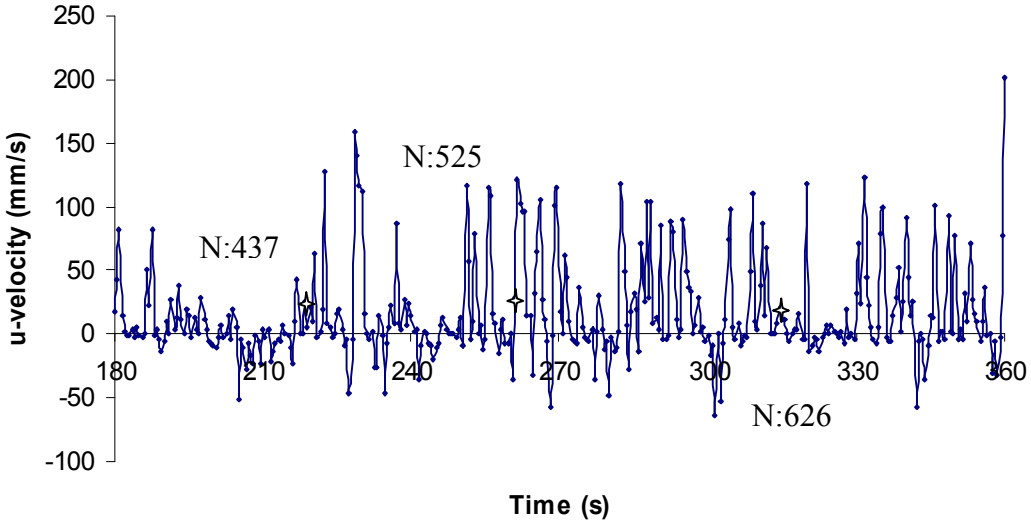

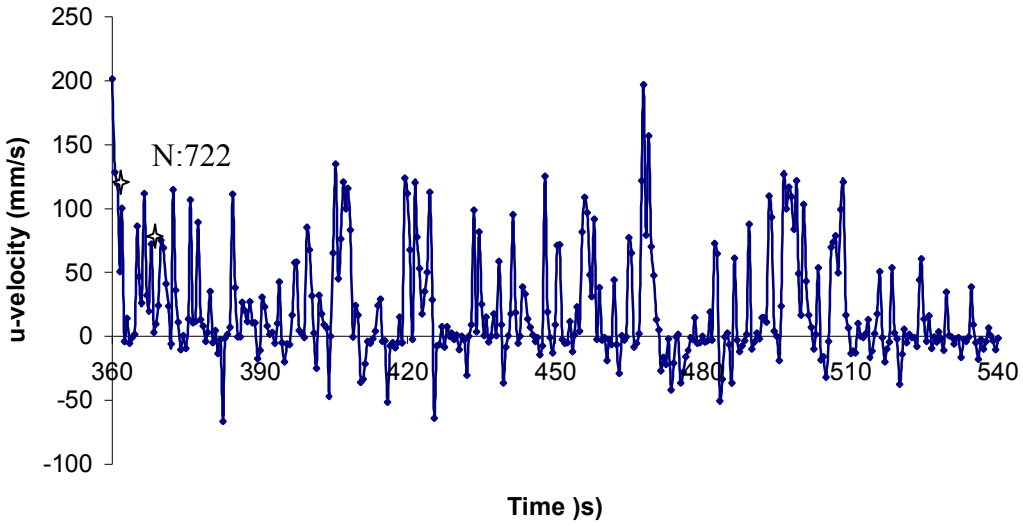

Figure 4.24. Instantaneous stream-wise velocity component for two side-by-side cylinders at x: 73.00mm, y : 65.52mm for H/D = 1.00, T/D = 1.25

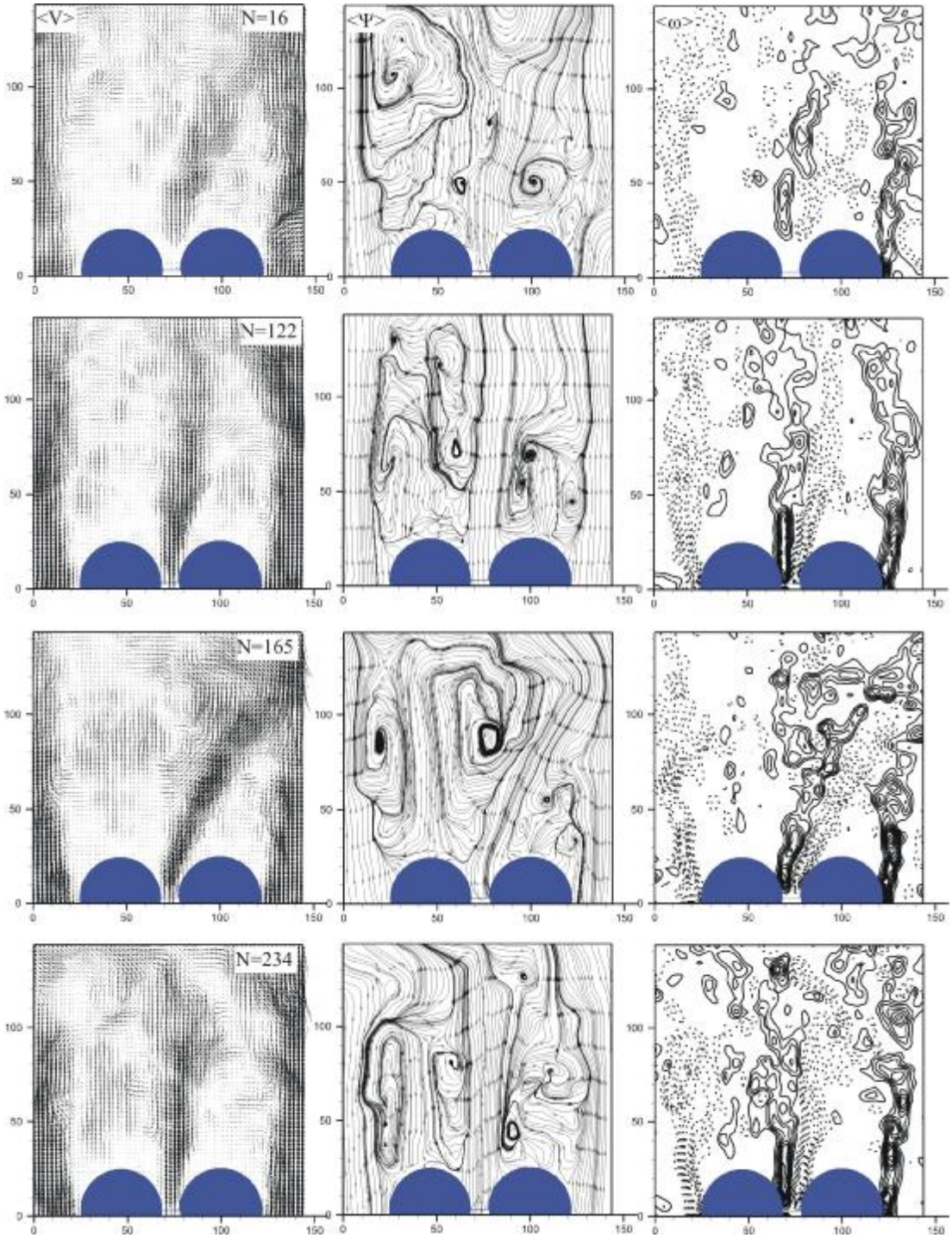
<V>
N=16
<Ψ>
<ω>
N=122
N=165
N=234

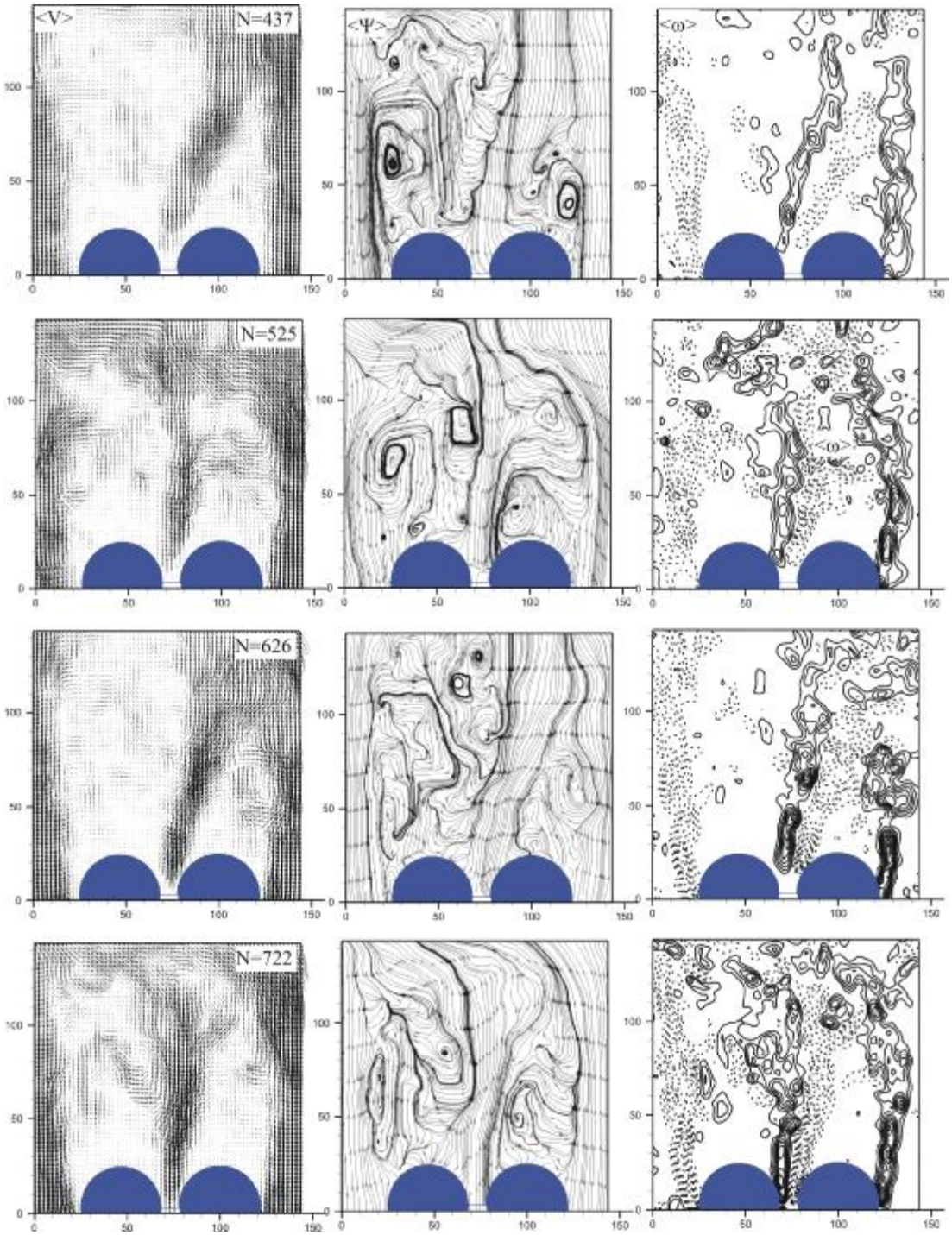

Figure 4.25. Instantaneous velocity vector field, vorticity contours and corresponding streamline topology for two side-by-side cylinders, H/D=1.00 T/D=1.25

Figure 4.26. shows the spectra of stream-wise velocity component at point 73.00 mm, 65.52 mm. The figure does not indicate any dominant frequency for this case.

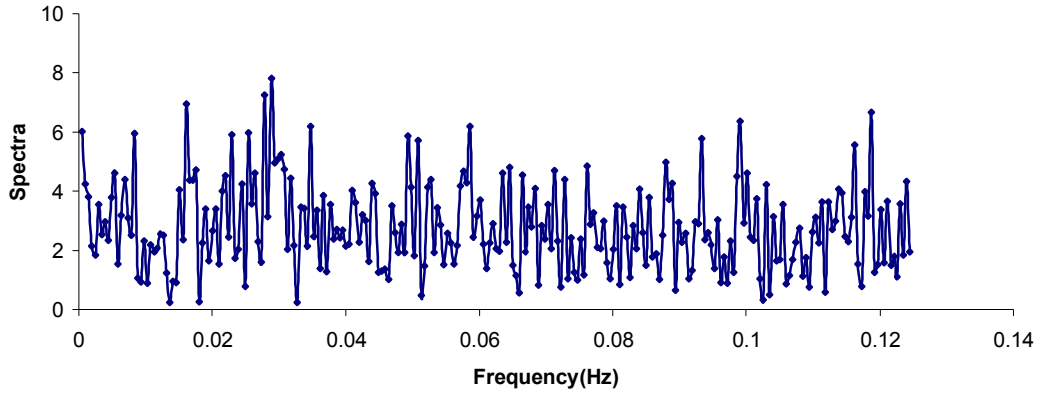

Figure 4.26. Spectra of stream-wise velocity component at point 73.00mm, 65.52mm

4.8. Two Side-by-Side Circular Cylinders with H/D=1.0 and T/D=1.5

In this case, the water height was adjusted to 40mm and the distance between side-by-side cylinders is 20mm which corresponds to the gap ratio of T/D=1.5. Figure 4.27. shows simultaneous time histories of stream-wise velocity component, u, behind two side-by-side circular cylinders at point (55.67 mm, 66.61 mm). The length of time between transitions appears to be random during first 720 seconds. As can be seen from time history, the wake of left cylinder was wider and dominant during first 180 seconds. However, for the second 160 seconds, the wake of right cylinder is wider for most of the time. The number of flopping is less than those obtained for other water heights.

Figure 4.28. instantaneous velocity vector fields, streamline topologies and corresponding vorticity contours downstream of two side-by-side circular cylinders at various times and flopping regimes for H/D=1.0 and T/D=1. 5 case.

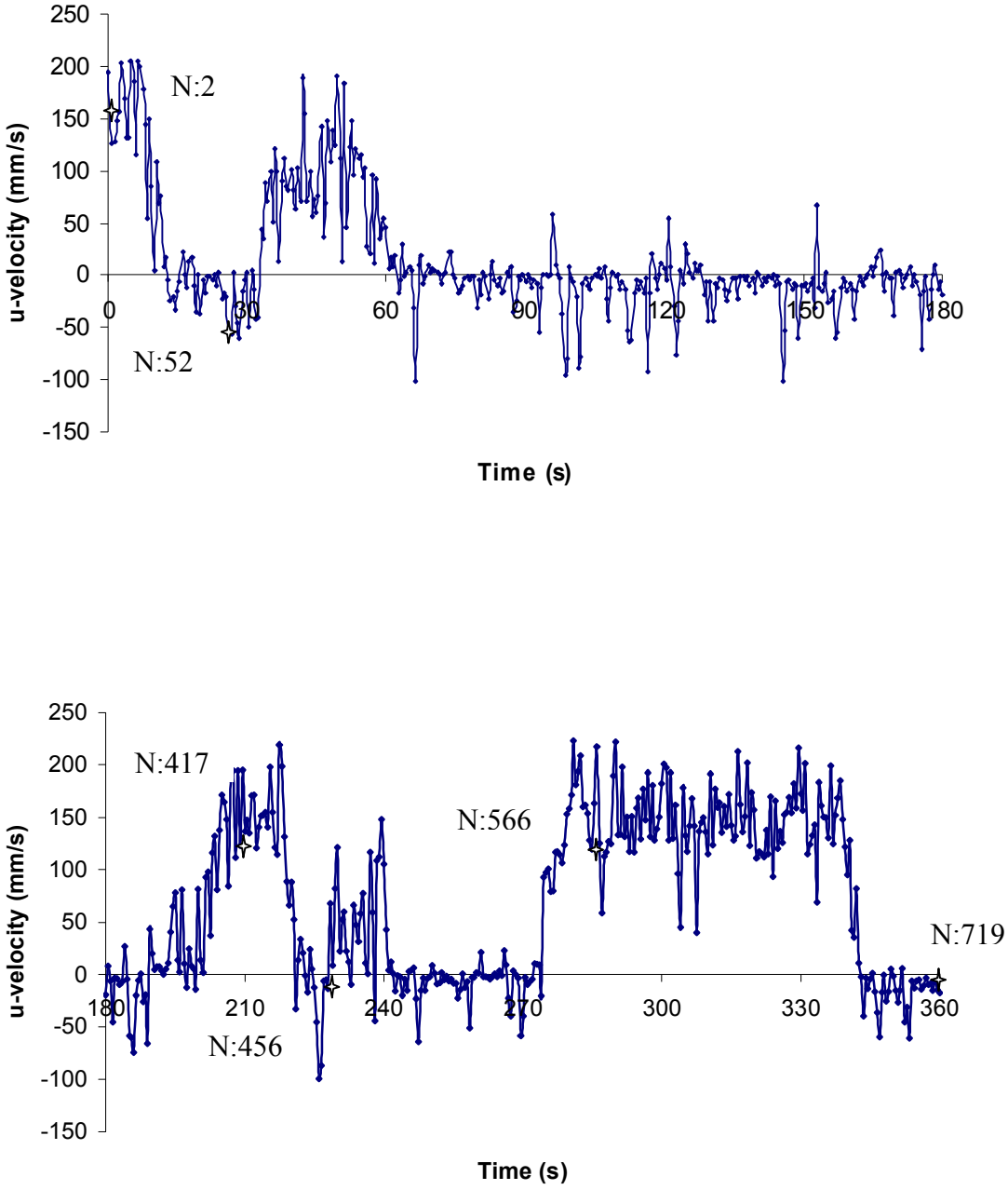

Figure 4.27. Instantaneous stream-wise velocity component for two side-by-side cylinders at x: 55.67mm, y: 66.61mm for H/D = 1.00, T/D = 1.50

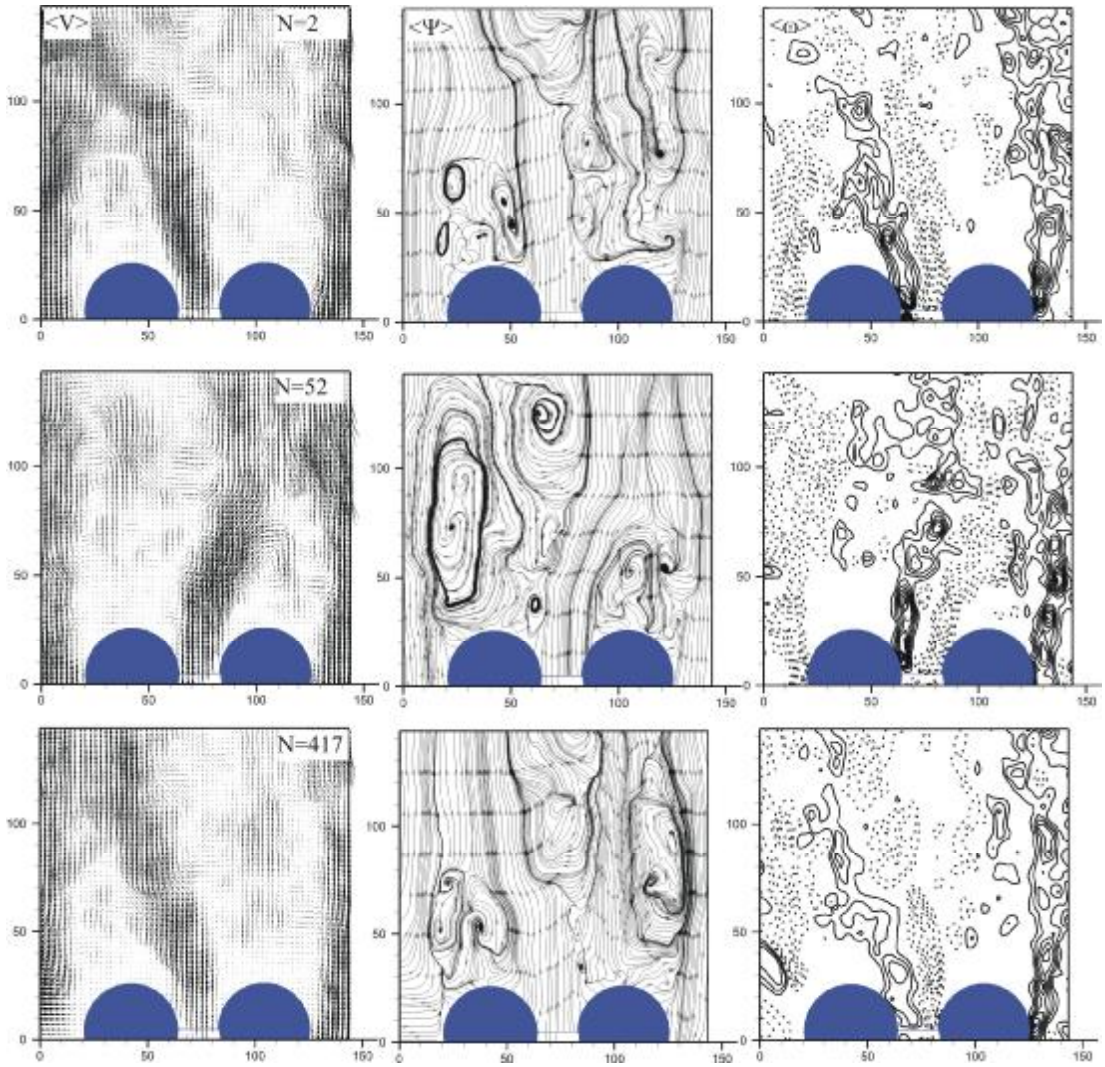
<V>
N=2
<Ψ>
<ω>
N=52
N=417

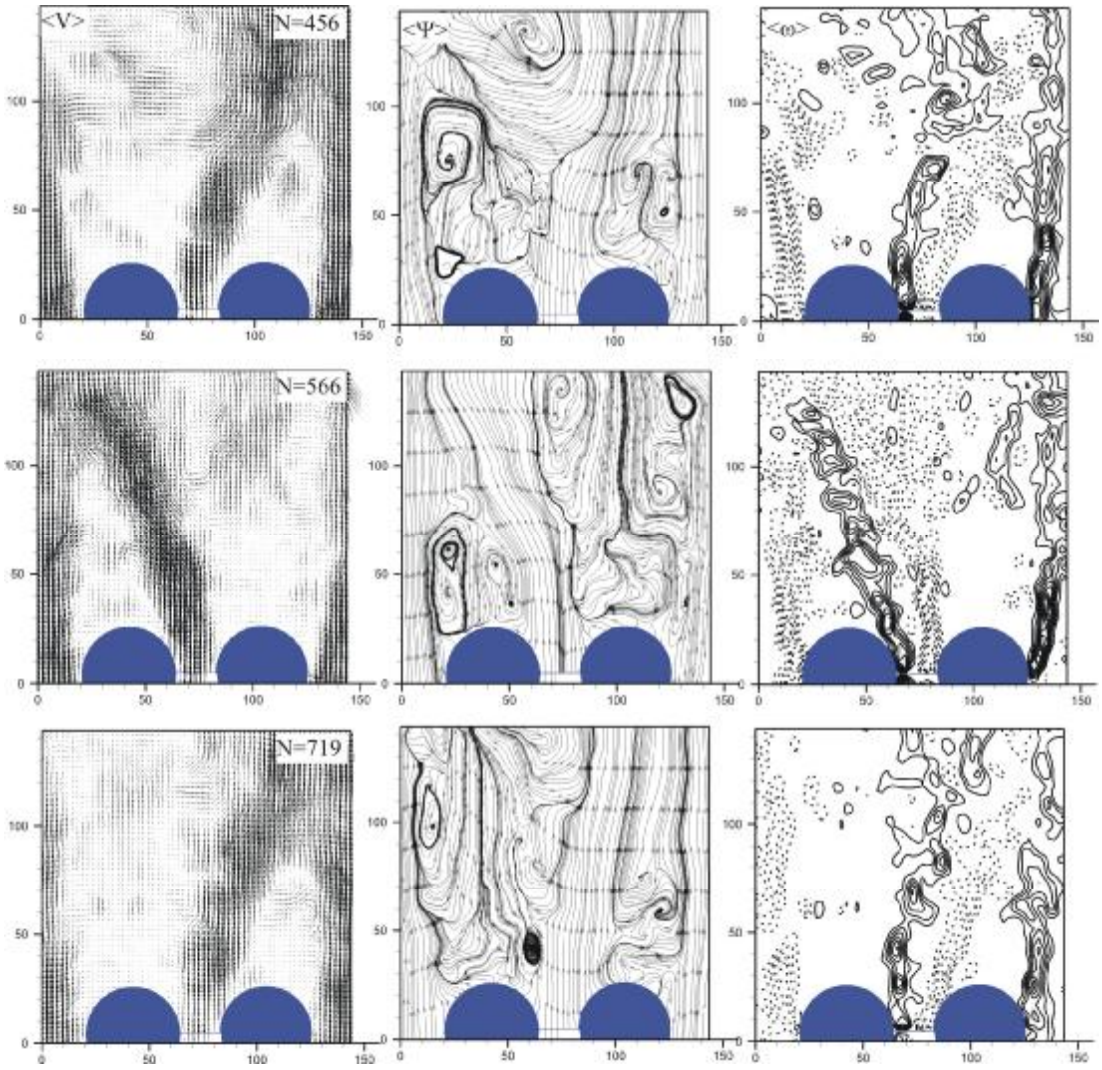

Figure 4.28. Instantaneous velocity vector field, vorticity contours and corresponding streamline topology for two side-by-side cylinders, H/D=1.00 T/D=1.50

Figure 4.29. shows the spectra of stream-wise velocity component at point 55.67 mm, 66.61 mm. The figure does not indicate any dominant frequency for this case.

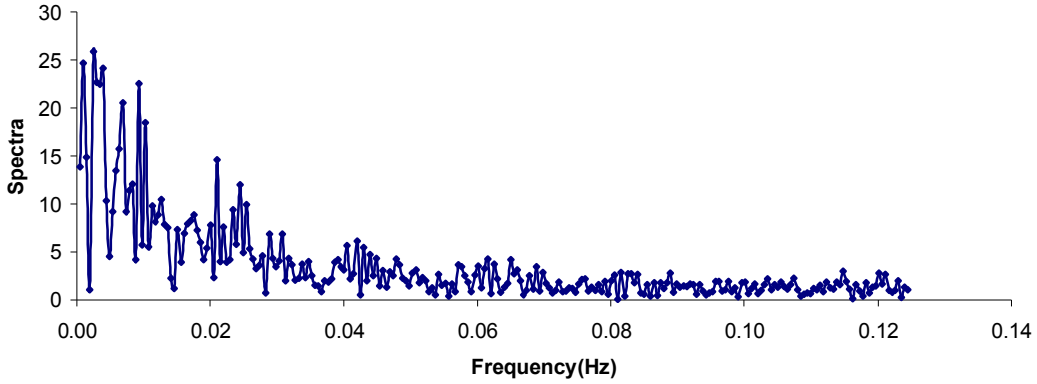

Figure 4.29 Spectra of stream-wise velocity component at point 55.67mm, 66.61mm

5. CONCLUSIONS AND RECOMMENDATIONS

In this study, flopping regime behind two and three side-by-side cylinders in shallow water flow was investigated by Particle Image Velocimetry Technique. Experiments were carried out at three different water heights (10mm, 20mm and 40mm) and three different spacing (10mm, 20 mm, 30 mm) between cylinders were used. Free-stream velocity was kept constant during experiments. Namely, experiments were carried out for just one Reynolds number.

Experiments show that one wide wake region and a small wake region occur downstream of two side-by-side circular cylinders and wide wake sometimes occur downstream of left cylinder and sometimes downstream of right cylinder. This kind of flow behavior is called as flopping in literature. Both instantaneous and time-averaged velocity vector field, corresponding vorticity contours and streamline topology were obtained from PIV experiments. Time history and spectra of stream-wise velocity vector field at various locations in the flow field for different cases does not show any dominant frequency of flopping regime. Flopping regime looks completely random process of flow. However, flopping occurs in between 10 and 60 seconds time period. Moreover, this time period decreases with decreasing water height.

Finally, for the flows where flopping regime occurs, instantaneous flow characteristics are more informative than the time-averaged flow characteristics.

AKILLI, H., AND ROCKWELL, D., 2002. Vortex formation from a cylinder in shallow water. Physics of Fluids, 14 (9): 2957-2967.

AKILLI, H., AKAR,A. and KARAKUS, C., 2004. Flow characteristics of circular cylinders arranged side-by-side in shallow water. Flow Measurement and Instrumentation,15,187-197.

AKILLI, H, SAHIN, B., and TUMEN, N.F., 2005, "Suppression of vortex shedding of circular cylinder in shallow water by a splitter plate", Flow measurement and Instrumentation, 16, pp.211-219.

ANDREOPOULUS, A., 1972. M.Sc. Project Report, Imperical College, London. 1972.

BALACHANDAR, R., CHU, V.H., AND ZHANG, J., 1997. Experimental study of turbulent concentration flow field in the wake of a bluff body. Journal of Fluids Engineering, 199: 263-270.

BALACHANDAR, R., TACHIE, T.M., AND CHU, V.H., 1999. Concentration profiles in shallow turbulent wakes. Journal of Fluids Engineering, 121: 34-43.

BALACHANDAR, R., RAMACHANDRAN, S., 1999. Turbulent boundary layers in low Reynolds number shallow open channel flows. Journal of Fluids Engineering, 121: 684-689.

BALACHANDAR, R., RAMACHANDRAN, S., AND TACHIE, M.F., 2000. Characteristic of shallow turbulent near wakes at low Reynolds number. Journal of Fluids Engineering, 122: 302-308.

BALACHANDAR, R., TACHIE, T.M., 2001. A study of boundary layer-wake interaction in shallow open channel flows. Experiments in Fluids, 30: 511-521.

BRADSHAW, P., DEAN, R.B., AND MCELIGOT, N.P, 1973. Trans. ASME I Journal Fluids Engineering 95, 214.

BEARMAN, P.W., AND WADCOCK, A.J., 1973. The interaction between a pair of circular cylinders normal to a stream. Journal of Fluid Mechanics, 61: 499-511.

BIERMANN, D., AND HERRNSTEIN, M., 1933. The interference between struts in various combinations, NACA Tech. Rep. 468.

BLOOR, M.S., 1964. The transition to turbulence in the wake of a circular cylinder. Journal of Fluid Mechanics, 19: 290-304.

CARMER, C.F.V., ANDREAS, C.R., AND JIRKA, G.H., 2002. Combined planar measurement of flow and mass concentration in shallow turbulent flow. Part 2: Application of coupled PIV-PCA to Turbulent shallow wakes flows. Proc. EVRI/IAHR International Conference on Hydraulic Measurements & Experimental Methods, Estes Park, USA.

CARMER, C.F.V., AND JIRKA, G.H., 2001. On turbulence and transport in shallow wake flows. Proceedings 29th IAHR Congress, Beijing, China.

CELİK, E., 2006. Oscillations of flow past a perforated plate: flow physics and suppression techniques. PhD Dissertation, Lehigh University.

CHEN, D., AND JIRKA, H., 1995. Experimental study of plane turbulent wakes in a shallow water layer. Fluid Dynamics Research, 16: 11-41.

CHEN, D., AND JIRKA, H., 1997. Absolute and convective instabilities of plane turbulent wakes in a shallow water layer. Journal of Fluid Mechanics, 338: 157-172.

CHENG, M., AND MORETTI, P.M., 1988. Experimental study of the flow field downstream of a single tube row. Experimental Thermal and Fluid Science, Journal 1:69-74.

CHU, H.V., WU, J.H., KHAYAT, R.E., 1991. Stability of transverse shear flows in shallow open channels. Journal of Hydraulic Engineering, 117(10): 1370-1388.

CHU, H.V. and S. BABARUTSI, 1988.Confinement and bed –friction effect in shallow turbulent mixing layers. J. Hydraulic Engineering 114: 1257-1274.

FABRIS, G., 1984. A conditional-sampling study of the interaction of two turbulent wakes. Journal of Fluid Mechanics, 140: 355-372.

FU, H., 2004. Shallow flow vortex formation and control. PhD Dissertation, Lehigh University.

FURUKAWA, K. AND WOLANSKI, E., 1998. Shallow-water frictional effects in island wakes. Coastal and Shelf Science, 46: 599-608.

GERRARD, J.H., 1978. The wakes of cylindrical bluff bodies at low Reynolds number. Phil. Trnas. R. Soc. London A, 288: 351-382.

GUILLAUME, D.W., AND LARUE, J.C., 1999. Investigation of the flopping regime with two-, three- and four-cylinder arrays. Experiments in Fluids 27: 145-156.

GUILLAUME, D.W., 1997. The effect of cylinder and plate arrays on the downstream velocity flowfield and the effect of a plate array on a flowfield with spatial and temporal unmıxedness. PhD Dissertation, University of California.

GRUBISIC, V., SMITH R.B., AND SCHAR, C., 1995. The effect of friction on shallow-water flow past an isolated obstacle. Journal of the Atmospheric Sciences, 52: 1985-2005.

HO, C.M., AND HUERRE, P., 1984. Perturbed free shear layers. Annu. Rev. Fluid Mechanics, 16: 365-424.

HORI, E., 1959. Experiments on flow around a pair of parallel circular cylinders. Proceedings of the 9th Japan National congress for Applied Mechanics, Paper III-11: 231-234.

INGRAM, R.G., AND CHU, V.H., 1987. Flow around island in Rupert Bay: An Investigation of the bottom friction effect. Journal of Geophysical Research, 92 (C13): 14521-14533.

ISHIGAI, S., NISHIKAWA, E., NISHIMURA, K., AND CHO, K., 1972. Experimental study of structures of gas flow in tube banks with tube axes normal to flow (Part I, Karman vortex flow from two tubes at various spacing). Bulletin of the JSME, 15: 949-956.

JENDRZEJCZYK, J.A., AND CHEN, S.S., 1986. Fluid forces on two circular cylinders in cross flow. In Flow-Induced Vibration- 1986: (eds Chen, S.S., Simonis, J.C., and Shin, Y.S.,) Chicago, IL, PVP,104: 1-13.

KAHRAMAN, A., SAHIN, B., AND ROCKWELL, D., 2002. Control of vortex formation a vertical cylinder in shallow water: Effect of localized roughness elements. Experiments in Fluids, 33: 54-65.

KAMEMOTO, K., 1976. Formation and interaction of two parallel vortex streets. Bulletin of the JSME, 19: 283-290.

KANG, S., 2003. Characteristics of flow over two circular cylinders in a side-by-side arrangement at low Reynolds numbers. Physics of fluids, 15: 2486-2498.

KUMADA, M., HIWADA, M., ITO, M., AND MABUCHI, I., 1984. Wake interference between three circular cylinders arranged side-by-side normal to a flow. Trans, Japanese. Soc. Mech. Eng., Ser. B 50, 1699 (in Japanese).

KIM, H.J., AND DURBIN, P.A., 1988. Investigation of the flow between a pair of circular cylinders in the flopping regime. Journal of Fluid Mechanics, 196: 431-448.

KIYA, M., ARIE, M., TAMURA, H., AND MORI, H., 1980. Vortex shedding from two circular cylinders in staggered arrangement. Trans. ASME, Journal of Fluid Engineering, 102: 166-173.

LEGAL, P., CHAUVE, M.P., LIMA, R., AND REZENDE, J., 1990. Coupled waked behind two circular cylinder. Physical Review A, 41: 4566-4569.

LEGAL, P., PESCHARD, I., CHAUVE, M.P AND TAKEDA, Y. 1996. Collective behaviour of wakes downstream of a row of cylinders. Physics of Fluids, 8: 2097-2106.

LLOYD, P.M., AND STANSBY, P.K., 1997. Shallow-water flow around model conical island of small side slope. I: Surface piercing. Journal of Hydraulic Engineering, 123: 1057-1067.

NEILL, S.P., AND ELLIOTT, A.J., 2004. Observations and simulations of an unsteady island wake in the firth of forth, Scotland. Ocean Dynamics, 54: 324-332.

PALMER, M.D., KEFFER, J.F., 1972. An experimental investigation of an asymmetrical turbulent wake. Journal of Fluid Mechanics, 53: 593-610.

PATTIARATCHI, C., JAMES, A., AND COLLINS, M., 1986. Island wakes and headland eddies: A comparison between remotely sensed data and laboratory experiments. Journal of Geophysical Research, 92: 783-784.

SCHAR, C., AND SMITH R.B., 1993. Shallow water flow past isolated topography. Part II: Transition to vortex shedding. Journal of the Atmospheric Sciences, 50: 1401-1412.

SUMNER, D., WONG, S., PRICE, S.J., AND PAIDOUSSIS, M.P., 1997. Two and three side-by-side circular cylinder in steady cross-flow. Proceeding of the 16th Canadian Congress of Applied Mechanics, 1: 273-274

SUMNER, D., WANG, S.S.T., PRICE, S. J., AND PAIDOUSSIS, M.P., 1999. Fluid Behavior of side-by- side circular cylinders in steady cross-flow. Journal of Fluids and Structures 13: 309-338.

SUMNER, D., PRICE, S. J., AND PAIDOUSSIS, M.P., 2000. Flow-pattern identification for two staggered circular cylinders in cross-flow. Journal of Fluid Mechanics, 411: 263-303.

SPIVACK, H.M., 1946. Vortex frequency and flow pattern in the wake of two parallel cylinders at varied spacing normal to an air stream. Journal of the Aeronautical Science, 13: 289-297.

TACHIE, T.M., BALACHANDAR, R., 2001. Shallow wakes generated on smooth and rough surfaces. Experiments in Fluids, 30:467-474.

ÜNAL, M.F., AND ROCKWELL, D., 1988. On vortex formation from a cylinder. Part I. The initial instability. Journal of Fluid Mechanics, 19: 491-512.

WEI, C.Y., AND CHANG, J.R., 1999. Study of base-bleed flow and wake downstream of two dimensional bluff bodies arranged side by side. The Sixth Military Academy Symposium on Fundamental Science, ROC.

WEI, T., AND SMITH, C.R., 1986. Secondary vortices in the wake of circular cylinder. Journal of Fluid Mechanics, 169:513-533.

WEIR, A.D., WOOD. D.H., AND BRADSHAW, P., 1981. Interacting turbulent shear layers in a plane jet. Journal of Fluid Mechanics, 107: 237-260.

WESTEWEEL, J., 1997. Fundamentals of digital particle image velocimetry. Measurement Science Technology, 8: 1379-1392.

WILLIAMSON, C.H.K., 1985. Evolution of a single wake behind a pair of bluff bodies. Journal of Fluid Mechanics, 159: 1-18.

WOLANSKI, E., IMBERGER, J., AND HERON, M.L., 1984. Island wakes in shallow coastal water. Journal of Geophysical Research, 89: 10553-10569.

ZHOU, Y., SO, R.M.C., LIU, M.H., AND ZHANG, H.J., 2000. Complex turbulent wakes generated by two and three side-by-side cylinders. International Journal of Heat and Fluid Flow 21: 125-123.

ZHOU, Y., WANG, Z.J., SO, R.M.C., XU, S.J., AND JIN, W., 2001. Free vibrations of two side-by-side cylinders in a cross-flow. Journal of Fluid Mechanics, 443; 197-229.

ZHOU, Y., 2003. Vortical structures behind three side-by-side cylinders. Experiments in Fluids, 34; 68-76.

ZDRAVKOVICH, M.M., 1968. Smoke observation of the wake of a group of three-cylinders at low Reynolds number. Journal of Fluid Mechanics, 32: 339-351.

ZDRAVKOVICH, M.M., AND STONEBANKS, K.I., 1990. Intrinsically nonuniform and metastable flow in and behind tube arrays. International Journal of Heat and Fluid Flow, 4: 305-319.

ZHANG, H.J., AND ZHOU, Y., 2001. Effect of unequal cylinder spacing on vortex streets behind three side-by-side cylinders. Physics of Fluids, 13 (12): 3675-3686.

CIRRICULUM VITAE

Ruken AKTAŞ was born on October 30, 1980 in Diyarbakır, Turkey. In 1997, she graduated from High School, and enrolled at Dicle University to study Mechanical Engineering .She graduated from Dicle University as a Mechanical Engineer in July 2001.She began her MSc education at the Department of Mechanical Engineering of Çukurova University. She is working in Atabar Ltd.Şti.,now